Transmission/Reflection and Short-Circuit Line Methods for Measuring Permittivity and Permeability

James Baker-Jarvis
Michael D. Janezic
John H. Grosvenor, Jr.
Richard G. Geyer

Electromagnetic Fields Division
Electronics and Electrical Engineering Laboratory
National Institute of Standards and Technology
325 Broadway
Boulder, Colorado 80303-3328

December 1993

U.S. DEPARTMENT OF COMMERCE, Ronald H. Brown, Secretary
TECHNOLOGY ADMINISTRATION, Mary L. Good, Under Secretary for Technology
NATIONAL INSTITUTE OF STANDARDS AND TECHNOLOGY, Arati Prabhakar, Director

National Institute of Standards and Technology Technical Note
Natl. Inst. Stand. Technol., Tech. Note 1355-R, 236 pages (December 1993)
CODEN:NTNOEF

U.S. GOVERNMENT PRINTING OFFICE
WASHINGTON: 1993

For sale by the Superintendent of Documents, U.S. Government Printing Office, Washington, DC 20402-9325

Contents

1 Introduction 1

2 Theory for Coaxial Line and Rectangular Waveguide Measurements of Permittivity and Permeability 6

2.1 Theory . . . 6
2.1.1 Decomposition into TE, TM, and TEM Modes . . . 6
2.1.2 Imperfect Sample Geometry . . . 9
2.1.3 Perfect Sample in Waveguide . . . 13
2.2 Permeability and Permittivity Calculation . . . 15
2.2.1 Nicolson-Ross-Weir Solutions (NRW) . . . 15
2.2.2 2-Port Solution Where Position is Determined Solely by $L_{airline}$ and L 17
2.2.3 Two Samples of Different Length . . . 18
2.3 Measurement Results . . . 19
2.3.1 Measurements without Gap Corrections . . . 20
2.3.2 Effects of Gaps between Sample and Waveguide . . . 20
2.4 Permeameter . . . 28
2.5 Uncertainty of Combined Permittivity and Permeability Determination . . . 29
2.5.1 One Sample at One Position . . . 30
2.5.2 Two Samples of Differing Lengths . . . 43
2.6 Uncertainty in Gap Correction . . . 49
2.6.1 Dielectric Materials . . . 49
2.6.2 Magnetic Materials . . . 50
2.6.3 Higher Order Modes . . . 50

3 Optimized Solution 52

3.1 Introduction . . . 52
3.2 Model for Permeability and Permittivity . . . 54
3.2.1 Relaxation Phenomena in the Complex Plane . . . 54
3.3 Numerical Technique . . . 57
3.3.1 Algorithm . . . 57

3.3.2 Numerical Results 59
3.4 Permittivity and Permeability 61
3.4.1 Measurements 61
3.4.2 Robustness of the Procedure 61
3.5 Discussion 65

4 Short-Circuit Line Methods **66**
4.1 Theory 66
4.1.1 Two Samples of Different Lengths 68
4.1.2 Single Sample at Two Short-Circuit Positions 70
4.2 Measurements 71
4.3 Uncertainty of Short-Circuit Line Measurements 73

5 Discussion **79**

6 References **83**

7 Appendices **86**

A Magnetism in Matter **87**
A.1 Description of Magnetic Phenomena 87
A.1.1 Field Description of Electromagnetic Phenomena 87
A.1.2 Types of Magnetism 89
A.2 Paramagnetism 89
A.2.1 Diamagnetism 90
A.2.2 Ferromagnetism 90
A.2.3 Ferrites and Antiferromagnetism 91
A.3 Equations of Motion for the Magnetization Vector 92
A.3.1 The Torque Equation 92
A.3.2 Magnetized Magnetic Material: The Polder Matrix 93

B Fields in Waveguides **96**
B.1 Summary of Maxwell's Equations 96
B.2 Modes 97
B.2.1 TE Modes 97
B.2.2 TM Modes 97
B.2.3 TEM Modes 98

C Gap Correction **99**
C.1 Frequency-Dependent Gap Correction 99
C.1.1 Waveguide 99

C.1.2 Coaxial Line 100
C.2 Frequency-Independent Approaches 101
C.2.1 Coaxial Capacitor Model for Dielectric Materials 101
C.2.2 Rectangular Waveguide Model 103
C.3 Gap Correction for Magnetic Materials 104
C.3.1 Coaxial Line 104
C.3.2 Waveguide 105
C.4 Gap Correction Formulas Derived Directly From Maxwell's Equations . . . 107
C.5 Mitigation of Air Gap Effects 108

D Causal Functions and Linear Response **110**
D.1 Introduction 110
D.2 Transfer Functions 111
D.3 Kramers-Kronig Relations 111

Abstract

The transmission/reflection and short-circuit line methods for measuring complex permittivity and permeability of materials in waveguides and coaxial lines are examined. Equations for complex permittivity and permeability are developed from first principles. In addition, new formulations for the determination of complex permittivity and permeability independent of reference plane position are derived. For the one-sample transmission/reflection method and two-position short-circuit line measurements, the solutions are unstable at frequencies corresponding to integral multiples of one-half wavelength in the sample. For two-sample methods the solutions are unstable for frequencies where both samples resonate simultaneously. Criteria are given for sample lengths to maintain stability. An optimized solution is also presented for the scattering parameters. This solution is stable over all frequencies and is capable of reducing scattering parameter data on materials with higher dielectric constant. An uncertainty analysis for the various techniques is developed and the results are compared. The errors incurred due to the uncertainty in scattering parameters, length measurement, and reference plane position are used as inputs to the uncertainty models.

Key words: Calibration; coaxial line; dielectric constant; loss factor; magnetic materials; microwave measurements; permeameter; permeability measurement; permittivity measurement; reflection method; short-circuit; transmission; uncertainty; waveguide.

Chapter 1

Introduction

The goal of this report is to review and critically evaluate various transmission line measurement algorithms for combined permeability and permittivity determination and to present results and uncertainty analysis for the techniques.

There is continual demand to measure accurately the magnetic and dielectric properties of solid materials. Over the years there has been an abundance of methods developed for measuring permeability and permittivity. Almost all possible perturbations or variations of existing methods have been proposed for measurements. These techniques include free-space methods, open-ended coaxial probe techniques, cavity resonators, full-body resonance techniques, and transmission-line techniques. Each method has its range of applicability and its own inherent limitations. For example, techniques based on cavities are accurate, but not broadband. Nondestructive techniques, although not most accurate, allow the maintenance of material integrity. Transmission line techniques are the simplest of the relatively accurate ways of measuring permeability and permittivity of materials. Transmission line measurements usually are made in waveguide or coaxial lines. Measurements are made in other types of transmission lines for special applications, but for precise measurements, rectangular waveguides and coaxial lines are usually used. The three major problems encountered in transmission line measurements are air gaps, half-wavelength resonances, and overmoding.

Coaxial lines are broadband in the TEM mode and therefore are attractive for permittivity and permeability measurements. The problem with coaxial lines, however, is that due to the discontinuity of the radial electric field, any air gap around the center conductor degrades the measurement by introducing a large measurement uncertainty. Belhadj-Tahar et al. [1] have attempted to circumvent these difficulties with the development of a technique for a plug of material at the end of a coaxial line. In Belhadj-Tahar's approach there is no center conductor hole. However, higher modes are excited at the transition between the plug and the center conductor which complicates the analysis. Due to the complexity

of the method it is not apparent at this time whether this approach will replace the more traditional single-mode models.

Transmission line techniques generally fall into the following categories:

- Off-resonance waveguide and coaxial line, full scattering parameter, 2-port measurements.
- Off-resonance short-circuit line, 1-port measurements.
- Open-circuit techniques.
- Resonant transmission-line techniques.

The topic of this report will be the first two categories. We will also examine direct inductance measurement, which uses permeameter techniques. The off-resonance techniques can be broadly grouped into two categories:

- Point-by-point or uncorrelated-point techniques.
- Multi-point or correlated-point techniques.

The point-by-point technique is at present the most widely used reduction technique and consists of solving the relevant scattering equations at single points. Multi-point techniques consist of solving the nonlinear scattering equations using nonlinear least square algorithms.

Due to their relative simplicity, the off-resonance waveguide and coaxial line transmission/reflection (TR) and short-circuit line (SCL) methods are presently widely used broadband measurement techniques. In these methods a precisely machined sample is placed in a section of waveguide or coaxial line and the scattering parameters are measured, preferably by an automatic network analyzer (ANA). The relevant scattering equations relate the measured scattering parameters to the permittivity and permeability of the material. One limitation of these techniques is that they require cutting of the sample and therefore these techniques do not fall under the general category of nondestructive testing methods. Another limitation is that these techniques require a small sample and therefore the resonance characteristics of large sheets of the material are not studied. Network analyzers have improved over the last years to a point where broad frequency coverage and accurate measurement of scattering parameters are possible. This broadband capability unearths another limitation of present algorithms, that is, the instability of the measurement in the vicinity of resonant frequencies.

In this report we assume that the materials under test are isotropic, homogeneous, and in a demagnetized state. The solutions obtained in this report are both single-frequency techniques and multiple frequency techniques. For the TR measurement, the system of equations contains as variables the complex permittivity and permeability, the two reference

plane positions, and, in some applications, the sample length. In the T/R procedure we have more data at our disposal than in SCL measurements, since we have all four of the scattering parameters. In SCL measurements the variables are complex permittivity and permeability, sample length, distance from sample to short-circuit termination, and reference plane positions. However, in most problems we know the sample length, reference plane position, and distance from the reflector to the sample. In these cases we have four unknown quantities (complex permittivity and permeability) and therefore require four independent real equations to solve for these variables. These equations can be generated by taking reflection coefficient data at two positions in the transmission line, thus yielding the equivalent of four real equations for the four unknown quantities. A problem encountered in measurements is the transformation of S-parameter measurements at the calibration reference planes to the air-sample interface. This transformation requires knowledge of the position of the sample in the sample holder. Information on reference plane position is limited in many applications. The port extension and gating features of network analyzers are of some help in determining reference plane position, but do not completely solve the problem. Equations that are independent of reference plane position are desirable.

Most of the present transmission-line techniques [2,3,4], with some variations, are based on the procedure developed by Nicolson and Ross [5] and Weir [6] for obtaining 2-port, off-resonance, broadband measurements of permeability and permittivity. In the Nicolson-Ross-Weir (NRW) procedure the equations for the scattering parameters are combined in such a fashion that the system of equations can be decoupled. This procedure yields an explicit expression for the permittivity and permeability as a function of the S-parameters. These equations are not well-behaved for low-loss materials at frequencies corresponding to integral multiples of one-half wavelength in the sample. In fact, the NRW equations are divergent, due to large phase uncertainties for very low-loss materials at integral multiples of one-half wavelength in the material. Many researchers avoid this problem by measuring samples which are less than one-half wavelength long at the highest measurement frequency. The advantage of the NRW approach is that it yields both permittivity and permeability over a large frequency band. As a special case of the NRW equations, Stuchly and Matuszewski [7] found solutions to the scattering equations for nonmagnetic materials and derived two explicit equations for the permittivity. Delecki and Stuchly [8] have studied the uncertainty analysis for infinitely long samples using the bilinear and Schwarz-Christoffel transformations. Franceschetti [9] was one of the first to perform a detailed uncertainty analysis for TR measurements. Ligthart [10] developed an analytical method for permittivity measurements at microwave frequencies using an averaging procedure. In Ligthardt's study, a single-moded cylindrical waveguide was filled with a homogeneous dielectric with a moving short-circuit termination positioned beyond the sample. This study focused primarily on single-frequency measurements rather than on broadband measurements.

The short-circuit line (SCL) method was introduced by Roberts and von Hippel [11] over fifty years ago as an accurate broadband measurement procedure. The SCL measure-

ment method uses data obtained from a short-circuit 1-port measurement to calculate the dielectric and magnetic properties. SCL is useful when 2-port measurements are not possible, for example, in high temperature measurements [12] and remote sensing applications. When an ANA is used, the sample is positioned in either a waveguide or coaxial line and the reflection coefficient is measured. The determination of the permittivity and permeability usually proceeds by solving a transcendental equation that involves the sample length, sample position, and reflection coefficient. With modern computer systems, iterative solutions of the resulting transcendental equations are easy to implement. However, they require an initial guess. The resultant nonlinear equations have an infinite number of solutions due to periodic functions. The physical solution can be determined by group delay arguments or by measuring two samples with differing lengths. Much of the theory developed for the SCL technique was developed for use with a slotted line. Present-day network analyzers usually measure scattering parameters. Therefore in this report we derive equations from a scattering approach.

The SCL method has endured over the years, and as a result there is an extensive literature. In this report we attempt to review only the most relevant work on the subject. Short-circuit line methods can be broadly separated into *two- position techniques* and *two-sample techniques.* In the *two-position technique* 1-port scattering parameters are measured for a sample in two different positions in the sample holder. In the *two-sample technique* two samples of different lengths are machined from the same material and scattering parameters are measured with each sample pressed against the short-circuit termination. Szendrenyi [13] developed an algorithm for the case in which the length of one sample is precisely twice the length of the other sample. In this special case, they found an explicit solution.

Mattar and Brodwin [14] have described a variable reactance termination technique for permittivity determination. Maze [15] has presented an optimized-solution technique where at each frequency scattering parameters are taken for various short-circuit termination positions. Dakin and Work [16] developed a procedure for low-loss materials and Bowie and Kelleher [17] presented a rapid graphical technique for solving the scattering equations. Other authors have presented methods using measurements on two or more sample lengths [18]. Most of the literature to date has focused on permittivity determination. In the few works that have addressed the combined permeability and permittivity problem, many details have been left unresolved.

Recently Chao [19] presented SCL measurements results with a slotted line and also an uncertainty analysis for single frequency measurements. Chao found that accuracy was reduced when the reflection coefficient is dominated by the front face contribution.

The SCL measurement may use either a fixed or movable short-circuit device. The advantage of a moving short-circuit termination [2] is the possibility for making many separate measurements at a given frequency with the sample placed in either a high electric or magnetic field region [15]. Generally, a maximum in electric field strength is advantageous for permittivity measurements, whereas a maximum in magnetic field strength is

advantageous for permeability measurements.

When only permittivity is required, a single measurement at a given frequency suffices, whereas when both permeability and permittivity are to be determined, it is necessary to carry out two independent measurements at each frequency. There are various contributions to the uncertainties in the SCL method. These uncertainties include network analyzer uncertainties, sample gaps, wall and reflection losses, and measurement of sample dimensions. There are also uncertainties in the location of the sample reference planes and in the distance from sample to the short-circuit termination. The uncertainty in the network analyzer parameters are sometimes documented by the manufacturer [3].

In this report we develop relevant equations from first principles. These equations apply to ANA systems. We will examine the various approaches for combined determination of permeability and permittivity, and study the uncertainty in the measurement process. The special case of repeated measurements on a sample of fixed length is treated in detail.

Chapter 2

Theory for Coaxial Line and Rectangular Waveguide Measurements of Permittivity and Permeability

2.1 Theory

The goal of this chapter is to present various approaches for obtaining both the permeability and permittivity from transmission line scattering data. In the TR measurement, a sample is inserted into either a waveguide or a coaxial line, and the sample is subjected to an incident electromagnetic field [see figure 2.1]. The scattering equations are found from an analysis of the electric field at the sample interfaces. In order to determine the material properties from scattering data, it is necessary to understand the structure of the electromagnetic field in waveguides. In developing the scattering equations usually only the fundamental waveguide mode is assumed to exist. In this report we develop the theory for multimode solutions. However, the numerical algorithms presented will be valid only for the fundamental mode.

2.1.1 Decomposition into TE, TM, and TEM Modes

In this section we briefly review the theory of modes in transmission lines. It is possible to decompose the fields in a waveguide at a given frequency into the complete set of TE, TM,

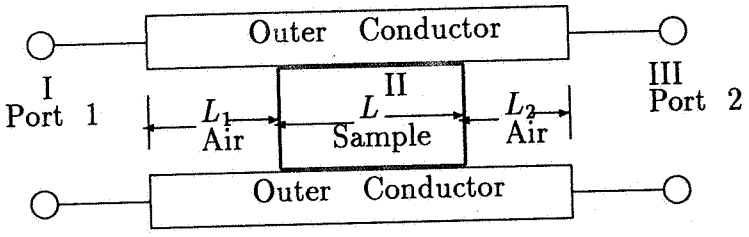

Figure 2.1: A dielectric sample in a transmission line and the incident and reflected electric field distributions in the regions I, II, and III. Port 1 and port 2 denote calibration reference plane positions.

and TEM modes. In our model at hand we assume:

- There is a propagation direction in the guide which we call $\vec{z}$.
- The cross-sectional area of the guide is perpendicular to $\vec{z}$ and constant throughout the length of the guide.

Electromagnetic fields in a sourceless region satisfy

$$\nabla \times \nabla \times \vec{E} = -j\omega\nabla\mu \times \vec{H} + k^2\vec{E} \ , \tag{2.1}$$

$$\nabla \times \nabla \times \vec{H} = j\omega\nabla\epsilon \times \vec{E} + k^2\vec{H} \ , \tag{2.2}$$

where $k = -j\gamma$ is the wave number.

In this report we assume that there are no sources of electric and magnetic fields in the guide ($\vec{J} = 0$) and there no free charge build up ($\nabla \cdot \vec{D} = 0$). Further we assume that the material parameters are not spatially dependent. However, step function discontinuities are assumed to exist between the sample and air gap. The step function discontinuities in the equations can contribute a delta function term in derivatives. With these assumptions, the fields satisfy homogeneous Helmholtz equations,

$$\nabla^2\vec{E} + k^2\vec{E} = 0 \ , \tag{2.3}$$

$$\nabla^2\vec{H} + k^2\vec{H} = 0 \ . \tag{2.4}$$

The time-dependent fields can be expanded in terms of modes

$$\vec{\mathcal{E}}(\vec{r},t) = \frac{1}{2\pi}\int_{-\infty}^{\infty} d\omega \sum_n \vec{E}_n(\vec{r}_T,\omega)\exp(\pm\gamma_n z)\exp(j\omega t) \ , \tag{2.5}$$

$$\vec{\mathcal{H}}(\vec{r},t) = \frac{1}{2\pi}\int_{-\infty}^{\infty} d\omega \sum_n \vec{H}_n(\vec{r}_T,\omega)\exp(\pm\gamma_n z)\exp(j\omega t)\ , \tag{2.6}$$

where $\vec{r}_T$ is a transverse vector, E_n, H_n are the amplitudes of the modes, and

$$\gamma_n = j\sqrt{\frac{\omega^2\mu_R^*\epsilon_R^*}{c_{vac}^2} - \left(\frac{2\pi}{\lambda_{nc}}\right)^2}\ , \tag{2.7}$$

$$\gamma_o = j\sqrt{\left(\frac{\omega}{c_{lab}}\right)^2 - \left(\frac{2\pi}{\lambda_{nc}}\right)^2}\ , \tag{2.8}$$

where γ_o, γ_n are the propagation constants in vacuum and material, respectively. Also $j = \sqrt{-1}$, c_{vac} and c_{lab} are the speed of light in vacuum and laboratory, ω is the angular frequency, λ_{nc} is the cutoff wavelength of the nth mode, ϵ_o and μ_o are the permittivity and permeability of vacuum, ϵ_R^* and μ_R^* are the complex permittivity and permeability relative to a vacuum.

Since these modes satisfy a Sturm-Liouville problem, we know that the totality of these waves forms a complete set of functions, and therefore an eigenfunction expansion property exists for this system. The Laplacian separates in the coordinate systems used in this report, and therefore the fields can be separated into transverse (T) and longitudinal (z) components:

$$\vec{E} = \vec{E}_T + E_z\vec{z}\ , \tag{2.9}$$

$$\vec{H} = \vec{H}_T + H_z\vec{z}\ . \tag{2.10}$$

The component E_z is the generator of the TM mode (see Appendix) and the H_z component is the generator of the TE mode. Since the TE, TM, and TEM modes form a complete set of functions, we can expand the transverse Fourier-transformed fields as

$$\begin{aligned}\vec{E}_T(\vec{r},\omega) = &\\ &\sum_{n=1}^{\infty}\{E_{nTE}^+\exp(-\gamma_n z) + E_{nTE}^-\exp(\gamma_n z)\}\vec{E}_{T(TE)}(\vec{r}_T)\\ &+\sum_{n=1}^{\infty}\{E_{nTM}^+\exp(-\gamma_n z) + E_{nTM}^-\exp(\gamma_n z)\}\vec{E}_{T(TM)}(\vec{r}_T)\\ &+\sum_{n=1}^{N-1}\{E_{nTEM}^+\exp(-\gamma_n z) + E_{nTEM}^-\exp(\gamma_n z)\}\vec{E}_{T(TEM)}(\vec{r}_T)\ ,\end{aligned} \tag{2.11}$$

$$\vec{H}_T(\vec{r},\omega) =$$

$$\sum_{n=1}^{\infty} \frac{1}{Z_{nTE}} \{E_{nTE}^{+} \exp(-\gamma_n z) - E_{nTE}^{-} \exp(\gamma_n z)\} (\vec{z} \times \vec{E}_{T(TE)})(\vec{r}_T))$$
$$+ \sum_{n=1}^{\infty} \frac{1}{Z_{nTM}} \{E_{nTM}^{+} \exp(-\gamma_n z) - E_{nTM}^{-} \exp(\gamma_n z)\} (\vec{z} \times \vec{E}_{T(TM)}(\vec{r}_T))$$
$$+ \sum_{n=1}^{N-1} \sqrt{\frac{\epsilon}{\mu}} \{E_{nTEM}^{+} \exp(-\gamma_n z) - E_{nTEM}^{-} \exp(\gamma_n z)\} (\vec{z} \times \vec{E}_{T(TEM)}(\vec{r}_T)) \quad (2.12)$$

where N is the number of disjoint conductors and $(\pm)$ denotes forward and backward traveling waves. The coefficients E_n depend on the transverse components, and the wave impedances are

$$Z_{TM} = \frac{\gamma_n}{j\omega\epsilon} , \quad (2.13)$$

$$Z_{TE} = \frac{j\omega\mu}{\gamma_n} . \quad (2.14)$$

Although the sums for the TE and the TM waves in eqs (3.11) and (2.12) approach ∞, in many problems of practical interest, some of the coefficients in the sums vanish. Two or more modes may have the same eigenvalue; the eigenvectors in these cases are called *degenerate*.

In order to solve eq (2.3) it is expeditious to break up the Laplacian into transverse and longitudinal components,

$$\nabla^2 \vec{E} = \nabla_T^2 \vec{E} + \frac{\nabla^2 \vec{E}}{\partial z^2} , \quad (2.15)$$

where

$$\frac{\partial^2 \vec{E}}{\partial z^2} = \gamma^2 \vec{E} , \quad (2.16)$$

and the transverse Laplacian satisfies by eq (2.3)

$$\nabla_T^2 \vec{E} = -(k^2 + \gamma^2)\vec{E} \equiv -k_c^2 \vec{E} , \quad (2.17)$$

where k_c is the cutoff wavenumber. If ϵ has a dependence on transverse coordinates in terms of a step discontinuity, then γ also has a transverse dependence. In Appendix A, the details of the derivations of the fields are reviewed.

2.1.2 Imperfect Sample Geometry

In the case of perfect or near perfect samples and sample holders, γ is independent of the transverse coordinates and therefore different eigenfunctions for the transverse components

in the air and sample regions possess an orthogonality condition [see Appendix A]. In such cases it is possible to match mode by mode, and the coefficients are decoupled. However, when samples and sample holder are not perfectly formed or are slightly inhomogeneous, both μ and ϵ have a weak dependence on the transverse coordinates of the guide and therefore the different transverse eigenfunctions in the sample are not orthogonal to the transverse eigenfunctions in the air section. The modes of imperfect samples cannot be separated and matched mode by mode. The imperfections in the sample generate evanescent waves at the sample-material interface. These modes may propagate in the sample, but they decay exponentially outside of the sample.

For an imperfect sample, the fields in the regions I, II, and III are found from an analysis of the electric field at the sample interfaces. We assume that the incident electric field is the TE_{10} mode in rectangular waveguide and TEM in coaxial line. As the wave propagates from the air-filled region into the sample, some of the energy carried in the wave will convert into higher order modes. However, it is necessary to consider only the transverse components of the fields when matching boundary conditions. In the following we assume that gaps or other imperfections can exist in and around the sample. We further assume that the imperfections are such that the Laplacian can be separated into transverse and longitudinal components. If the imperfections are azimuthally symmetric, then only the H_ϕ magnetic field component is assumed to exist. If we assume the vector component of the normalized electric fields E_I, E_{II}, and, E_{III}[1] in the regions I, II, and III, we can write for N modes

$$E_I = \underbrace{\exp(-\gamma_{o1}z)}_{\text{incident wave}} + S_{11}\exp(\gamma_{o1}z) + \sum_{i=2}^{N}\underbrace{C_i(\vec{z}_T)\exp(\gamma_{oi}z)]}_{\text{evanescent}}\,, \tag{2.18}$$

$$E_{II} = \sum_{i=1}^{N}[D_i(\vec{z}_T)\exp(-\gamma_{mi}z) + E_i(\vec{z}_T)\exp(\gamma_{mi}z)]\,, \tag{2.19}$$

$$E_{III} = S_{21}\underbrace{\exp(-\gamma_{o1}(z-L))}_{\text{transmitted wave}} + \sum_{i=2}^{N}\underbrace{[F_i(\vec{z}_T)\exp(-\gamma_{oi}(z-L))]}_{\text{evanescent}}\,, \tag{2.20}$$

where C_i, D_i, E_i, F_i are the modal coefficients, which may depend on the transverse coordinates. Also γ_{oi}, γ_{mi} are the propagation constants of the ith mode in vacuum and material respectively. We assume that we are operating the waveguide at such a frequency that only the fundamental mode is a propagating mode in the air section of the guide. The other modes are evanescent in the air section of the guide, but may be propagating in the material-filled section. There may be additional modes produced by mode conversion for

[1]TEM mode in a coaxial line or the TE_{10} mode in a waveguide (with a time dependence of $\exp(j\omega t)$ suppressed)

the other components of the electric field, but these are not necessary for specification of the boundary conditions.

In general, the amplitudes in eqs (2.18) to (2.20) are functions of the transverse coordinates. To find the coefficients, it is necessary to match tangential electric and magnetic fields at the interfaces and integrate over the cross- sectional area. Since different transverse eigenfunctions in the air are not orthogonal to transverse eigenfunctions in the sample we cannot separate a particular mode in the sample and match it to the analogous mode in the air. The tangential electric field matching yields

$$\delta_{k1} + (1 - \delta_{k1})c_k = \sum_{j=1}^{N}[A_{kj}d_j + A_{kj}e_j] \ , \tag{2.21}$$

$$[d_k \exp(-\gamma_{mk}L) + e_k \exp(\gamma_{mk}L) = \sum_{j=1}^{N} A_{jk}f_j \ , \tag{2.22}$$

where δ_{ij} is the Kronecker delta and c, e, and f are the integrated coefficients, N is the number of modes, and A_{kj} is the matrix of the coefficients of the integrated transverse eigenfunctions. The transverse component of the magnetic field can be obtained from Maxwell's equations using eqs (2.21) and (2.22). If we match the tangential magnetic field components and integrate over the transverse variables we have

$$[-\frac{\gamma_{01}}{\mu_0}\delta_{k1} + \frac{\gamma_{0k}}{\mu_0}(1 - \delta_{k1})c_k] = \sum_{j=1}^{N}\frac{\gamma_{mj}}{\mu}[-A_{kj}d_j + A_{kj}e_j] \ , \tag{2.23}$$

$$[-d_k\frac{\gamma_{mk}}{\mu}\exp(-\gamma_{mk}L) + \frac{\gamma_{mk}}{\mu}e_k \exp(\gamma_{mk}L) = -\sum_{j=1}^{N} A_{jk}f_j\frac{\gamma_{0j}}{\mu_0} \ , \tag{2.24}$$

where L is the sample length and

$$L_{air} = L + L_1 + L_2 \ . \tag{2.25}$$

These boundary conditions yield a linear system of equations for the coefficients. Various cutoff frequencies and operating frequencies are given in tables 2.1 and 2.2.

The difficulties in solving the full mode problem in eqs (2.21) to (2.24) is that the coefficients of the matrix A_{kj} are not generally known precisely unless the complete boundary value problem is solved for each sample. These coefficients are known only for simple, well-defined geometries and not for samples with unknown air gaps or complicated inhomogeneities.

Table 2.1: Cutoff frequencies for TE_{10} mode in rectangular waveguide.

EIA WR	Band	Cutoff frequency(GHz)
650	L	0.908
430	W	1.372
284	S	2.078
187	C	3.152
90	X	6.557
42	K	14.047
22	Q	26.342

Table 2.2: Rectangular waveguide dimensions and operating frequencies in air.

EIA WR	Band	a (cm)	b (cm)	TE_{10} Operating frequency(GHz)
650	L	16.510	8.255	1.12 - 1.70
430	W	10.922	5.461	1.70 - 2.60
284	S	7.710	3.403	2.60 - 3.95
187	C	4.754	2.214	3.95 - 5.85
90	X	2.286	1.016	8.20 - 12.40
42	K	1.067	0.432	18.0 - 26.5
22	Q	0.569	0.284	33.0 - 50.0

2.1.3 Perfect Sample in Waveguide

As a special case of the formalism developed in the previous section we consider a perfect sample in a perfect waveguide as indicated in figure 2.1. In this case no mode conversion occurs because the eigenfunctions in the air and sample regions are orthogonal with respect to cross-sectional coordinates. Therefore the modes may be decoupled and the evanescent modes are not of concern. This is a special case of eqs (2.21) to (2.25). In this case we nced to be concerned only with the fundamental mode in the guide. The electric fields in the sample region $z \in (0, L)$ for a coaxial line with a matched load and with the radial dependence written explicitly are

$$E_I = \frac{1}{r}[\exp(-\gamma_o z) + S_{11}\exp(\gamma_o z)] \ , \tag{2.26}$$

$$E_{II} = \frac{1}{r}C_2[\exp(-\gamma_1 z) + C_3\exp(\gamma_1 z)] \ , \tag{2.27}$$

$$E_{III} = \frac{1}{r}[S_{21}\exp(-\gamma_o(z-L))] \ . \tag{2.28}$$

When these equations are integrated over the cross-sectional surface area, the radial dependence is the same for each region of the waveguide.

The constants in the field equations are again determined from the boundary conditions. The boundary condition on the electric field is the continuity of the tangential component at the interfaces. The tangential component can be calculated from Maxwell's equations given an electric field with only a radial component. The higher modes in eqs (2.18) to (2.20) are evanescent in the air-filled section of the guide. TM modes can be treated similarly. The details of the boundary matching for the TE_{10} case are described in a previous report on dielectric materials [26,27]. The boundary condition for the magnetic field requires the additional assumption that no surface currents are generated. If this condition holds, then the tangential component of the magnetic field is continuous across the interface. The tangential component can be calculated from Maxwell's equations for an electric field with only a radial component. For a 2-port device the expressions for the measured scattering parameters are obtained by solving eqs (2.18) through (2.20) subject to the boundary conditions. We assume that $S_{12} = S_{21}$. The explicit expressions for a sample in a waveguide a distance L_1 from the port-1 reference plane to the sample front face and L_2 from the sample back face to the port-2 calibration plane are related. The S-parameters measured by the device reference planes are related to the S- parameters at the sample face S' by [26]

$$\overline{\overline{S}}' = \overline{\overline{\Phi}}\,\overline{\overline{S}}\,\overline{\overline{\Phi}} \ , \tag{2.29}$$

where

$$\overline{\overline{\Phi}} = \begin{pmatrix} \exp(j\phi_1) & 0 \\ 0 & \exp(j\phi_2) \end{pmatrix} , \tag{2.30}$$

and $\phi_1 = j\gamma_0 L_1$ and $\phi_2 = j\gamma_0 L_2$. The S-parameters are defined in terms of the reflection coefficient Γ and transmission coefficient z by:

$$S_{11} = R_1^2 \left[\frac{\Gamma(1-z^2)}{1-\Gamma^2 z^2} \right] , \tag{2.31}$$

$$S_{22} = R_2^2 \left[\frac{\Gamma(1-z^2)}{1-\Gamma^2 z^2} \right] , \tag{2.32}$$

$$S_{21} = R_1 R_2 \left[\frac{z(1-\Gamma^2)}{1-\Gamma^2 z^2} \right] , \tag{2.33}$$

where

$$R_1 = \exp(-\gamma_o L_1) , \tag{2.34}$$

$$R_2 = \exp(-\gamma_o L_2) , \tag{2.35}$$

are the respective reference plane transformations. Equations (2.31) through (2.33) are not new and are derived in detail elsewhere [5,28]. We also have an expression for the transmission coefficient Z:

$$Z = \exp(-\gamma L) . \tag{2.36}$$

We define a reflection coefficient by

$$\Gamma = \frac{\frac{\mu}{\gamma} - \frac{\mu_0}{\gamma_0}}{\frac{\mu}{\gamma} + \frac{\mu_0}{\gamma_0}} . \tag{2.37}$$

For coaxial line the cutoff frequency approaches 0, ($\omega_c \to 0$) and therefore Γ reduces to

$$\Gamma = \frac{\frac{c_{vac}}{c_{lab}} \sqrt{\frac{\mu_R^*}{\epsilon_R^*}} - 1}{\frac{c_{vac}}{c_{lab}} \sqrt{\frac{\mu_R^*}{\epsilon_R^*}} + 1} . \tag{2.38}$$

Additionally, S_{21} for the empty sample holder is

$$S_{21}^0 = R_1 R_2 \exp(-\gamma_0 L_a) . \tag{2.39}$$

For nonmagnetic materials, eqs (2.31), (2.32), (2.33) contain ϵ'_R, ϵ''_R, L, and L_a, and the reference plane transformations R_1, R_2 as unknown quantities. Since the equations for S_{12} and S_{21} are theoretically equivalent for isotropic non-gyromagnetic materials, we have four complex equations, eqs (2.31), (2.32), (2.33), (2.39), plus the equation for the length of the air line (2.25), or equivalently, nine real equations for the six unknowns. However, in many applications we know the sample length to high accuracy. For magnetic materials we have eight unknowns. However, we have frequency data for each measurement. Since the lengths are independent of frequency we have an over-determined system of equations. This abundance of information will be exploited in the next chapter.

2.2 Permeability and Permittivity Calculation

2.2.1 Nicolson-Ross-Weir Solutions (NRW)

Nicolson and Ross [5], and Weir [6] combined the equations for S_{11} and S_{21} and discovered a formula for the permittivity and permeability. Their procedure works well at off-resonance where the sample length is not a multiple of one-half wavelength in the material. Near resonance, however, the solution completely breaks down. In the NRW algorithm the reflection coefficient

$$\Gamma_1 = X \pm \sqrt{X^2 - 1} \tag{2.40}$$

is given explicitly in terms of the scattering parameters where

$$X = \frac{1 - V_1 V_2}{V_1 - V_2} , \tag{2.41}$$

and

$$V_1 = S_{21} + S_{11} , \tag{2.42}$$

$$V_2 = S_{21} - S_{11} . \tag{2.43}$$

Note that in the Nicolson-Ross solution the S-parameters must be rotated to the plane of the sample faces in order for the correct group delay to be calculated. The correct root is chosen in eq (2.40) by requiring $|\Gamma_1| \leq 1$. The transmission coefficient Z_1 for the NRW procedure is given by

$$Z_1 = \frac{S_{11} + S_{21} - \Gamma_1}{1 - (S_{11} + S_{21})\Gamma_1} . \tag{2.44}$$

If we define

$$\frac{1}{\Lambda^2} = -[\frac{1}{2\pi L}\ln(\frac{1}{Z_1})]^2 \ , \tag{2.45}$$

then we can solve for the permeability

$$\mu_R^* = \frac{1+\Gamma_1}{(1-\Gamma_1)\Lambda\sqrt{\frac{1}{\lambda_0^2}-\frac{1}{\lambda_c^2}}} \ , \tag{2.46}$$

where λ_0 is the free space wavelength and λ_c is the cutoff wavelength. The permittivity is given by

$$\epsilon_R^* = \frac{\lambda_0^2}{\mu_R^*}[\frac{1}{\lambda_c^2} - [\frac{1}{2\pi L}\ln(\frac{1}{Z_1})]^2] \ . \tag{2.47}$$

Equation (2.45) has an infinite number of roots for magnetic materials, since the logarithm of a complex number is multi-valued. In order to pick out the correct root it is necessary to compare the measured group delay to the calculated group delay. The calculated group delay is related to the change of the wave number k with respect to the angular frequency

$$\tau_{calc.group} =$$

$$-L\frac{d}{df}\sqrt{\frac{\epsilon_R^*\mu_R^* f^2}{c^2} - \frac{1}{\lambda_c^2}} \tag{2.48}$$

$$= -\frac{1}{c^2}\frac{f\epsilon_R^*\mu_R^* + f^2\frac{1}{2}\frac{d(\epsilon_R^*\mu_R^*)}{df}}{\sqrt{\frac{\epsilon_R^*\mu_R^* f^2}{c^2} - \frac{1}{\lambda_c^2}}}L \ . \tag{2.49}$$

The measured group delay is

$$\tau_{meas.group} = \frac{1}{2\pi}\frac{d\phi}{df} \ , \tag{2.50}$$

where ϕ is the phase of Z_1. To determine the correct root, the calculated group delays are found from eq (2.49) for various values of n in the logarithm term in eq (2.45), where $\ln Z = \ln|Z| + j(\theta + 2\pi n)$, where $n = 0, \pm 1, \pm 2, ...$ The calculated and measured group delays are compared to yield the correct value of n. Many researchers think of the NRW solution as an explicit solution; however, due to the phase ambiguity, it is not in the strict sense. Where there is no loss in the sample under test, the NRW solution is divergent at integral multiples of one-half wavelength in the sample. This occurs because the phase of S_{11} cannot be accurately measured for small $|S_{11}|$. Also in this limit both of the scattering equations reduce to the relation $Z^2 \rightarrow 1$, which is only a relation for the phase velocity and

therefore solutions for ϵ_R^* and μ_R^* are not separable. This singular behavior can be minimized in cases where permeability is known *a priori*, as shown in previous work performed by Baker-Jarvis [26].

For magnetic materials there are other methods for solution of the S-parameter equations. In the next section we will describe various solution procedures.

2.2.2 2-Port Solution Where Position is Determined Solely by $L_{airline}$ and L

In order to obtain both the permittivity and the permeability from the S-parameter relations, it is necessary to have at least two independent measurements. These independent measurements could be two samples of different lengths, it could be a full 2-port measurement, or it could be a 1-port SCL measurement of the sample in two different positions in the line. In the full S-parameter solution we solve equations that are invariant to reference planes for ϵ and μ. A set of equations for single-sample magnetic measurements is

$$S_{11}S_{22} - S_{21}S_{12} = \exp\{-2\gamma_0(L_{air} - L)\}\frac{\Gamma^2 - Z^2}{1 - \Gamma^2 Z^2}\ , \tag{2.51}$$

$$(S_{21} + S_{12})/2 = \exp\{-\gamma_0(L_{air} - L)\}\frac{Z(1 - \Gamma^2)}{1 - \Gamma^2 Z^2}\ . \tag{2.52}$$

Equation (2.51) is the determinant of the scattering matrix.

Iterative Solution

Equations (2.51) and (2.52) can be solved iteratively or by a technique similar to the NRW technique. In an iterative approach, Newton's numerical method for root determination works quite well. To solve the system it is best to separate the system into four real equations. The iterative solution works well if good initial guesses are available.

Explicit Solution

It is also possible to obtain an explicit solution to eqs (2.51) and (2.52). Let $x = (S_{21}S_{12} - S_{11}S_{22})\exp\{2\gamma_0(L_{air} - L)\}$ and $y = \{(S_{21} + S_{12})/2\}\exp\{\gamma_0(L_{air} - L)\}$, then it can be shown that the physical roots for the transmission coefficient are

$$Z = \frac{x+1}{2y} \pm \sqrt{\left(\frac{x+1}{2y}\right)^2 - 1}\ . \tag{2.53}$$

The reflection coefficient is

$$\Gamma_2 = \pm\sqrt{\frac{x - Z^2}{xZ^2 - 1}} \ . \tag{2.54}$$

The ambiguity in the plus-or-minus sign in eq (2.54) can be resolved by considering the reflection coefficient calculated from S_{11} alone

$$\Gamma_3 = \frac{\alpha(Z^2 - 1) \pm \sqrt{\alpha^2 Z^4 + 2Z^2(2S_{11} - \alpha^2) + \alpha^2}}{2S_{11}Z^2} \ , \tag{2.55}$$

where $\alpha = \exp(-2\gamma_0 L_1)$. The correct root for Γ_3 is picked by requiring $|\Gamma_3| \leq 1$. Note that an estimate of L_1 is needed in eq (2.55). If Γ_2 is compared with Γ_3 then the plus-or-minus sign ambiguity in eq (2.54) can be resolved and therefore Γ_2 is determined. The permeability and permittivity are then

$$\mu_R^* = -\frac{1 + \Gamma_2}{1 - \Gamma_2}\frac{1}{\gamma_0 L}(\ln Z + 2\pi jn) \ , \tag{2.56}$$

$$\epsilon_R^* = \frac{c^2}{\omega^2}[(\frac{2\pi}{\lambda_c})^2 - \frac{1}{L^2}(\ln Z + 2\pi jn)^2]/\mu_R^* \ . \tag{2.57}$$

The correct value of n is picked using the group delay comparison as described in the Nicolson-Ross-Weir technique. At low frequencies the correct roots are more easily identified since they are more widely spaced.

2.2.3 Two Samples of Different Length

Solutions for the material parameters exist when scattering parameters on two samples of differing lengths are measured. Let us consider two samples, one of length L and one of length $\alpha_1 L$ as indicated in figure 2.2.

For independent measurements on two samples where $|S_{21}| > -50dB$ over the frequency band of interest we use only S_{21} measurements. The measurements obtained on the two samples are designated as $S_{21(1)}$ and $S_{21(2)}$ for first and second measurements:

$$S_{21(1)} = \exp\{-\gamma_0(L_{air} - L)\}\frac{Z(1 - \Gamma^2)}{1 - Z^2\Gamma^2} \ , \tag{2.58}$$

$$S_{21(2)} = \exp\{-\gamma_0(L_{air} - \alpha_1 L)\}\frac{Z^{\alpha_1}(1 - \Gamma^2)}{1 - Z^{2\alpha_1}\Gamma^2} \ , \tag{2.59}$$

where

$$Z = \exp(-\gamma L) \ , \tag{2.60}$$

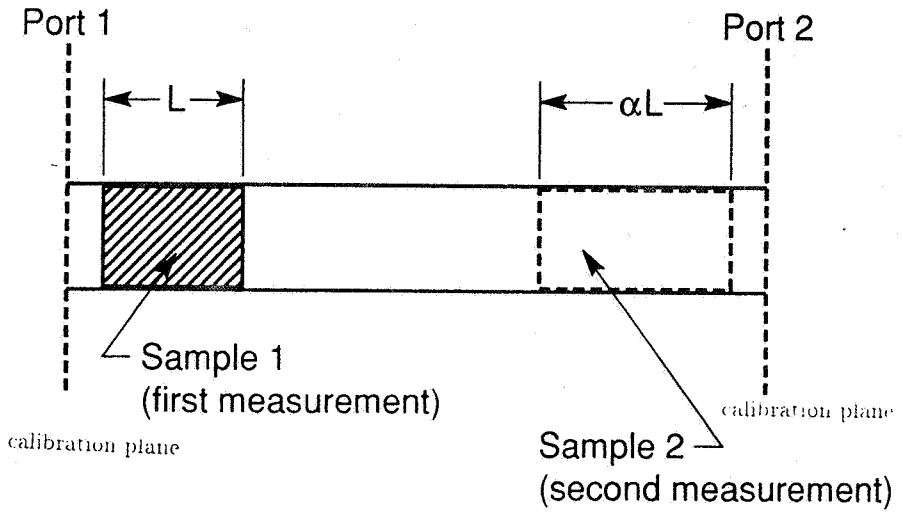

Figure 2.2: A dielectric sample in a transmission line for two sample magnetic measurements

and

$$Z^{\alpha_1} = \exp(-\alpha_1 \gamma L) \ . \tag{2.61}$$

The reflection coefficient is given by eq (2.37). Equations (2.58) and (2.59) can be solved iteratively for ϵ_R^* and μ_R^*.

This solution is unstable for low-loss materials at certain frequencies if the sample lengths, L and $\alpha_1 L$, are related so that both materials resonate at a certain frequency simultaneously. Also with this technique two-sample length measurements are required, and this increases the uncertainty.

2.3 Measurement Results

The measurement consists of inserting a well-machined sample into a coaxial line or waveguide and measuring the scattering parameters. For waveguide measurements it is important to have a section of waveguide of length about two free space wavelengths between the coax-to waveguide adapter and the sample holder. This acts as a mode filter for filtering out higher evanescent modes. There are many roots to the equations for the permeability and permittivity and caution must be exercised when selecting out the correct root. At lower frequencies ($<$ 1 GHz) the roots are usually more widely spaced and therefore root selection is simplified. Another approach to root selection is the measurement of two samples of differing lengths where the results compared to determine the correct root.

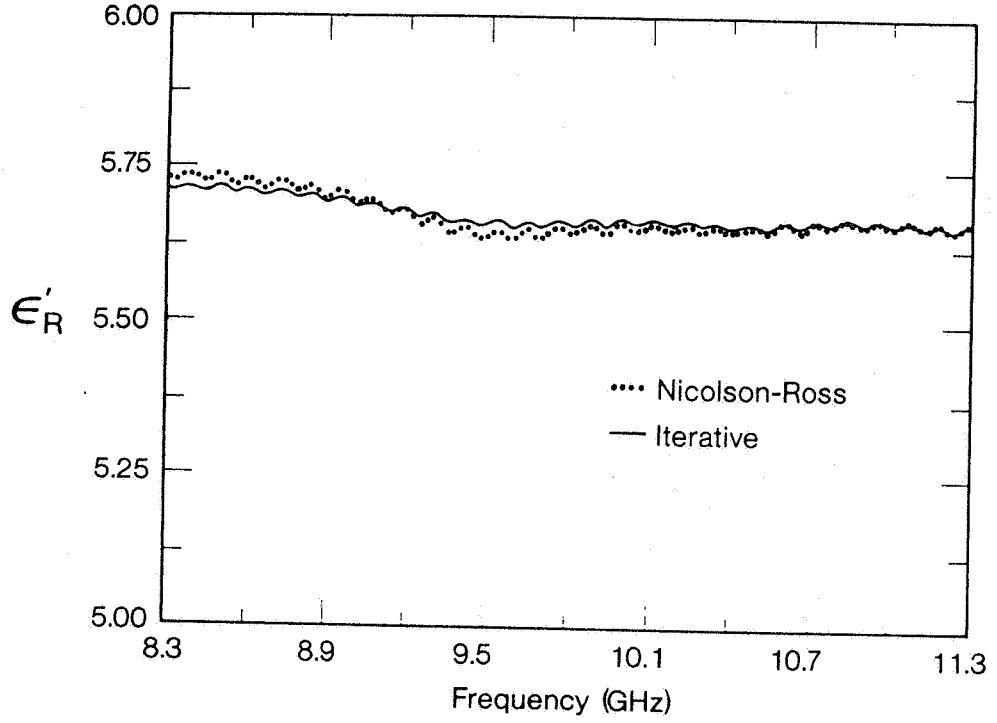

Figure 2.3: ϵ'_R of a loaded polymer in a X-band waveguide with the full S-parameter iterative technique.

2.3.1 Measurements without Gap Corrections

Various measurements have been made in waveguide and coaxial line. Some of the results of these measurements are reported in figures 2.3 through 2.14 for the full S-parameter technique and in figures 2.15 and 2.16 for the two-sample length method. The measurements reported in this section are not corrected for gaps around the sample. The effect of the air gaps is to measure values of the material parameters that are lower than the actual values. In the next section we will discuss ways of mitigating the effects of air gaps.

2.3.2 Effects of Gaps between Sample and Waveguide

Gaps between the sample holder and sample either may be corrected with the formulas given in the appendix or a conducting paste can be applied to the external surfaces of the sample that are in contact with the sample holder before insertion into the sample holder. In figure 2.17 we show a measurement of a nickel-zinc ferrite with and without a gap-filling grease. The dielectric loss factor is increased slightly by the gap filling. We suspect that part of this increase is due to the finite conductivity of the conducting grease.

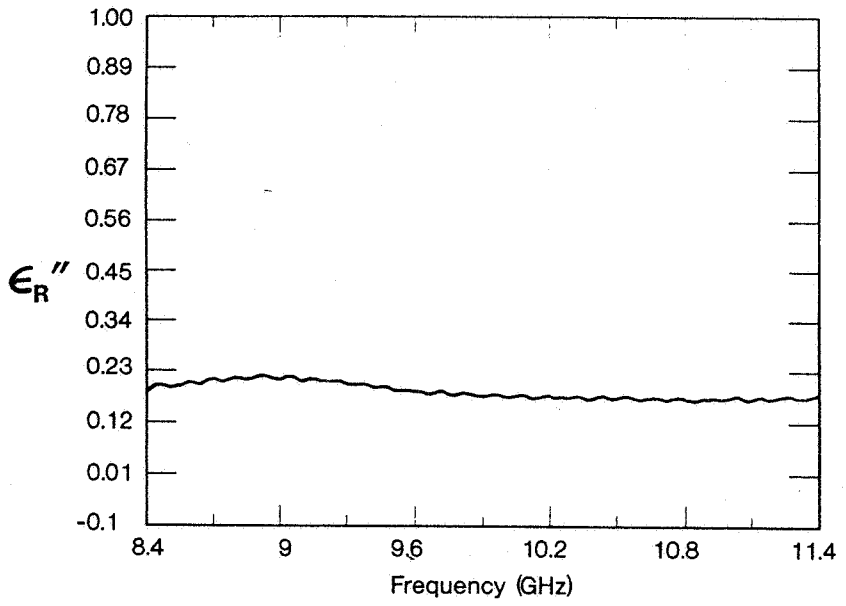

Figure 2.4: ϵ_R'' of a loaded polymer in a X- band waveguide with the full S-parameter iterative technique.

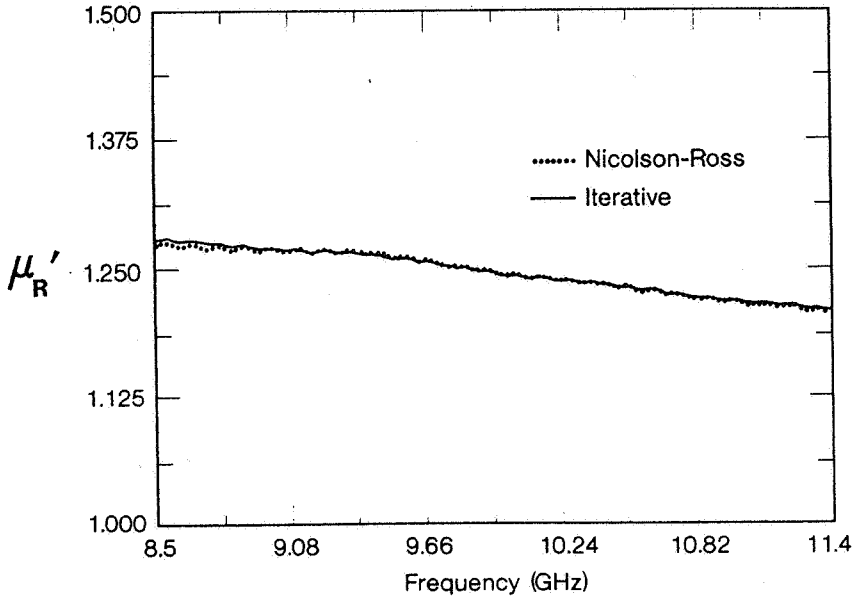

Figure 2.5: μ_R' of a loaded polymer in a X-band waveguide with the full S-parameter iterative technique.

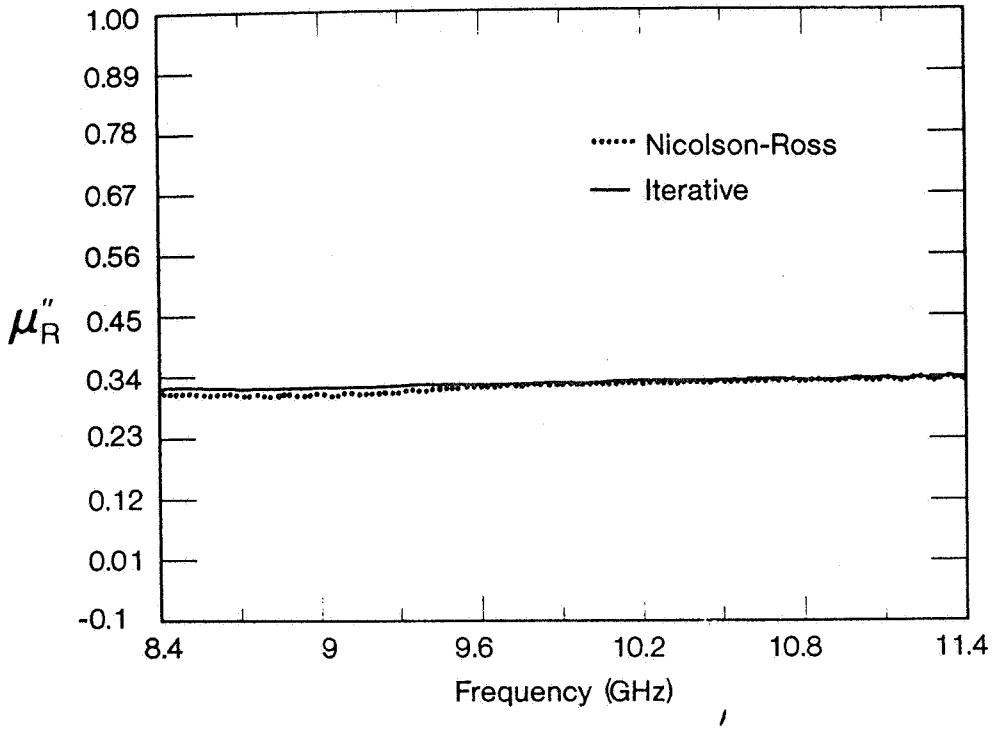

Figure 2.6: μ''_R of a loaded polymer in a X-band waveguide with the full S-parameter iterative technique.

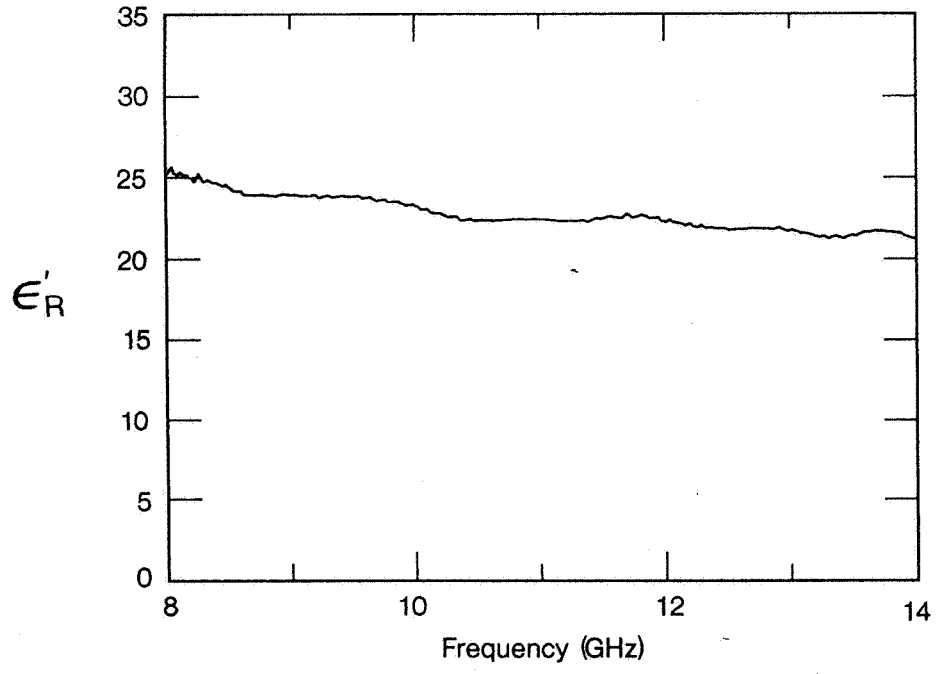

Figure 2.7: ϵ'_R of a ferrite in a X-band waveguide with the full S-parameter iterative technique.

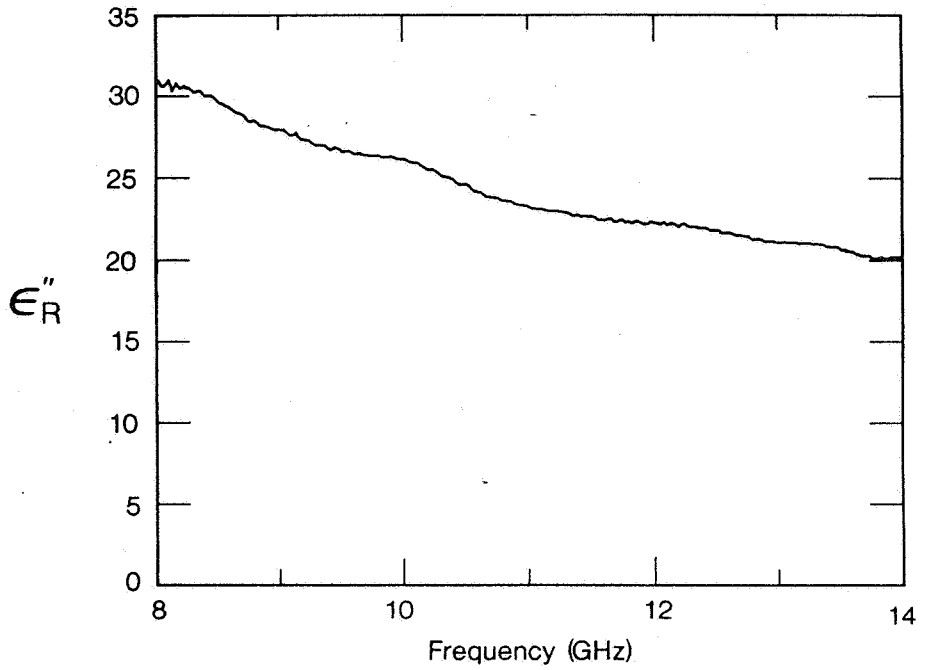

Figure 2.8: ϵ''_R of a ferrite in a X-band waveguide with the full S-parameter iterative technique.

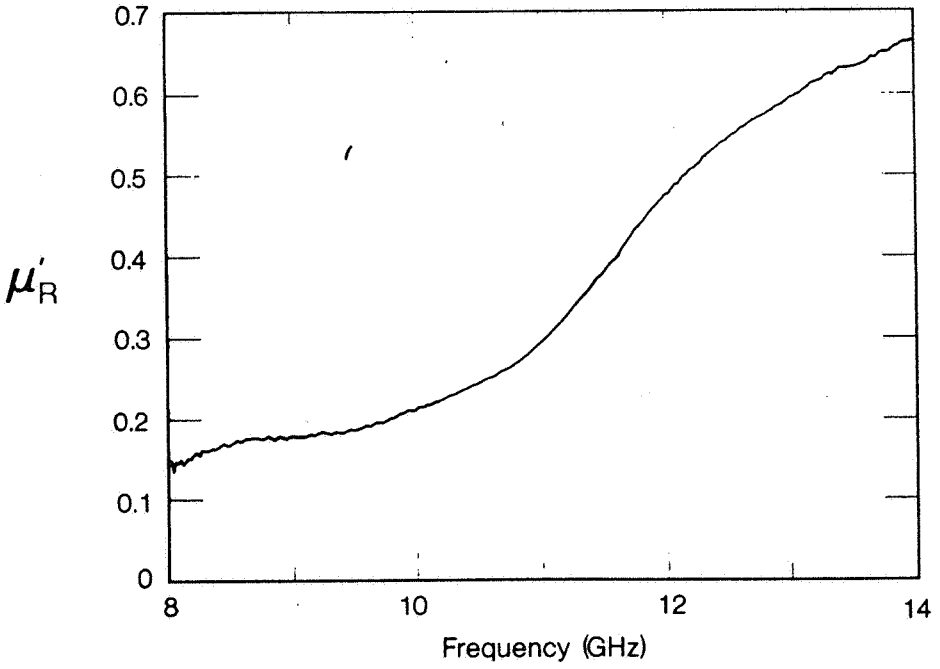

Figure 2.9: μ'_R of a ferrite in a X-band waveguide with the full S-parameter iterative technique.

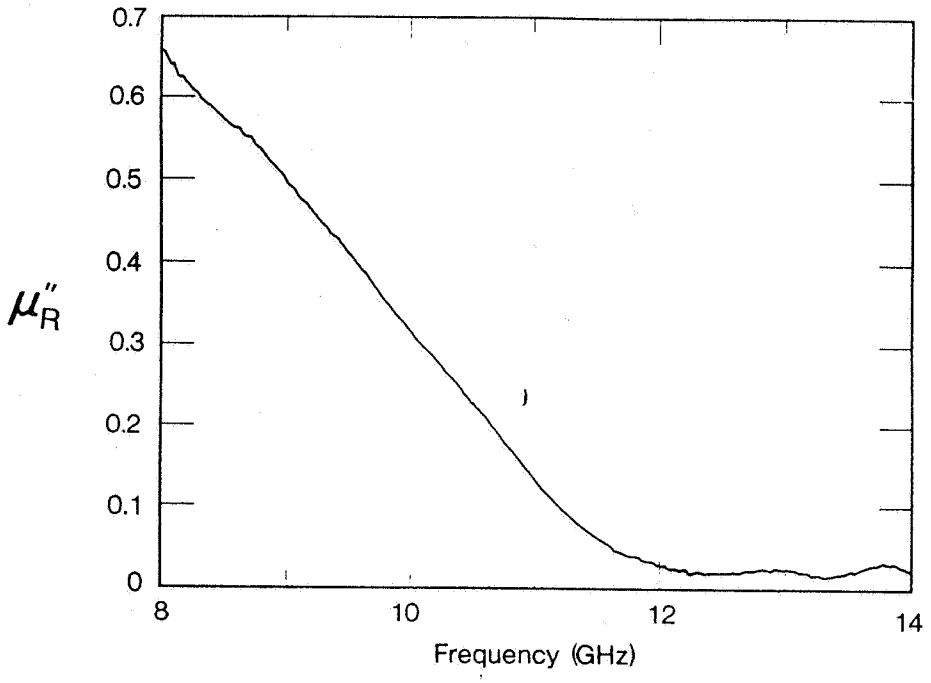

Figure 2.10: μ''_R of a ferrite in a X-band waveguide with the full S-parameter iterative technique.

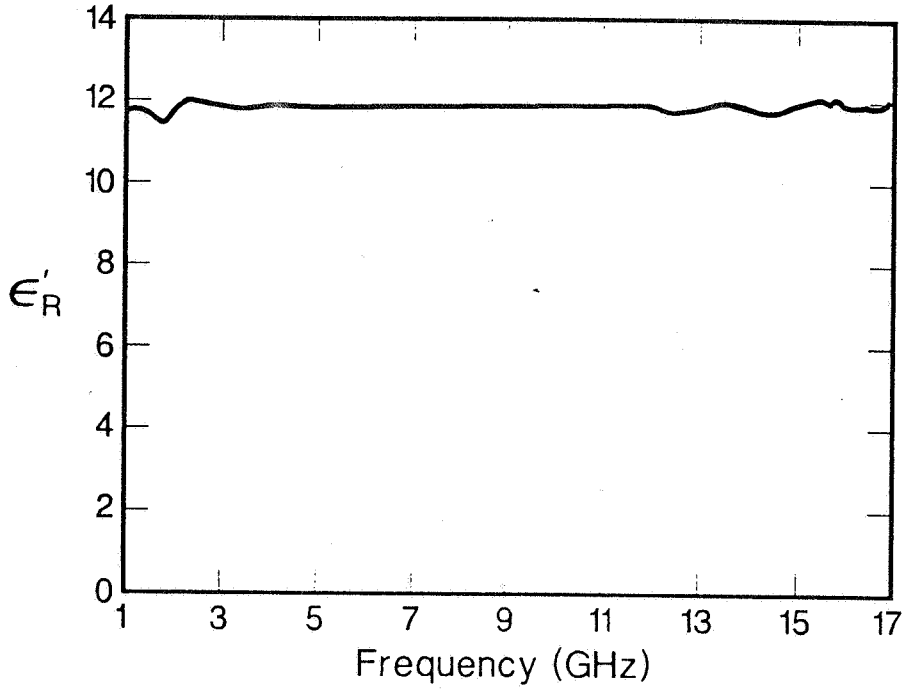

Figure 2.11: ϵ'_R of a loaded polymer in coaxial line with the full S-parameter iterative technique.

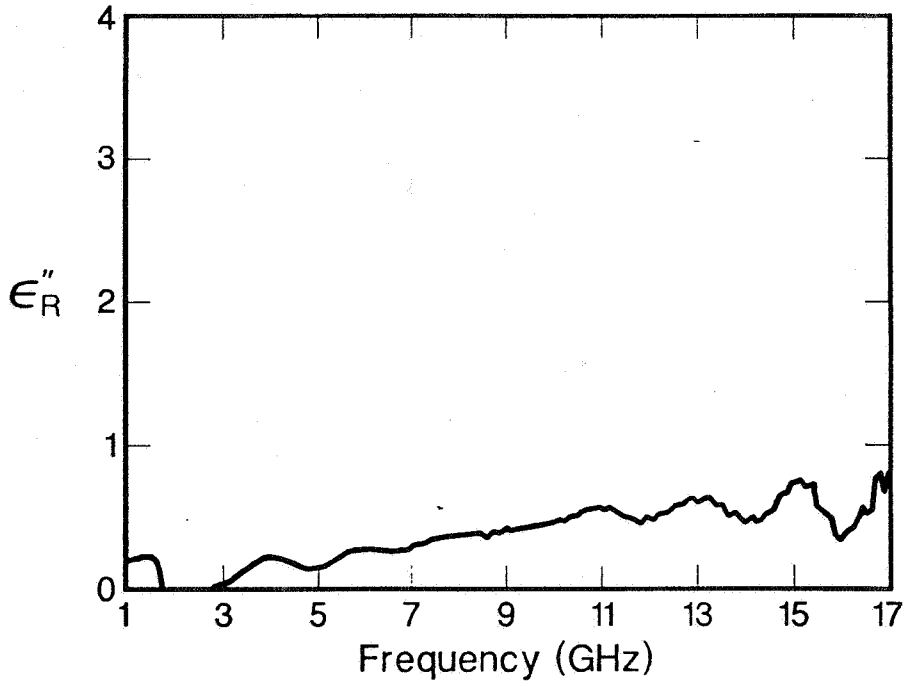

Figure 2.12: ϵ''_R of a loaded polymer in coaxial line the full S-parameter iterative technique.

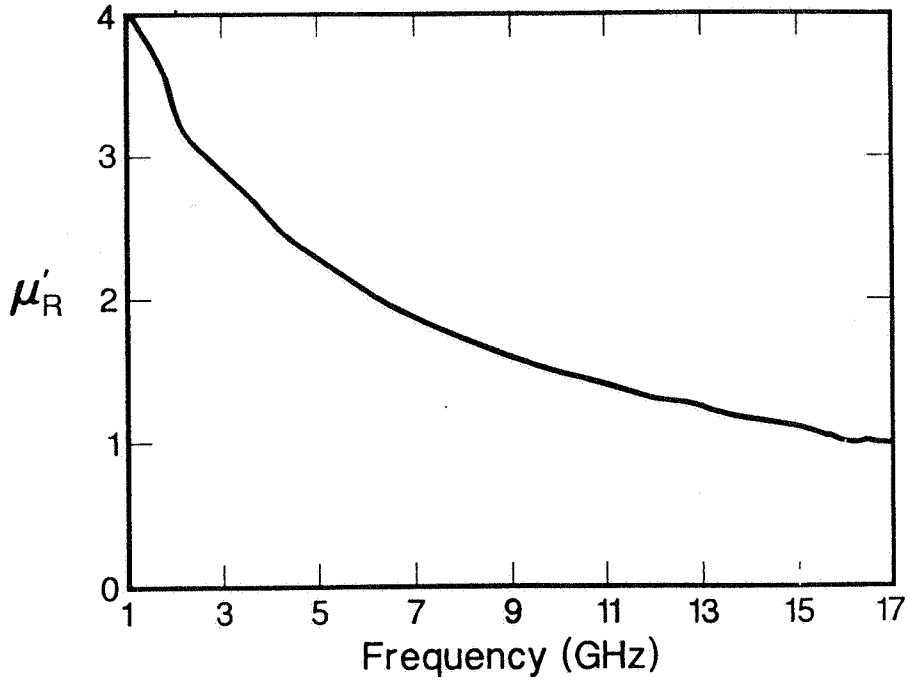

Figure 2.13: μ'_R of a loaded polymer in coaxial line with the full S-parameter iterative technique.

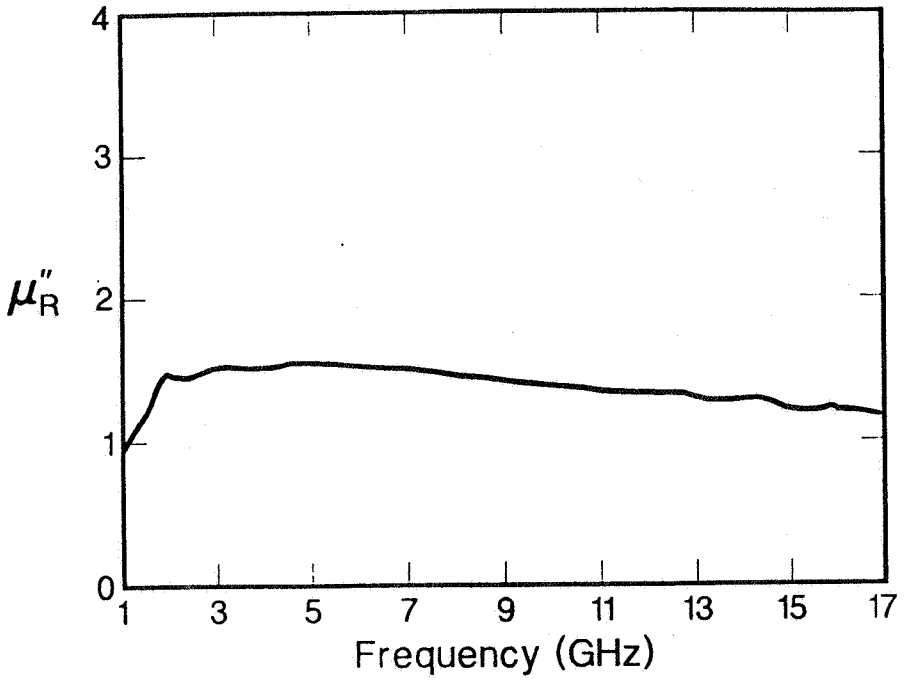

Figure 2.14: μ''_R of a loaded polymer in coaxial line with the full S-parameter iterative technique.

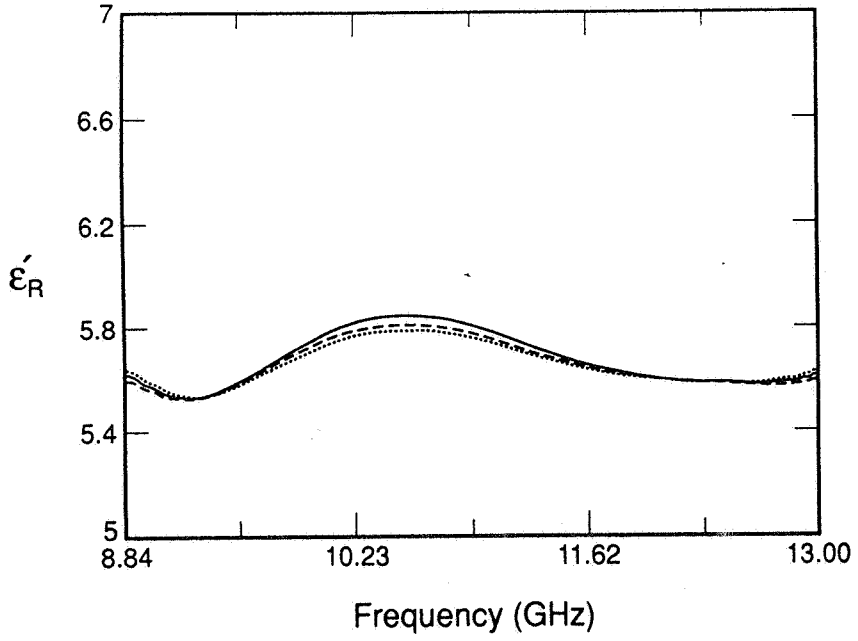

Figure 2.15: ϵ'_R of a loaded polymer in a X-band waveguide with TR method for two sample technique, for three different samples.

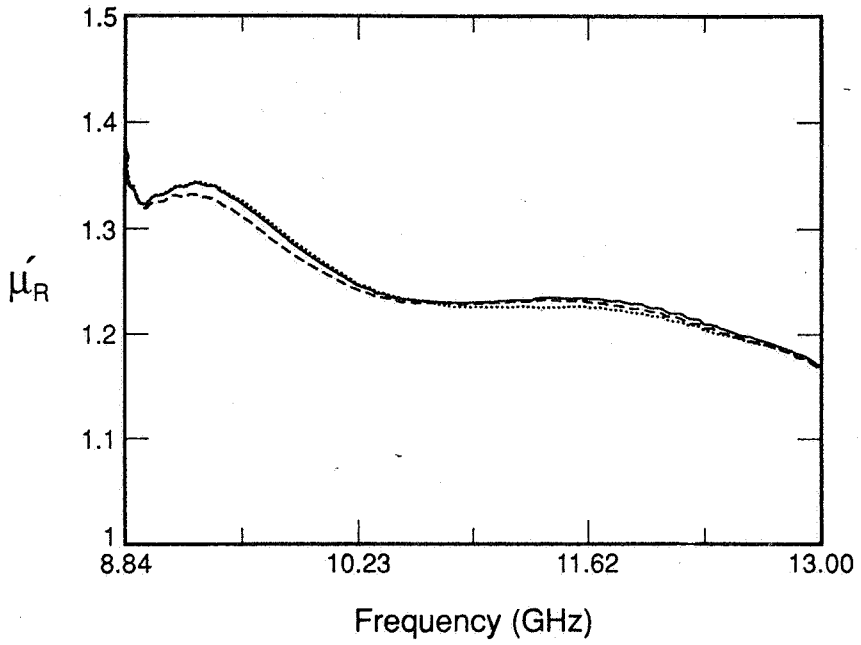

Figure 2.16: μ'_R of a loaded polymer in a X-band waveguide with TR method for two sample technique, for three different samples.

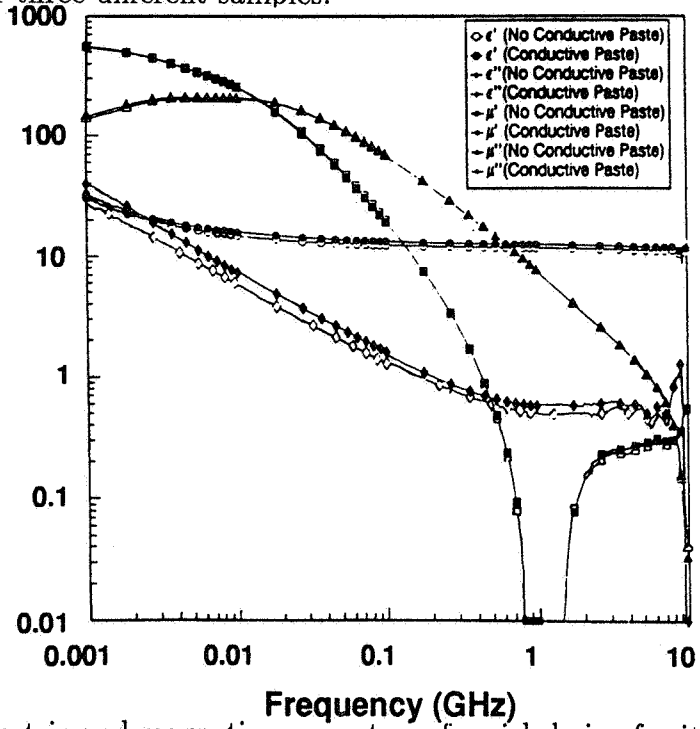

Figure 2.17: The dielectric and magnetic parameters of a nickel-zinc ferrite in a coaxial line from 1 MHz to 10 GHz with the full S-parameter iterative technique.

2.4 Permeameter

In the past permeameters have been used for high permeability materials. Rasmussen [29], Hoer [30], Powell [31], and Goldfarb [32] have all described various permeameter setups. In this section we wish to review the theory behind the permeameter.

If a toroidal sample is inserted into an azimuthal magnetic field region, the inductance is changed. If the inductance of the empty sample holder is compared to the inductance of the filled holder then it is possible to extract the complex permeability of the material.

Consider a toroid of inner diameter a and outer diameter b and height h. The material contributes an inductance of [32]

$$L_m = \frac{\mu' h \ln(b/a)}{2\pi} , \tag{2.62}$$

and the inductance of the air space is

$$L_a = \frac{\mu_0 h \ln(b/a)}{2\pi} . \tag{2.63}$$

The net change in the sample inductance when the sample is inserted into the holder is

$$\Delta L = L_m - L_a , \tag{2.64}$$

and therefore

$$\mu'_R = 1 + \frac{2\pi \Delta L}{\mu_0 h \ln(b/a)} . \tag{2.65}$$

The magnetic loss may be obtained from consideration of the core loss ΔR or resistance

$$\mu''_R = \frac{\Delta R}{\mu_0 f h \ln(b/a)} . \tag{2.66}$$

These equations are a special case of the scattering equations for short-circuit line (see eq (4.7)) in the limit as $\omega \rightarrow 0$ and through use of relation $H_\phi = E_\rho / Z$.

2.5 Uncertainty of Combined Permittivity and Permeability Determination

In this section an uncertainty analysis is presented. The sources of error in the permeability and permittivity TR measurement include

- Errors in measuring the magnitude and phase of the scattering parameters,
- Gaps between the sample and sample holder,
- Sample holder dimensional variations,
- Uncertainty in sample length,
- Line losses and connector mismatch, and
- Uncertainty in reference plane positions.

A technique for correcting errors arising from gaps around the sample is given in Appendix B [33,34,35]. Gaps between holder and sample either may be corrected using the formulas given in the appendix or conducting liquid solder can be painted on the external surfaces of the sample that are in contact with the sample holder before insertion into the sample holder, thereby minimizing gap problems. The formulas given in the literature generally under-correct for the real part of the permittivity and over-correct for the imaginary part of the permittivity. We assume that all measurements of permittivity have been corrected for air gaps around the sample before the uncertainty analysis is applied. In order to evaluate the uncertainty introduced by the measured scattering parameters and sample dimensions, a differential uncertainty analysis is assumed applicable with the uncertainty due to S_{11} and S_{21} evaluated separately. We assume that the S-parameters are functions of $S_{ij}(|S_{11}|, |S_{21}|, \theta_{11}, \theta_{21}, L, d)$. We assume that the total uncertainty in ϵ'_R, where d is the air gap between the sample and waveguide. We assume that the uncertainties for the physically measured parameters are

$$\frac{\Delta\epsilon'_R}{\epsilon'_R} = \frac{1}{\epsilon'_R}\sqrt{\sum_\alpha \left[\left(\frac{\partial\epsilon'_R}{\partial|S_\alpha|}\Delta|S_\alpha|\right)^2 + \left(\frac{\partial\epsilon'_R}{\partial\theta_\alpha}\Delta\theta_\alpha\right)^2\right] + \left(\frac{\partial\epsilon'_R}{\partial L}\Delta L\right)^2 + \left(\frac{\partial\epsilon'_R}{\partial d}\Delta d\right)^2}, \quad (2.67)$$

$$\frac{\Delta\epsilon''_R}{\epsilon''_R} = \frac{1}{\epsilon''_R}\sqrt{\sum_\alpha \left[\left(\frac{\partial\epsilon''_R}{\partial|S_\alpha|}\Delta|S_\alpha|\right)^2 + \left(\frac{\partial\epsilon''_R}{\partial\theta_\alpha}\Delta\theta_\alpha\right)^2\right] + \left(\frac{\partial\epsilon''_R}{\partial L}\Delta L\right)^2 + \left(\frac{\partial\epsilon''_R}{\partial d}\Delta d\right)^2}, \quad (2.68)$$

where $\alpha = 11$ or 21, $\Delta\theta$ is the uncertainty in the phase of the scattering parameter, $\Delta|S_\alpha|$ is the uncertainty in the magnitude of the scattering parameter, Δd is the uncertainty in the air gap around the sample, and ΔL is the uncertainty in the sample length. The derivatives with respect to air gap, $\partial\epsilon'_R/\partial d$, have been presented previously [26]. The uncertainties used for the S-parameters depend on the specific ANA used for the measurements. This type of uncertainty analysis assumes that changes in independent variables are sufficiently small so that a Taylor series expansion is valid. Of course there are many other uncertainty sources of lesser magnitude such as repeatability of connections and torquing of flange bolts. Estimates for these uncertainties could be added to the uncertainty budget.

2.5.1 One Sample at One Position

For the uncertainty analysis it is necessary to take implicit derivatives of the S-parameter equations with respect to the assumed independent parameters. It is assumed that the functions are analytic over the region of interest with respect to the differentiation variables. The independent variables are assumed to be $|S_{21}|$, $|S_{11}|$, θ_{11}, θ_{21}, and L. The derivatives of the S-parameter eqs (2.31) through (2.33) can be found analytically

$$\frac{\partial S_{11}}{\partial Z}\left[\frac{\partial Z}{\partial \epsilon_R^*}\frac{\partial \epsilon_R^*}{\partial |S_{11}|} + \frac{\partial Z}{\partial \mu_R^*}\frac{\partial \mu_R^*}{\partial |S_{11}|}\right] + \frac{\partial S_{11}}{\partial \Gamma}\left[\frac{\partial \Gamma}{\partial \epsilon_R^*}\frac{\partial \epsilon_R^*}{\partial |S_{11}|} + \frac{\partial \Gamma}{\partial \mu_R^*}\frac{\partial \mu_R^*}{\partial |S_{11}|}\right] = \exp(j\theta_{11}) , \quad (2.69)$$

$$\frac{\partial S_{11}}{\partial Z}\left[\frac{\partial Z}{\partial \epsilon_R^*}\frac{\partial \epsilon_R^*}{\partial |S_{21}|} + \frac{\partial Z}{\partial \mu_R^*}\frac{\partial \mu_R^*}{\partial |S_{21}|}\right] + \frac{\partial S_{11}}{\partial \Gamma}\left[\frac{\partial \Gamma}{\partial \epsilon_R^*}\frac{\partial \epsilon_R^*}{\partial |S_{21}|} + \frac{\partial \Gamma}{\partial \mu_R^*}\frac{\partial \mu_R^*}{\partial |S_{21}|}\right] = 0 , \quad (2.70)$$

$$\frac{\partial S_{21}}{\partial Z}\left[\frac{\partial Z}{\partial \epsilon_R^*}\frac{\partial \epsilon_R^*}{\partial |S_{11}|} + \frac{\partial Z}{\partial \mu_R^*}\frac{\partial \mu_R^*}{\partial |S_{11}|}\right] + \frac{\partial S_{21}}{\partial \Gamma}\left[\frac{\partial \Gamma}{\partial \epsilon_R^*}\frac{\partial \epsilon_R^*}{\partial |S_{11}|} + \frac{\partial \Gamma}{\partial \mu_R^*}\frac{\partial \mu_R^*}{\partial |S_{11}|}\right] = 0 , \quad (2.71)$$

$$\frac{\partial S_{21}}{\partial Z}\left[\frac{\partial Z}{\partial \epsilon_R^*}\frac{\partial \epsilon_R^*}{\partial |S_{21}|} + \frac{\partial Z}{\partial \mu_R^*}\frac{\partial \mu_R^*}{\partial |S_{21}|}\right] + \frac{\partial S_{21}}{\partial \Gamma}\left[\frac{\partial \Gamma}{\partial \epsilon_R^*}\frac{\partial \epsilon_R^*}{\partial |S_{21}|} + \frac{\partial \Gamma}{\partial \mu_R^*}\frac{\partial \mu_R^*}{\partial |S_{21}|}\right] = \exp(j\theta_{21}) . \quad (2.72)$$

We can rewrite eq (2.69) - (2.72) as

$$\underbrace{\left(\frac{\partial S_{11}}{\partial Z}\frac{\partial Z}{\partial \epsilon_R^*} + \frac{\partial S_{11}}{\partial \Gamma}\frac{\partial \Gamma}{\partial \epsilon_R^*}\right)}_{A}\frac{\partial \epsilon_R^*}{\partial |S_{11}|} + \underbrace{\left(\frac{\partial S_{11}}{\partial Z}\frac{\partial Z}{\partial \mu_R^*} + \frac{\partial S_{11}}{\partial \Gamma}\frac{\partial \Gamma}{\partial \mu_R^*}\right)}_{B}\frac{\partial \mu_R^*}{\partial |S_{11}|} = \exp(j\theta_{11}) , \quad (2.73)$$

$$\underbrace{\left(\frac{\partial S_{11}}{\partial Z}\frac{\partial Z}{\partial \epsilon_R^*}+\frac{\partial S_{11}}{\partial \Gamma}\frac{\partial \Gamma}{\partial \epsilon_R^*}\right)}_{A}\frac{\partial \epsilon_R^*}{\partial |S_{21}|}+$$
$$\underbrace{\left(\frac{\partial S_{11}}{\partial Z}\frac{\partial Z}{\partial \mu_R^*}+\frac{\partial S_{11}}{\partial \Gamma}\frac{\partial \Gamma}{\partial \mu_R^*}\right)}_{B}\frac{\partial \mu_R^*}{\partial |S_{21}|}=0\ , \tag{2.74}$$

$$\underbrace{\left(\frac{\partial S_{21}}{\partial Z}\frac{\partial Z}{\partial \epsilon_R^*}+\frac{\partial S_{21}}{\partial \Gamma}\frac{\partial \Gamma}{\partial \epsilon_R^*}\right)}_{C}\frac{\partial \epsilon_R^*}{\partial |S_{11}|}+$$
$$\underbrace{\left(\frac{\partial S_{21}}{\partial Z}\frac{\partial Z}{\partial \mu_R^*}+\frac{\partial S_{21}}{\partial \Gamma}\frac{\partial \Gamma}{\partial \mu_R^*}\right)}_{D}\frac{\partial \mu_R^*}{\partial |S_{11}|}=0\ , \tag{2.75}$$

$$\underbrace{\left(\frac{\partial S_{21}}{\partial Z}\frac{\partial Z}{\partial \epsilon_R^*}+\frac{\partial S_{21}}{\partial \Gamma}\frac{\partial \Gamma}{\partial \epsilon_R^*}\right)}_{C}\frac{\partial \epsilon_R^*}{\partial |S_{21}|}+$$
$$\underbrace{\left(\frac{\partial S_{21}}{\partial Z}\frac{\partial Z}{\partial \mu_R^*}+\frac{\partial S_{21}}{\partial \Gamma}\frac{\partial \Gamma}{\partial \mu_R^*}\right)}_{D}\frac{\partial \mu_R^*}{\partial |S_{21}|}=\exp(j\theta_{21})\ , \tag{2.76}$$

where we have defined parameters A, B, C, and D. If we let

$$E=-\frac{\partial S_{11}}{\partial Z}\frac{\partial Z}{\partial L}\ , \tag{2.77}$$

$$F=-\frac{\partial S_{21}}{\partial Z}\frac{\partial Z}{\partial L}\ , \tag{2.78}$$

we can solve for the derivatives that have been taken with respect to the independent parameters in eqs (2.73)- (2.75):

$$\frac{\partial \epsilon_R^*}{\partial |S_{11}|}=\frac{\exp(j\theta_{11})}{[A-\frac{BC}{D}]}\ , \tag{2.79}$$

$$\frac{\partial \mu_R^*}{\partial |S_{11}|} = -\frac{C}{D}\frac{\partial \epsilon_R^*}{\partial |S_{11}|} , \tag{2.80}$$

$$\frac{\partial \epsilon_R^*}{\partial L} = \frac{BF - DE}{BC - AD} , \tag{2.81}$$

$$\frac{\partial \mu_R^*}{\partial L} = \frac{E - A\frac{\partial \epsilon_R^*}{\partial L}}{B} , \tag{2.82}$$

$$\frac{\partial \epsilon_R^*}{\partial \theta_{11}} = j|S_{11}|\frac{\partial \epsilon_R^*}{\partial |S_{11}|} , \tag{2.83}$$

$$\frac{\partial \mu_R^*}{\partial \theta_{11}} = j|S_{11}|\frac{\partial \mu_R^*}{\partial |S_{11}|} , \tag{2.84}$$

$$\frac{\partial \epsilon_R^*}{\partial \theta_{21}} = j|S_{21}|\frac{\partial \epsilon_R^*}{\partial |S_{21}|} , \tag{2.85}$$

$$\frac{\partial \mu_R^*}{\partial \theta_{21}} = j|S_{21}|\frac{\partial \mu_R^*}{\partial |S_{21}|} , \tag{2.86}$$

$$\frac{\partial S_{11}}{\partial \Gamma} = -\frac{(1+\Gamma^2 Z^2)(Z^2-1)}{(1-\Gamma^2 Z^2)^2} , \tag{2.87}$$

$$\frac{\partial S_{11}}{\partial Z} = \frac{2Z\Gamma(\Gamma^2-1)}{(1-\Gamma^2 Z^2)^2} , \tag{2.88}$$

$$\frac{\partial S_{21}}{\partial Z} = \frac{(1-\Gamma^2)(Z^2\Gamma^2+1)}{(1-\Gamma^2 Z^2)^2} , \tag{2.89}$$

$$\frac{\partial S_{21}}{\partial \Gamma} = \frac{2Z\Gamma(Z^2-1)}{(1-\Gamma^2 Z^2)^2} , \tag{2.90}$$

$$\frac{\partial \Gamma}{\partial \epsilon_R^*} = \frac{\gamma_0 \mu_R^{2*} \epsilon_0 \mu_0 \omega^2}{\gamma(\gamma+\gamma_0\mu_R^*)^2} , \tag{2.91}$$

$$\frac{\partial \Gamma}{\partial \mu_R^*} = \frac{\epsilon_R^*}{\mu_R^*}\frac{\partial \Gamma}{\partial \epsilon_R^*} + \frac{2\gamma_0\gamma}{(\gamma+\gamma_0\mu_R^*)^2} , \tag{2.92}$$

$$\frac{\partial Z}{\partial L} = -\gamma \exp(-\gamma L) , \tag{2.93}$$

$$\frac{\partial Z}{\partial \epsilon_R^*} = \frac{L\mu_R^*\omega^2\epsilon_0\mu_0}{2\gamma}\exp(-\gamma L) , \tag{2.94}$$

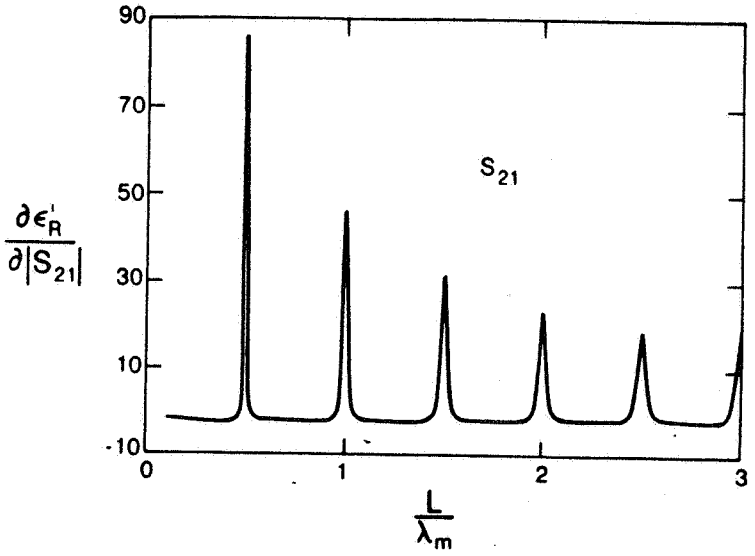

Figure 2.18: The derivative of ϵ'_R by $|S_{21}|$ vs L/λ_m with $\epsilon^*_R = (5.0, 0.02)$, $\mu^*_R = (2.0, 0.03)$.

$$\frac{\partial Z}{\partial \mu^*_R} = \frac{L\epsilon^*_R \omega^2 \epsilon_0 \mu_0}{2\gamma} \exp(-\gamma L) \; . \tag{2.95}$$

The measurement bounds for S-parameter data are obtained from specifications for a network analyzer. The dominant uncertainty is in the phase of S_{11} as $\mid S_{11} \mid \rightarrow 0$. The uncertainty in $|S_{21}|$ is relatively constant until $|S_{21}| \leq$ -50 dB, when it increases abruptly. The various derivatives are plotted in figures 2.18 through 2.27.

In figures 2.28 through 2.31 the total uncertainty in ϵ^*_R and μ^*_R computed from S_{21} and S_{11} is plotted as a function of normalized sample length. For low-loss and high-loss materials at 3 GHz with various values of ϵ^*_R and the guided wavelength in the material given by

$$\lambda_m = \frac{2\pi}{\sqrt{\omega^2 \frac{(\sqrt{\epsilon'^2 + \epsilon''^2} + \epsilon')}{2} \mu' - (\frac{2\pi}{\lambda_c})^2}} \; . \tag{2.96}$$

In figures 2.28 through 2.31 the error due to the gap correction is not included, nor are there uncertainties included for connector repeatability or flange bolt torquing. The maximum uncertainty for low-loss materials occurs at multiples of one-half wavelength. Generally, we see a decrease in uncertainty as a function of increasing sample length. Also, the uncertainties in the S-parameters have some frequency dependence with higher frequencies having larger uncertainties in phase.

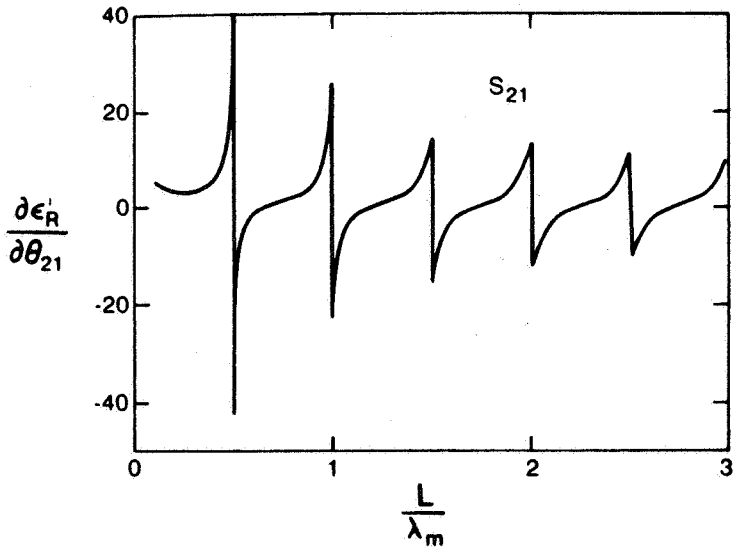

Figure 2.19: The derivative of ϵ'_R by θ_{21} using S_{21} vs L/λ_m with $\epsilon^*_R = (5.0, 0.01)$, $\mu^*_R = (2.0, 0.03)$.

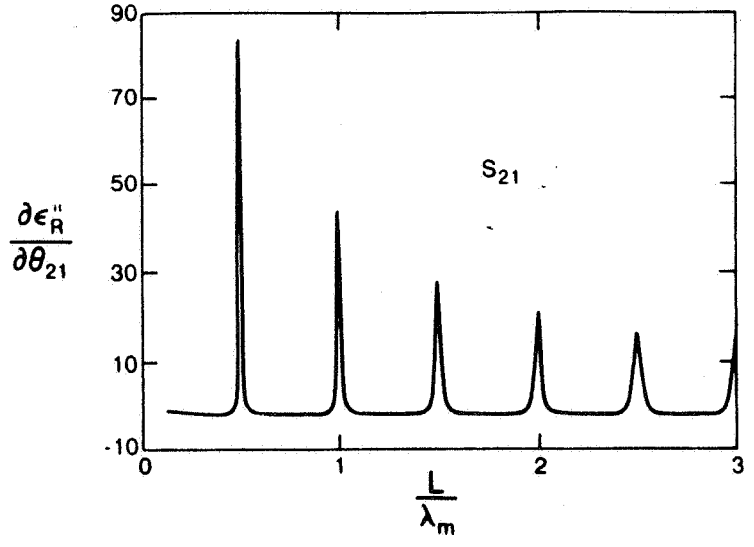

Figure 2.20: The derivative of ϵ''_R with respect to θ_{21} using S_{21} with $\epsilon^*_R = (5.0, 0.01), \mu^*_R = (2.0, 0.03)$.

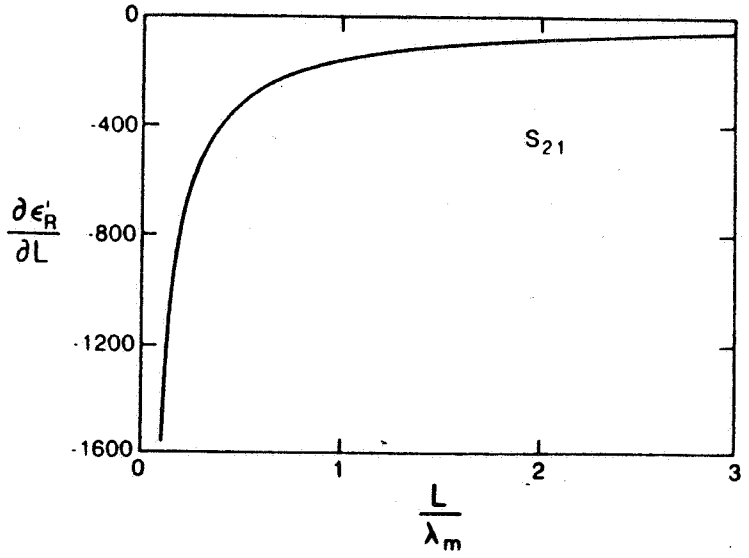

Figure 2.21: The derivative of ϵ'_R with respect to L using S_{21} with $\epsilon^*_R = (5.0, 0.01)$, $\mu^*_R = (2.0, 0.03)$.

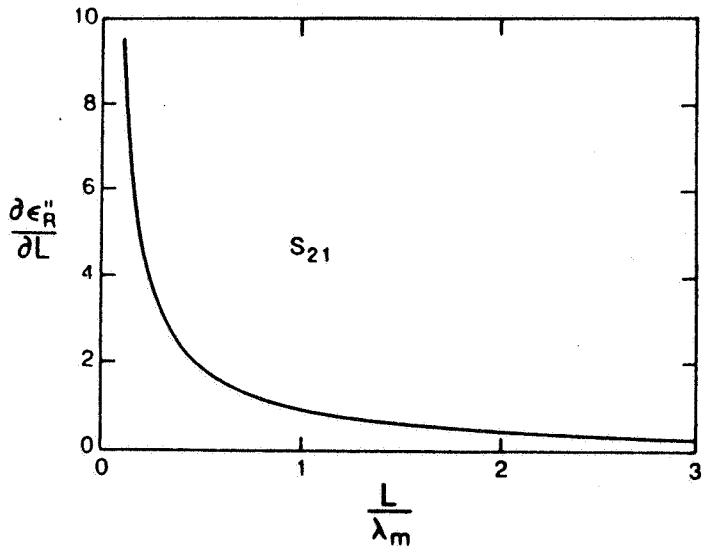

Figure 2.22: The derivative of ϵ''_R with respect to L using S_{21} with $\epsilon^*_R = (5.0, 0.01), \mu^*_R = (2.0, 0.03)$.

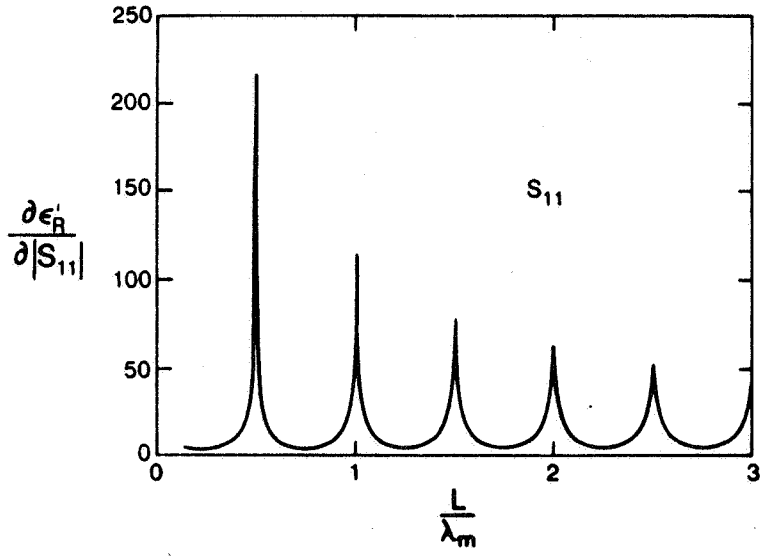

Figure 2.23: The derivative of ϵ'_R with respect to $|S_{11}|$ with $\epsilon^*_R = (5.0, 0.01), \mu^*_R = (2.0, 0.03)$.

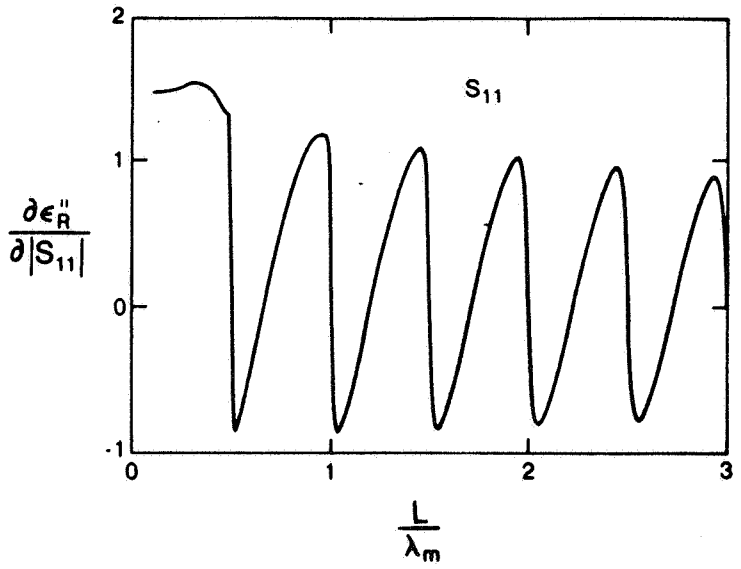

Figure 2.24: The derivative of ϵ''_R with respect to $|S_{11}|$ with $\epsilon^*_R = (5.0, 0.01), \mu^*_R = (2.0, 0.03)$.

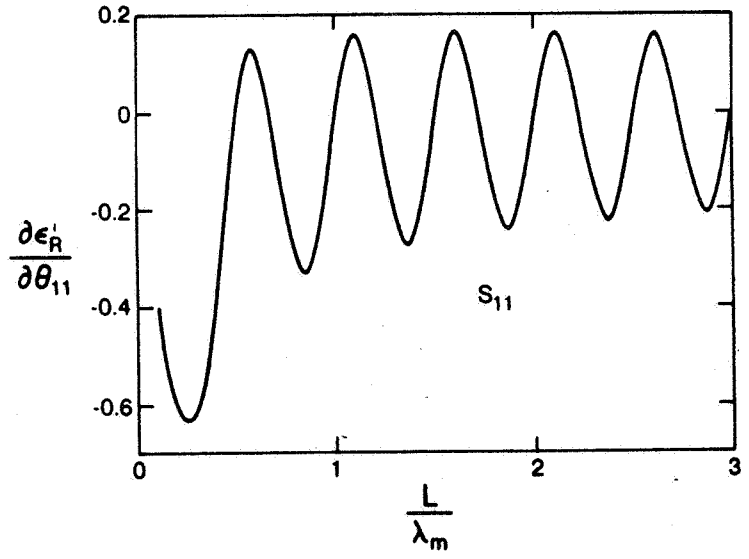

Figure 2.25: The derivative of ϵ_R' with respect to θ_{11} using S_{11} with $\epsilon_R^* = (5.0, 0.01), \mu_R^* = (2.0, 0.03)$.

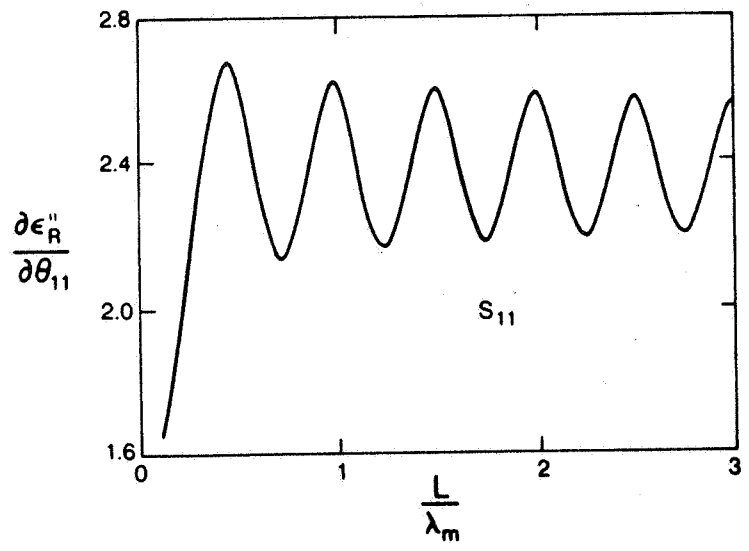

Figure 2.26: The derivative of ϵ_R'' with respect to θ_{11} using S_{11} with $\epsilon_R^* = (5.0, 0.01), \mu_R^* = (2.0, 0.03)$.

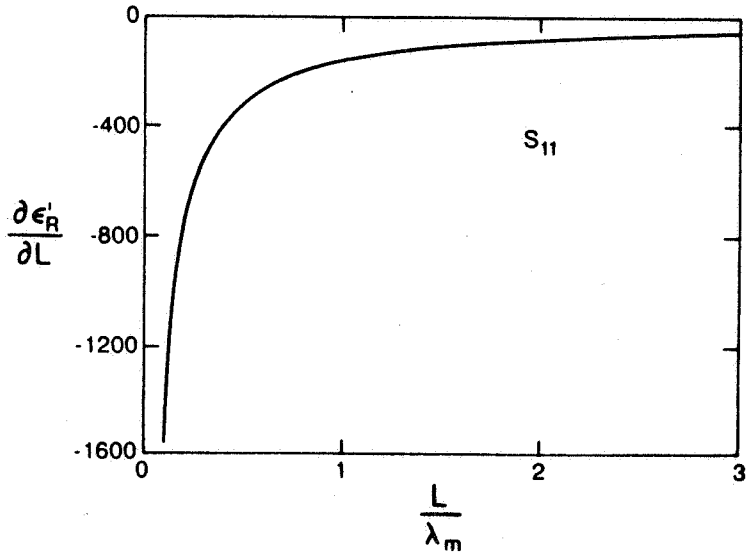

Figure 2.27: The derivative of ϵ'_R with respect to L using S_{11} with $\epsilon^*_R = (5.0, 0.01), \mu^*_R = (2.0, 0.03)$.

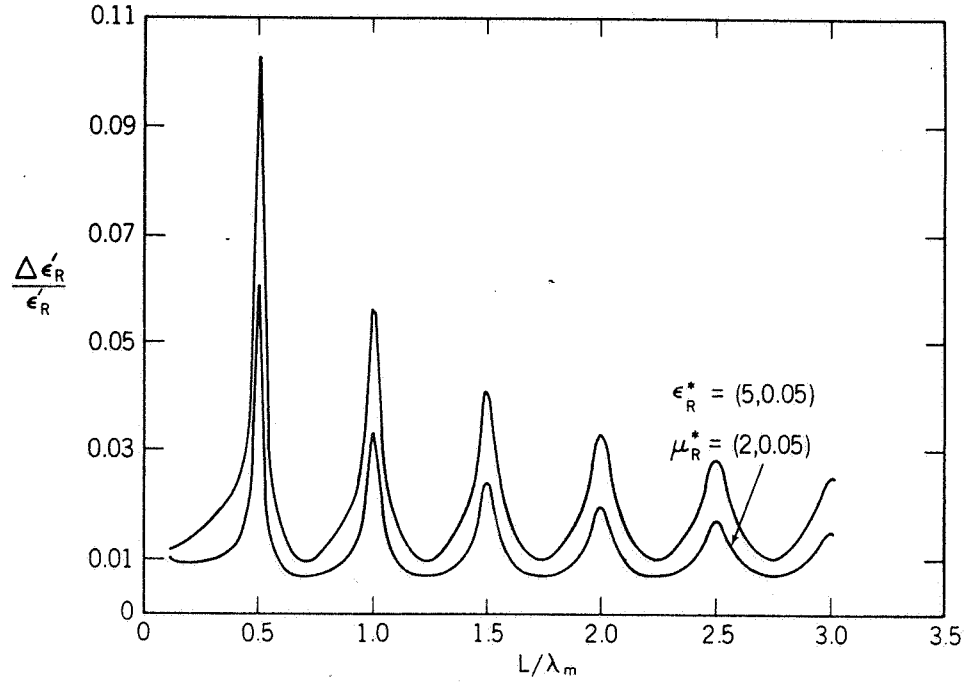

Figure 2.28: The relative uncertainty in $\epsilon'_R(\omega)$ for a low-loss material as a function of normalized length, with $\mu^*_R = (2, 0.05)$, $\epsilon^*_R = (10, 0.05)$ and $(5, 0.05)$.

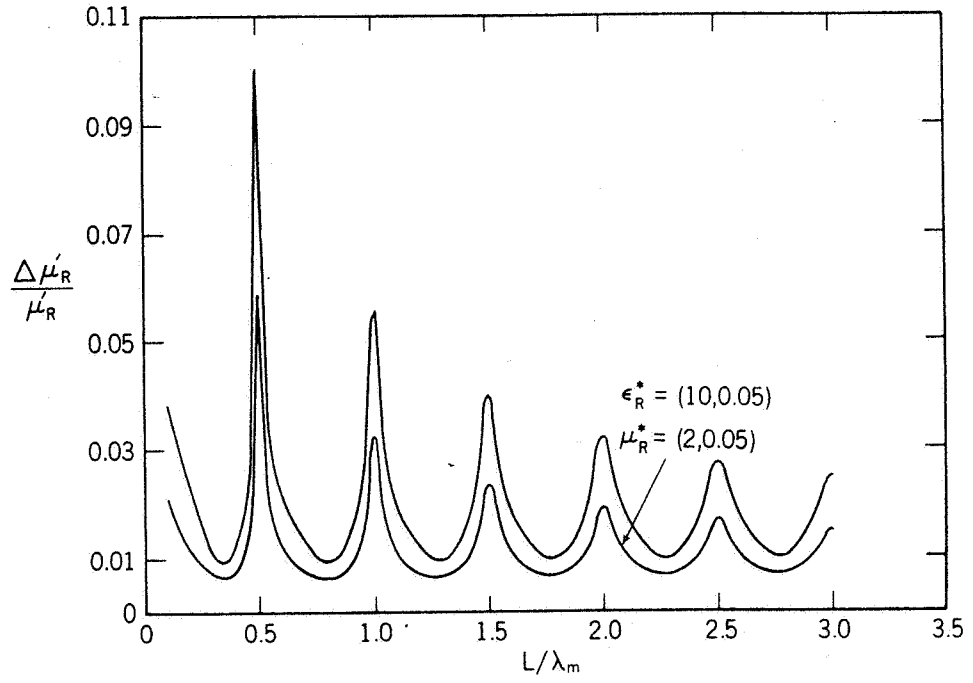

Figure 2.29: The relative uncertainty in $\mu'_R(\omega)$ for a low-loss material as a function of normalized length, with $\mu^*_R = (2, 0.05)$, $\epsilon^*_R = (10, 0.05)$ and $(5, 0.05)$.

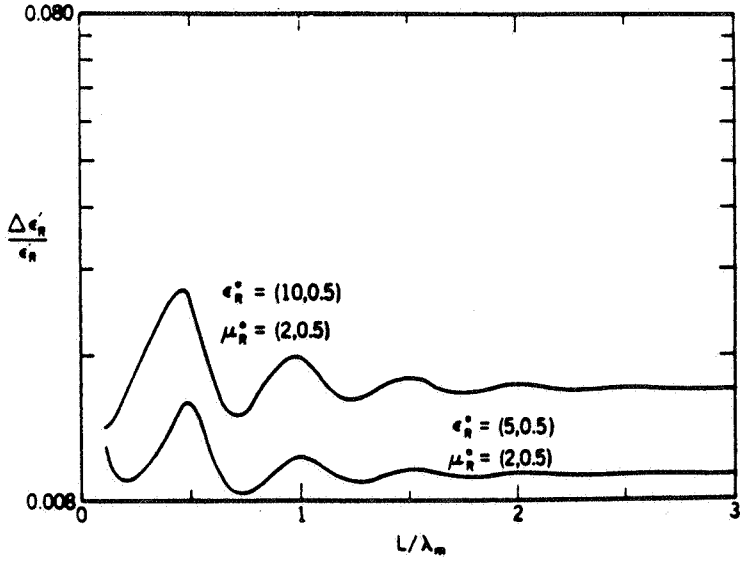

Figure 2.30: The relative uncertainty in $\epsilon'_R(\omega)$ for a high-loss material as a function of normalized length, with $\mu^*_R = (2, 0.5)$, $\epsilon^*_R = (10, 0.5)$ and $(5, 0.5)$.

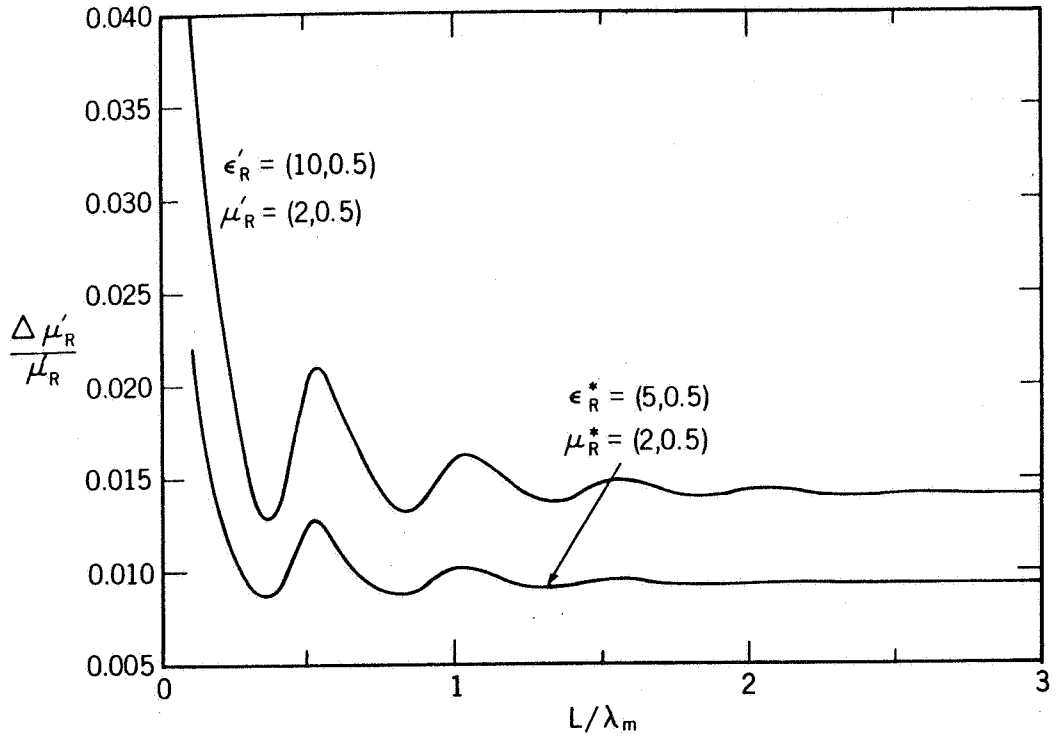

Figure 2.31: The relative uncertainty in $\mu'_R(\omega)$ for a high-loss material as a function of normalized length, with $\mu^*_R = (2.0, 0.5)$, $\epsilon^*_R = (10.0, 0.5)$ and $(5.0, 0.5)$.

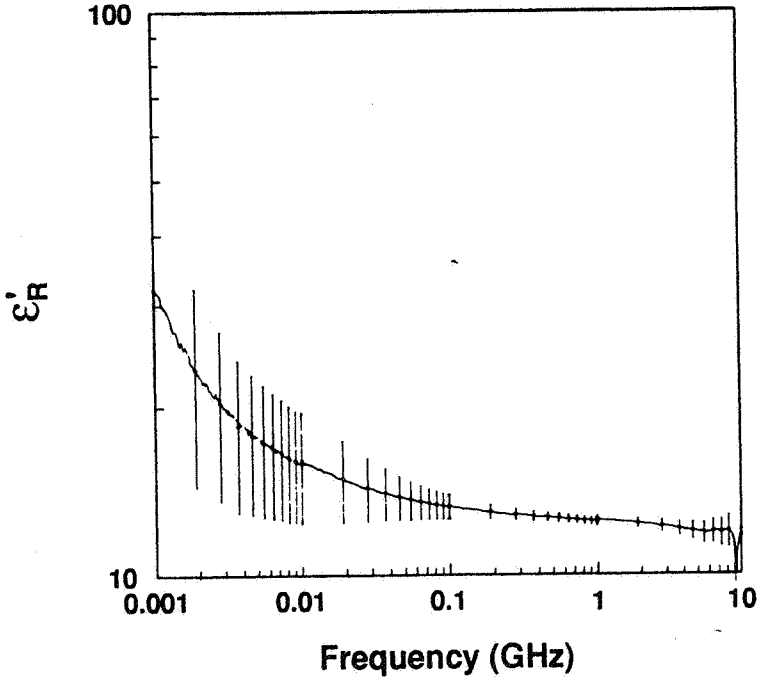

Figure 2.32: The real part of the relative permittivity $\epsilon'_R(\omega)$ for a nickel-zinc compound with uncertainties.

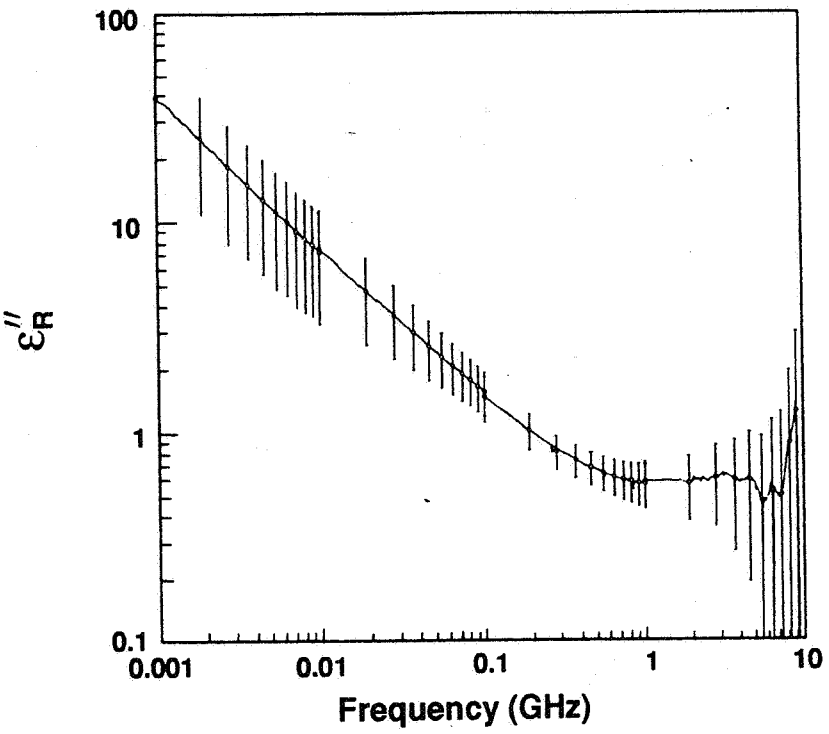

Figure 2.33: The imaginary part of the relative permittivity $\epsilon''_R(\omega)$ for a nickel-zinc compound with uncertainties.

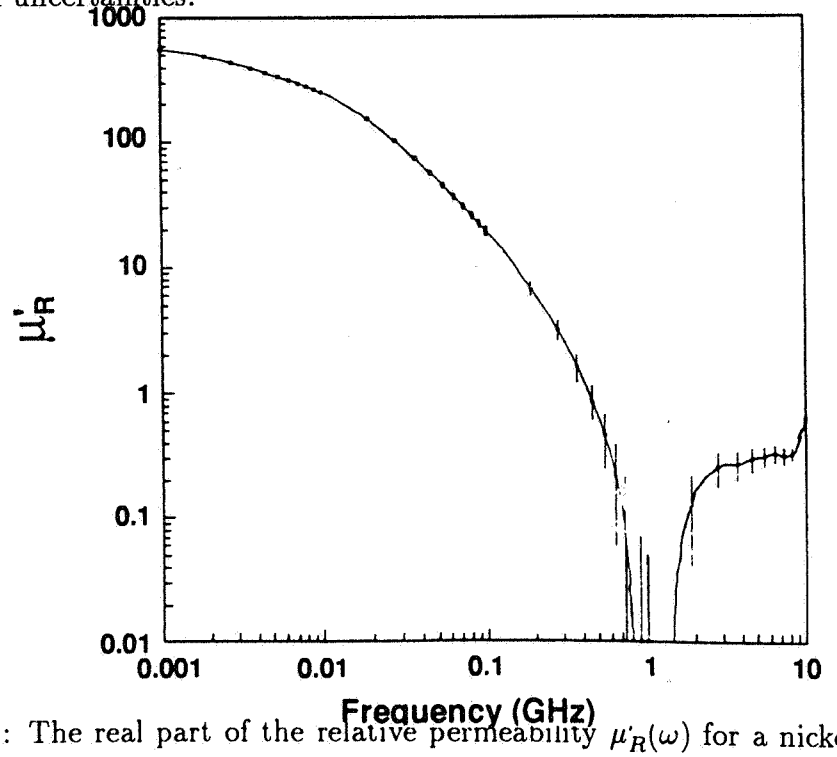

Figure 2.34: The real part of the relative permeability $\mu'_R(\omega)$ for a nickel-zinc compound with uncertainties.

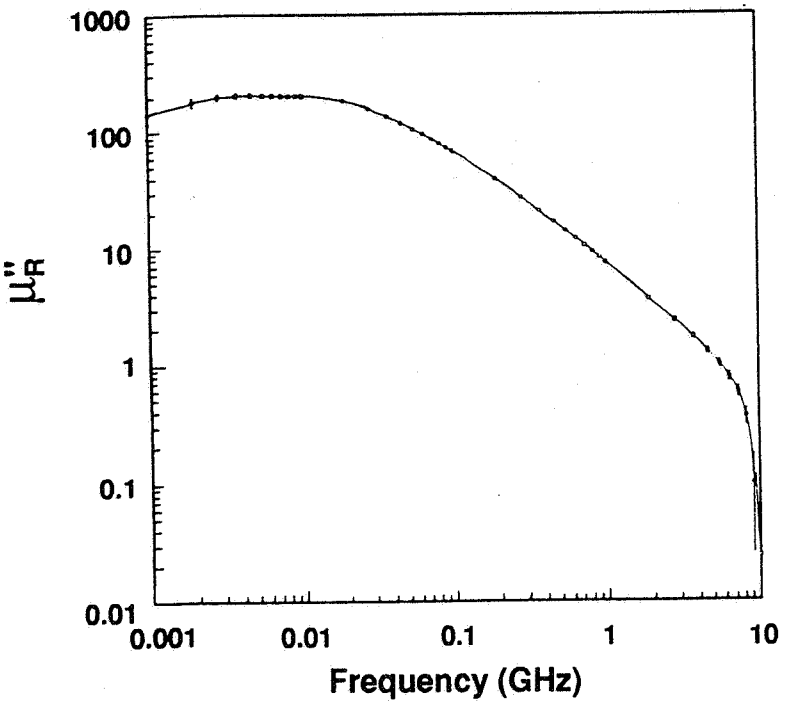

Figure 2.35: The imaginary part of the relative permeability $\mu''_R(\omega)$ for a nickel-zinc compound with uncertainties.

In figures 2.32 through 2.35 a measurement of a nickel-zinc ferrite compound is given with associated uncertainties. Uncertainties increase at high and low frequencies. At high and low frequency extremes the uncertainties in phase increase. Also, the scale is logarithmic which distorts the lengths of the error bars.

2.5.2 Two Samples of Differing Lengths

Another method to determine permittivity and permeability is the measurement of two samples with differing lengths. The advantage of this method is that each sample resonates at a different frequency and therefore S_{11} can be appreciable over the entire frequency band.

We assume the S-parameters are functions of $S_{ij}(|S_{mn}|, \theta_{mn}, L_1, L_2)$. The parameters used for measurements on materials of low to medium loss are

$$S_{21(i)} = \frac{Z_i(1-\Gamma^2)}{1-Z_i^2\Gamma^2} \ , \tag{2.97}$$

since it is acceptable down to -40 dB. We assume that the lengths of the samples are L_1 and $L_2 = \alpha L_1$. Due to the two lengths, there are transmission coefficients for each sample

$$Z_1 = \exp(-\gamma L_1) \ , \tag{2.98}$$

$$Z_2 = \exp(-\alpha\gamma L_1) \ . \tag{2.99}$$

The relevant partial derivatives of eqs (2.97) are:

$$\begin{aligned} &\frac{\partial S_{21(1)}}{\partial Z_1}\left[\frac{\partial Z_1}{\partial \epsilon_R^*}\frac{\partial \epsilon_R^*}{\partial |S_{21(1)}|} + \frac{\partial Z_1}{\partial \mu_R^*}\frac{\partial \mu_R^*}{\partial |S_{21(1)}|}\right] + \\ &\frac{\partial S_{21(1)}}{\partial \Gamma}\left[\frac{\partial \Gamma}{\partial \epsilon_R^*}\frac{\partial \epsilon_R^*}{\partial |S_{21(1)}|} + \frac{\partial \Gamma}{\partial \mu_R^*}\frac{\partial \mu_R^*}{\partial |S_{21(1)}|}\right] \\ &= \exp(j\theta_1) \ , \end{aligned} \tag{2.100}$$

$$\frac{\partial S_{21(2)}}{\partial Z_2}\left[\frac{\partial Z_2}{\partial \epsilon_R^*}\frac{\partial \epsilon_R^*}{\partial |S_{21(1)}|} + \frac{\partial Z_2}{\partial \mu_R^*}\frac{\partial \mu_R^*}{\partial |S_{21(1)}|}\right] + \frac{\partial S_{21(2)}}{\partial \Gamma}\left[\frac{\partial \Gamma}{\partial \epsilon_R^*}\frac{\partial \epsilon_R^*}{\partial |S_{21(1)}|} + \frac{\partial \Gamma}{\partial \mu_R^*}\frac{\partial \mu_R^*}{\partial |S_{21(1)}|}\right] = 0 \ , \tag{2.101}$$

$$\frac{\partial S_{21(1)}}{\partial Z_1}\left[\frac{\partial Z_1}{\partial \epsilon_R^*}\frac{\partial \epsilon_R^*}{\partial |S_{21(2)}|} + \frac{\partial Z_1}{\partial \mu_R^*}\frac{\partial \mu_R^*}{\partial |S_{21(2)}|}\right] + \frac{\partial S_{21(1)}}{\partial \Gamma}\left[\frac{\partial \Gamma}{\partial \epsilon_R^*}\frac{\partial \epsilon_R^*}{\partial |S_{21(2)}|} + \frac{\partial \Gamma}{\partial \mu_R^*}\frac{\partial \mu_R^*}{\partial |S_{21(2)}|}\right] = 0 \ , \tag{2.102}$$

$$\frac{\partial S_{21(2)}}{\partial Z_2}[\frac{\partial Z_2}{\partial \epsilon_R^*}\frac{\partial \epsilon_R^*}{\partial |S_{21(2)}|}+\frac{\partial Z_2}{\partial \mu_R^*}\frac{\partial \mu_R^*}{\partial |S_{21(2)}|}]$$
$$+\frac{\partial S_{21(2)}}{\partial \Gamma}[\frac{\partial \Gamma}{\partial \epsilon_R^*}\frac{\partial \epsilon_R^*}{\partial |S_{21(2)}|}+\frac{\partial \Gamma}{\partial \mu_R^*}\frac{\partial \mu_R^*}{\partial |S_{21(2)}|}]$$
$$=\exp(j\theta_2)\ . \tag{2.103}$$

We can rewrite eqs (2.100) through (2.103) as

$$\underbrace{(\frac{\partial S_{21(1)}}{\partial Z_1}\frac{\partial Z_1}{\partial \epsilon_R^*}+\frac{\partial S_{21(1)}}{\partial \Gamma}\frac{\partial \Gamma}{\partial \epsilon_R^*})}_{A_1}\frac{\partial \epsilon_R^*}{\partial |S_{21(1)}|}$$
$$+\underbrace{(\frac{\partial S_{21(1)}}{\partial Z_1}\frac{\partial Z}{\partial \mu_R^*}+\frac{\partial S_{21(1)}}{\partial \Gamma}\frac{\partial \Gamma}{\partial \mu_R^*})}_{B_1}\frac{\partial \mu_R^*}{\partial |S_{21(1)}|}=\exp(j\theta_1)\ , \tag{2.104}$$

$$\underbrace{(\frac{\partial S_{21(2)}}{\partial Z_2}\frac{\partial Z_2}{\partial \epsilon_R^*}+\frac{\partial S_{21(2)}}{\partial \Gamma}\frac{\partial \Gamma}{\partial \epsilon_R^*})}_{A_2}\frac{\partial \epsilon_R^*}{\partial |S_{21(1)}|}$$
$$+\underbrace{(\frac{\partial S_{21(2)}}{\partial Z_2}\frac{\partial Z_2}{\partial \mu_R^*}+\frac{\partial S_{21(2)}}{\partial \Gamma}\frac{\partial \Gamma}{\partial \mu_R^*})}_{B_2}\frac{\partial \mu_R^*}{\partial |S_{21(1)}|}=0\ , \tag{2.105}$$

$$\underbrace{(\frac{\partial S_{21(1)}}{\partial Z_1}\frac{\partial Z_1}{\partial \epsilon_R^*}+\frac{\partial S_{21(1)}}{\partial \Gamma}\frac{\partial \Gamma}{\partial \epsilon_R^*})}_{A_1}\frac{\partial \epsilon_R^*}{\partial |S_{21(2)}|}$$
$$+\underbrace{(\frac{\partial S_{21(1)}}{\partial Z_1}\frac{\partial Z_1}{\partial \mu_R^*}+\frac{\partial S_{21(1)}}{\partial \Gamma}\frac{\partial \Gamma}{\partial \mu_R^*})}_{B_1}\frac{\partial \mu_R^*}{\partial |S_{21(2)}|}=0\ , \tag{2.106}$$

$$\underbrace{\left(\frac{\partial S_{21(2)}}{\partial Z_2}\frac{\partial Z_2}{\partial \epsilon_R^*}+\frac{\partial S_{21(2)}}{\partial \Gamma}\frac{\partial \Gamma}{\partial \epsilon_R^*}\right)}_{A_2}\frac{\partial \epsilon_R^*}{\partial |S_{21(2)}|}$$
$$+\underbrace{\left(\frac{\partial S_{21(2)}}{\partial Z_2}\frac{\partial Z_2}{\partial \mu_R^*}+\frac{\partial S_{21(2)}}{\partial \Gamma}\frac{\partial \Gamma}{\partial \mu_R^*}\right)}_{B_2}\frac{\partial \mu_R^*}{\partial |S_{21(2)}|}=\exp(j\theta_2)\ , \tag{2.107}$$

where we have defined parameters A_1, B_1, A_2, and B_2. Also for the relevant derivatives with respect to length, we find

$$\underbrace{\left(\frac{\partial S_{21(1)}}{\partial Z_1}\frac{\partial Z_1}{\partial \epsilon_R^*}+\frac{\partial S_{21(1)}}{\partial \Gamma}\frac{\partial \Gamma}{\partial \epsilon_R^*}\right)}_{A_1}\frac{\partial \epsilon_R^*}{\partial L_1}$$
$$+\underbrace{\left(\frac{\partial S_{21(1)}}{\partial Z_1}\frac{\partial Z_1}{\partial \mu_R^*}+\frac{\partial S_{21(1)}}{\partial \Gamma}\frac{\partial \Gamma}{\partial \mu_R^*}\right)}_{B_1}\frac{\partial \mu_R^*}{\partial L_1}+\underbrace{\frac{\partial S_{21(1)}}{\partial Z_1}\frac{\partial Z_1}{\partial L_1}}_{E_1}=0\ , \tag{2.108}$$

$$\underbrace{\left(\frac{\partial S_{21(2)}}{\partial Z_2}\frac{\partial Z_2}{\partial \epsilon_R^*}+\frac{\partial S_{21(2)}}{\partial \Gamma}\frac{\partial \Gamma}{\partial \epsilon_R^*}\right)}_{A_2}\frac{\partial \epsilon_R^*}{\partial L_1}$$
$$+\underbrace{\left(\frac{\partial S_{21(2)}}{\partial Z_2}\frac{\partial Z_2}{\partial \mu_R^*}+\frac{\partial S_{21(2)}}{\partial \Gamma}\frac{\partial \Gamma}{\partial \mu_R^*}\right)}_{B_2}\frac{\partial \mu_R^*}{\partial L_1}+\underbrace{\frac{\partial S_{21(2)}}{\partial Z_2}\frac{\partial Z_2}{\partial L_1}}_{F2}=0\ . \tag{2.109}$$

We now can solve for the derivatives that have been taken with respect to the independent parameters in eqs (2.104) through (2.107)

$$\frac{\partial \epsilon_R^*}{\partial |S_{21(1)}|}=\frac{B_2\exp(j\theta_1)}{A_1B_2-B_1A_2}\ , \tag{2.110}$$

$$\frac{\partial \mu_R^*}{\partial |S_{21(1)}|}=-\frac{A_2}{B_2}\frac{\partial \epsilon_R^*}{|S_{21(1)}|}\ , \tag{2.111}$$

$$\frac{\partial \epsilon_R^*}{\partial |S_{21(2)}|}=\frac{B_1\exp(j\theta_2)}{A_2B_1-B_2A_1}\ , \tag{2.112}$$

$$\frac{\partial \mu_R^*}{\partial |S_{21(2)}|}=-\frac{A_1}{B_1}\frac{\partial \epsilon_R^*}{|S_{21(2)}|}\ , \tag{2.113}$$

$$\frac{\partial \epsilon_R^*}{\partial L_1} = \frac{E_1 B_2 - F_2 B_1}{B_1 A_2 - A_1 B_2} , \tag{2.114}$$

$$\frac{\partial \mu_R^*}{\partial L_1} = -\frac{E_1 + A_1 \frac{\partial \epsilon_R^*}{\partial L}}{B_1} , \tag{2.115}$$

$$\frac{\partial \epsilon_R^*}{\partial \theta_1} = j|S_{21(1)}| \frac{\partial \epsilon_R^*}{\partial |S_{21(1)}|} , \tag{2.116}$$

$$\frac{\partial \mu_R^*}{\partial \theta_1} = j|S_{21(1)}| \frac{\partial \mu_R^*}{\partial |S_{21(1)}|} , \tag{2.117}$$

$$\frac{\partial \epsilon_R^*}{\partial \theta_2} = j|S_{21(2)}| \frac{\partial \epsilon_R^*}{\partial |S_{21(2)}|} , \tag{2.118}$$

$$\frac{\partial \mu_R^*}{\partial \theta_2} = j|S_{21(2)}| \frac{\partial \mu_R^*}{\partial |S_{21(2)}|} , \tag{2.119}$$

$$\frac{\partial S_{21(i)}}{\partial Z_i} = \frac{(1 + \Gamma^2 Z_i^2)(Z_i^2 - 1)}{(1 - \Gamma^2 Z_i^2)^2} , \tag{2.120}$$

$$\frac{\partial S_{21(i)}}{\partial \Gamma} = \frac{2 Z_i \Gamma (Z_i^2 - 1)}{(1 - \Gamma^2 Z_i^2)^2} , \tag{2.121}$$

$$\frac{\partial \Gamma}{\partial \epsilon_R^*} = \frac{\gamma_0 \mu_R^{2*} \epsilon_0 \mu_0 \omega^2}{\gamma (\mu_0 \gamma + \gamma_0 \mu)^2} , \tag{2.122}$$

$$\frac{\partial \Gamma}{\partial \mu_R^*} = \frac{\epsilon_R^*}{\mu_R^*} \frac{\partial \Gamma}{\partial \epsilon_R^*} + \frac{2 \gamma_0 \gamma}{(\gamma + \gamma_0 \mu)^2} , \tag{2.123}$$

$$\frac{\partial Z}{\partial L} = -\gamma \exp(-\gamma L) , \tag{2.124}$$

$$\frac{\partial Z}{\partial \epsilon_R^*} = \frac{L \epsilon_0 \mu \omega^2}{2\gamma} \exp(-\gamma L) , \tag{2.125}$$

$$\frac{\partial Z}{\partial \mu_R^*} = \frac{L \epsilon \mu_0 \omega^2}{2\gamma} \exp(-\gamma L) . \tag{2.126}$$

In figures 2.36 through 2.37, the total uncertainty in ϵ_R^* and μ_R^* computed from S_{21} is plotted as a function of normalized sample length, for low-loss and high-loss materials at 3 GHz with various values of ϵ_R^*.

When the length of one sample is twice the length of the other sample, we see instability at frequencies corresponding to $n\lambda_m/2$. Generally, we see a decrease in uncertainty as a

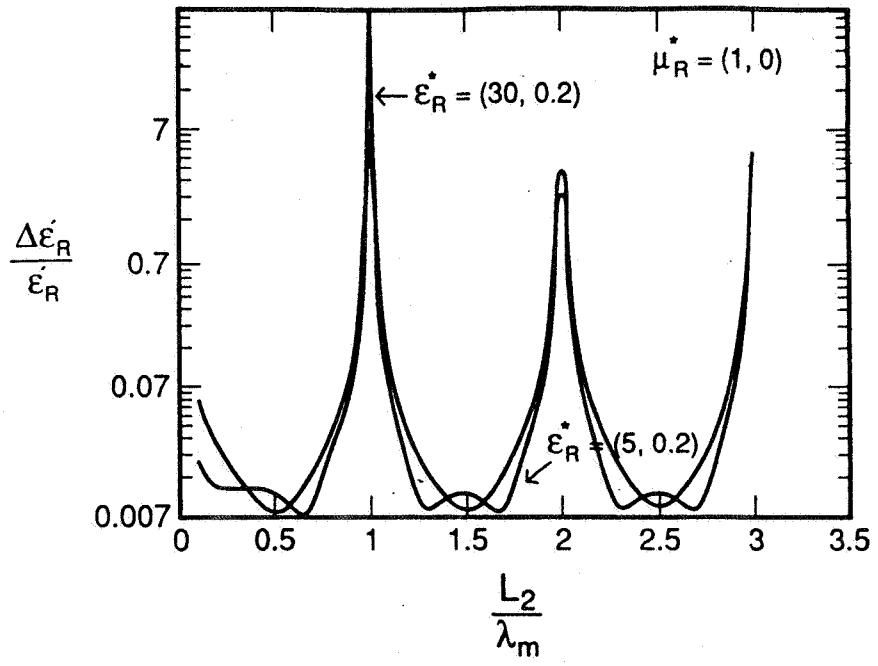

Figure 2.36: The relative uncertainty in $\epsilon_R'(\omega)$ for a low-loss material as a function of normalized length for the case when $L_1 = 0.5L_2$ for two different permittivities.

function of increasing sample length. Also, the uncertainties in the S-parameters show some frequency dependence. In figure 2.37 the ratio of sample lengths is $\sqrt{2}$. In this case we see greater stability over the frequency range than in the case where the range is 0.5. Resonances in the solutions will occur when $L = n\lambda_m/2$ and $\alpha L = m\lambda_m/2$ simultaneously, where m is an integer.

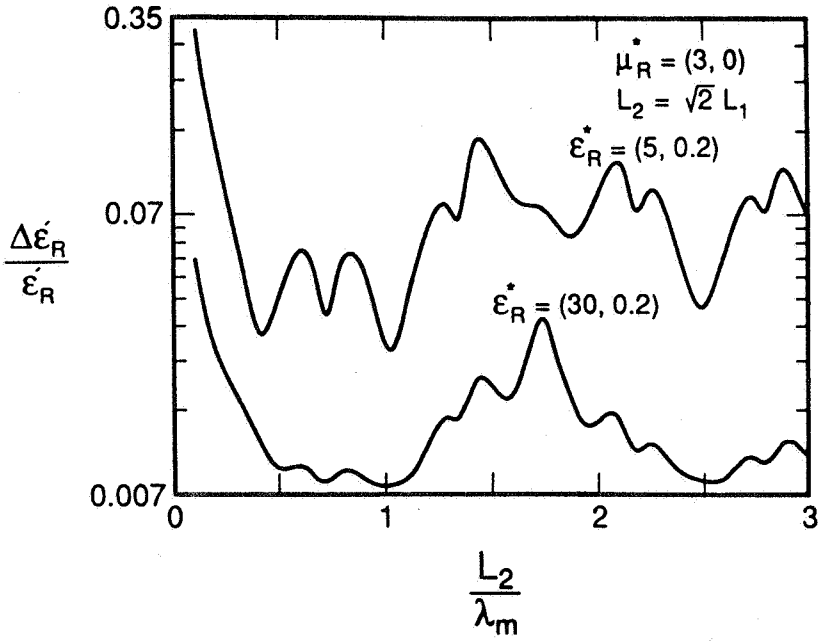

Figure 2.37: The relative uncertainty in $\epsilon_R'(\omega)$ for a low-loss material as a function of normalized length for the case when $L_2^2 = 2L_1^2$ for two different permittivities.

2.6 Uncertainty in Gap Correction

The correction for an air gap between the wall of the sample holder and sample is very important for measurements of high permittivity materials. In addition, the uncertainty in the gap correction is very important for high permittivity materials and may actually dominant the uncertainties of the measurement. In appendix C the gap correction is worked out in detail. In this section the uncertainty in the gap correction will be worked out.

2.6.1 Dielectric Materials

Waveguide Gap Uncertainty

The uncertainty due to an air gap between sample and holder can be calculated from the partial derivatives of ϵ_R^* with respect to sample thicknesses, d. The relevant derivatives for waveguide are given by

$$\frac{\partial \epsilon'_{cR}}{\partial d} = \epsilon'_{mR}\left[\frac{1}{b-(b-d)\epsilon'_{mR}}\right] - \epsilon'^2_{mR}\frac{d}{[b-(b-d)\epsilon'_{mR}]^2}\,, \tag{2.127}$$

$$\frac{\partial \epsilon''_{cR}}{\partial d} = -\epsilon''_{mR}\epsilon'_R\frac{b}{[b-(b-d)\epsilon'_{mR}]^2}\,. \tag{2.128}$$

Coaxial Gap Correction

For coaxial line the relevant derivatives are given by

$$\frac{\partial \epsilon'_{cR}}{\partial R_2} = -\epsilon'_{mR}\frac{1}{R_2(L_3-\epsilon'_{mR}L_1)} + \epsilon'^2_{mR}\frac{L_2}{R_2(L_3-\epsilon'_{mR}L_1)^2}\,, \tag{2.129}$$

$$\frac{\partial \epsilon'_{cR}}{\partial R_3} = \epsilon'_{mR}\frac{1}{R_3(L_3-\epsilon'_{mR}L_1)} + \epsilon'^2_{mR}\frac{L_2}{R_3(L_3-\epsilon'_{mR}L_1)^2}\,, \tag{2.130}$$

$$\frac{\partial \epsilon''_{cR}}{\partial R_2} = \epsilon''_{mR}\epsilon'_{mR}\left[\frac{1}{L_2R_2} + \frac{L_1}{L_2^2R_2}\right]\,, \tag{2.131}$$

$$\frac{\partial \epsilon''_{cR}}{\partial R_3} = -\epsilon''_{mR}\epsilon'_{mR}\left[\frac{1}{L_2R_3} + \frac{L_1}{L_2^2R_3}\right]\,. \tag{2.132}$$

2.6.2 Magnetic Materials

Waveguide Gap Uncertainty

The uncertainty due to an air gap between sample and holder can be calculated from the partial derivatives of μ_R^* with respect to gap thicknesses, d. The relevant derivatives for waveguide are given by

$$\frac{\partial \mu'_{cR}}{\partial d} = (1 - \mu'_{mR})\frac{b}{d^2} , \tag{2.133}$$

$$\frac{\partial \mu''_{cR}}{\partial d} = -\mu'_{mR}\frac{b}{d^2} . \tag{2.134}$$

Coaxial Gap Correction

For coaxial line the relevant derivatives are calculated using

$$K_1 = \ln R_2/R_1 , \tag{2.135}$$

$$K_2 = \ln R_3/R_2 , \tag{2.136}$$

$$K_3 = \ln R_4/R_3 , \tag{2.137}$$

$$K_4 = \ln R_4/R_1 , \tag{2.138}$$

as follows

$$\frac{\partial \mu'_{cR}}{\partial R_2} = \frac{1}{R_2 K_2}[\mu'_{mR}\frac{K_4}{K_2} - \frac{K_1}{K_2} - 1 - \frac{K_3}{K_2}] , \tag{2.139}$$

$$\frac{\partial \mu'_{cR}}{\partial R_3} = \frac{1}{R_3 K_2}[-\mu'_{mR}\frac{K_4}{K_2} + \frac{K_1}{K_2} + 1 + \frac{K_3}{K_2}] , \tag{2.140}$$

$$\frac{\partial \mu''_{cR}}{\partial R_2} = \mu''_{mR}\frac{K_1}{R_2 K_2^2} , \tag{2.141}$$

$$\frac{\partial \mu''_{cR}}{\partial R_3} = -\mu''_{mR}\frac{K_1}{R_3 K_2^2} . \tag{2.142}$$

2.6.3 Higher Order Modes

The field model assumes a single mode of propagation in the sample. Propagation of higher order modes becomes possible in inhomogeneous samples of high dielectric constant due to changes in cutoff. Air gaps also play an important role in mode conversion. Generally, the appearance of higher order modes manifests itself as a sudden dip in $|S_{11}|$. This dip is a result of resonance of the excited higher order mode. We can expect point-by-point

TR models to break down near higher order mode resonances for materials of high dielectric constant or inhomogeneous samples. Optimized, multi-frequency solution techniques fare better in this respect. The characteristic of the higher order modes are anomalies in the scattering matrix at and around resonance. Higher order modes require a coupling mechanism in order to begin propagating. In waveguide and coaxial line the asymmetry of the sample promotes higher order mode propagation. In order to minimize the effects of higher order modes, shorter samples can be used to maintain the electrical length less than one-half guided wavelength. Also well machined sample are important in suppressing modes. Higher order modes will not appear if the sample length is less than one-half guided wavelength of the fundamental mode in the material.

Mode Suppression

It is possible to remove some of the higher order modes by mode filters. This would be particularly helpful in cylindrical waveguide. One way to do this is to helically wind a fine wire about the inner surface of the waveguide sample holder, thus eliminating longitudinal currents and therefore TM modes. Another approach is to insert cuts in the waveguide walls to minimize current loops around the waveguide.

Chapter 3

Optimized Solution

3.1 Introduction

As indicated in the previous chapters, various numerical strategies have been employed for reducing 1-port and 2-port scattering data for both nonmagnetic and magnetic materials. The vast majority of the work in this area has involved the determination of permittivity and permeability by the reduction of scattering data frequency by frequency, that is, by the explicit or implicit solution of a system of nonlinear scattering equations at each frequency (see [11,33]; as an example of a multifrequency approach see Maze et al.[15]).

What is lacking in the literature are practical, robust, numerical reduction techniques for more accurate determination of permittivity and permeability in transmission lines. Reliable broadband permeability and permittivity results for low-loss, medium-to-high dielectric constant materials are hard to obtain with transmission line techniques. Coaxial line measurements are particularly hard to obtain due to air gap influences and overmoding. Traditional transmission line numerical techniques have difficulties to an extent that render these techniques of limited use for low-loss materials and for high dielectric constant materials. Difficulties arise with these methods for magnetic materials in that numerical singularities can occur at frequencies corresponding to integral multiples of one half wavelength. These instabilities arise from the fact that for low-loss materials both S_{21} and S_{11} become equations for the phase velocity, and the permittivity and permeability therefore enter as a product. These instabilities limit the acquisition of precise broadband dielectric and magnetic results in the neighborhood of a resonance. Another problem pertains to high dielectric constant materials. High dielectric constant materials are usually hard to measure since the theoretical models are limited to a single, fundamental mode and the data contain both fundamental and higher order mode responses. Further, point-by-point reduction techniques for magnetic materials contain large random uncertainties due

to the propagation of uncertainties through the equations. For nonmagnetic materials the propagation of errors is less of a problem.

In our search for better reduction techniques we have found that nonlinear optimization, which minimizes the squared error, are a viable alternative solution. Optimization-based data reduction has an advantage over point-by-point schemes in that correlations are allowed between frequency measurements. In nonlinear regression, if deemed appropriate, it is not necessary to even include S_{11} data in the constraint equations. Another advantage of regression is that constraints such as causality and positivity can be incorporated into the solution.

This chapter presents a method for obtaining complex permittivity and permeability spectra from scattering parameter data on isotropic, homogeneous materials using nonlinear regression. We solve the scattering equations in a nonlinear least-squares sense with a regression algorithm over the entire frequency measurement range. The complex permittivity and permeability are obtained by determining estimates for the coefficients of a truncated Laurent series expansion for these parameters consistent with linearity and causality constraints. The procedure has been successfully used for accurate permittivity and permeability characterization of a number of different samples where point-by-point schemes have proven to be inadequate. The details of the numerical method have been presented in [36]. The problem applied to microwave measurements is presented in this chapter. The method can easily be extended to the analysis of multi-mode problems and the determination of experimental systematic uncertainty. The novel features of our algorithm are:

- The algorithm finds a "best fit" to the 2-port scattering equations using a nonlinear least-squares solution for the permittivity and permeability.
- The algorithm uses fitting functions that satisfy causality requirements.
- The numerical technique allows slight variations in the sample and reference position lengths to compensate for measurement errors and sample imperfections.
- The method allows the de-emphasis of frequency points with large phase uncertainty.
- Statistics related to the solution parameters are automatically generated.
- The technique can force positivity of the fit functions.
- It is possible to determine both complex permittivity and permeability from measurements of a single scattering parameter on a 1-port or a 2-port taken over a frequency band.

3.2 Model for Permeability and Permittivity

In the optimization procedure the S-parameter eqs (2.31) through (2.33) for single-mode problems, or eqs (2.21) through (2.24) for problems with higher order modes are solved for the material parameters by the optimization routine. For higher order mode problems the matrix elements A_{jk} in eqs (2.21) through (2.24), which corresponds to the voltage in each mode, can be determined by the optimization routine. However, we usually consider only the primary mode.

The unknown quantities are L_1, L_2, L, λ_c, and $\mu_R^*(\omega)$ and $\epsilon_R^*(\omega)$. Some of these parameters, such as the lengths and cutoff wavelength, are known accurately within measurement uncertainty. Obviously the parameters of interest cannot be allowed to vary into non-physical realms. The problem is to use an optimization routine to determine the model parameters that are consistent with the scattering data and the physics of the problem.

3.2.1 Relaxation Phenomena in the Complex Plane

The numerical model requires an explicit functional form for μ_R^* and ϵ_R^* to reproduce the four S-parameters consistent with the data, for all the n frequency observations.

The general form for $\mu_R^*(\omega)$ and $\epsilon_R^*(\omega)$ should be causal see Appendix C; that is, it must satisfy a Kramers-Kronig relation. If the zeros and poles of a complex function are known over the complex plane, the function itself is known.

The Laplace transform of the real, time-dependent permittivity satisfies

$$\epsilon(\vec{r}, s) = \int_0^\infty \epsilon(\vec{r}, t) e^{-st} dt \ . \tag{3.1}$$

For stability, there can be no poles in the right-half side of the s-plane. Since $\epsilon(t)$ is real it can be shown that the poles and zeros are confined to the negative real s-axis of the s-plane, and the poles which are off the real s- axis must occur in complex conjugate pairs [37].

Assuming linear response a constitutive relationship in an isotropic medium between the displacement and electric fields is

$$\vec{D}(\vec{x}, t) = \epsilon_0 \vec{E}(\vec{x}, t) + \epsilon_0 \int_0^\infty G(\tau) \vec{E}(\vec{x}, t - \tau) d\tau \ . \tag{3.2}$$

With this definition the permittivity is

$$\epsilon_R^*(\omega) = 1 + \int_0^\infty G(\tau) e^{-j\omega\tau} d\tau \ . \tag{3.3}$$

The response function $G(\tau)$ for an incident electric field can sometimes be represented as a series of damped sinusoids of the form

$$G(t) = \sum_n A_n \exp(-(a_n + jb_n)t) \ . \tag{3.4}$$

We assume that the material parameters can be adequately modeled by a series of simple poles. The terms $e^{-a_n t}$ relate to relaxation and the terms $e^{-jb_n t}$ relate to resonant phenomena. Since the Laplace transform of eq (3.4) is

$$G(s) = \sum_n A_n \frac{1}{s + a_n + jb_n} \ , \tag{3.5}$$

for stability (no increasing time domain exponentials) there can be no poles or zeros in the right half-side of the s-plane [37], [38]. In order to maintain the reality of $\epsilon(s)$, any poles off the imaginary axis in the ω-plane must be conjugate poles of the form $\omega = ja \pm b$ where a and b are real, positive numbers as indicated in figure 3.1. These conjugate poles are of the form

$$\frac{1}{s + a + jb} + \frac{1}{s + a - jb} \ , \tag{3.6}$$

and are related to resonant phenomena.

We assume that the permittivity can be expressed as

$$\epsilon_R^* = C \left[\prod_n \frac{(j\omega + z_n)}{(j\omega + p_n)} + \sum_n [\frac{1}{j\omega + a_n + jb_n} + \frac{1}{j\omega + a_n - jb_n}] \right] \ . \tag{3.7}$$

Here z_n and p_n are the zeros and poles due to damped exponentials respectively, $(a_n \pm jb_n)$ are the complex conjugate poles, and C is a complex constant.

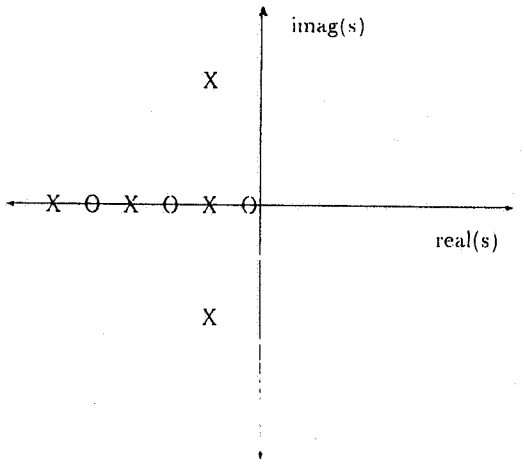

Figure 3.1: Poles (X) and zeros (O) in the complex s-plane and conjugate poles off the real s-axis.

For more complicated polarization phenomena other relations for permittivity could be used. For a continuous distribution of relaxation times

$$\epsilon' = \epsilon_\infty + [\epsilon(0) - \epsilon_\infty] \int_0^\infty \frac{y(\tau)}{1+\omega^2\tau^2} d\tau \ , \tag{3.8}$$

$$\epsilon'' = [\epsilon(0) - \epsilon_\infty] \int_0^\infty \frac{\omega\tau y(\tau)}{1+\omega^2\tau^2} d\tau \ , \tag{3.9}$$

where $y(\tau)$ is a distribution function. Various expressions for y yield various relations for permittivity. Presently we use eqs (3.11) and (3.12) in our calculations. The Havriliak-Negami model for materials assumes a single nonsimple pole on the negative, real s-plane axis:

$$\epsilon_R^* = C + \frac{A}{(1+[j|B|\omega]^{1-\alpha})^\beta} \ , \tag{3.10}$$

where β and α are in the interval $[0,1]$ and B is real. Limiting cases of this model are (1) the Cole-Davidson model when $\alpha = 0$; this model works well for some liquids and solid polymers, (2) the Cole-Cole model when $\beta = 1$; this model has been used to describe relaxation behavior of amorphous solids and many liquids. A simple Debye model ($\beta = 1$ and $\alpha = 1$) is very limited and works well only for materials that contain a single relaxation time in the frequency range of interest.

Heterogeneous materials and polymers usually have a very broad relaxation spectrum and as such have a response of the form of a power law such as s^{-a}. This behavior can be obtained from the Cole-Davidson model when $|B|\omega >> 1$.

In our present algorithm we assume a more general model than the single Debye relaxation model a truncated Laurent series is used for $\mu_R^*(\omega)$ and $\epsilon_R^*(\omega)$. This expansion has

generally yielded excellent results

$$\mu_R^*(\omega) = A_0 + \frac{A_1}{1 + j|B_1|\omega} + \frac{A_2}{(1 + j|B_2|\omega)^2} , \tag{3.11}$$

$$\epsilon_R^*(\omega) = D_0 + \frac{A_3}{1 + j|B_3|\omega} + \frac{A_4}{(1 + j|B_4|\omega)^2} , \tag{3.12}$$

where B_i are real numbers. The pole information yields constraints on the constants used in the Laurent series expansion. For example, it is required that B_i is a real number.

For a typical measurement on a network analyzer there may be 400 frequency points and at each point all four scattering parameters are taken. The problem is overdetermined since for n frequency measurements, if we assume known lengths, there are $8n$ real equations for the unknown quantities in the Laurent series. This over determination can be used at frequencies in the gigahertz range to find corrections to sample position and cut off wavelength.

The approach for determining the complex parameters A_j, B_j is to minimize the sum of the squares of the differences between the predicted and observed S-parameters,

$$\min \parallel \sum_{ij} \vec{S}_{ij} - \vec{P}_{ij} \parallel , \tag{3.13}$$

where the measured vectors are denoted by $\vec{S}_{ij} = (S_{ij}(\omega_1), S_{ij}(\omega_2), .., S_{ij}(\omega_n))$ and where $\vec{P}_{ij}$ is the predicted vector. Hence, the problem consists of finding the norm solution to these equations.

3.3 Numerical Technique

3.3.1 Algorithm

The solution currently uses a software routine called orthogonal distance regression pack ODRPACK [39] developed at the National Institute of Standards and Technology. This routine is an extended form of the Levenberg-Marquardt approach. This procedure allows for both ordinary nonlinear least-squares, in which the uncertainties are assumed to be only in the dependent variable, and, orthogonal distance regression, where the uncertainties appear in both dependent and independent variables. First-order derivatives for the Jacobian matrices can be numerically approximated (finite difference approximation) or can be user-supplied analytical derivatives. The procedure performs automatic scaling of the variables if necessary, as well as determining the accuracy of the model in terms of machine precision. The trust region approach enables the procedure to adaptively determine the region in which the linear approximation adequately represents the nonlinear model.

Iterations are stopped by ODRPACK when any one of three criteria are met. These criteria are: (1) the difference between observed and predicted values is small, (2) the convergence to a predicted value is sufficiently small, and (3) a specified limit on the number of iterations has been reached.

Initial guesses for ϵ_R^* and μ_R^* are obtained from explicit solutions of Stuchly [7] or Weir [6]. The most significant input parameters for modeling permittivity and permeability are the initial values for A_i and B_i. Sensitivity to the initial solution for these parameters is discussed below. All additional parameters are initialized to 0.

When measurements of length and scattering parameters of a sample are taken, there are systematic uncertainties.

An orthogonal distance regression model provides the modeler with the additional ability to assume that the independent variable, in this case, frequency, may contain some uncertainty as well. Allowances for these types of uncertainty can, in some cases, greatly improve the approximation. For this model and the samples tested, the errors in the independent variables are sufficiently small that an ordinary least-squares approximation is adequate.

Model parameters such as sample length, sample position in the waveguide, and cutoff wavelength could contain a systematic uncertainty. These parameters were allowed to vary over a limited region, and the optimization procedure chooses optimum values for the parameter. This procedure assumes that systematic measurement errors can be detected by the routine. For example, inserting a sample into a sample holder introduces an uncertainty in the sample position L_1, so we include with L_1 an additional optimization parameter β_{L1} in R_1 to account for positioning uncertainties,

$$R_1 = \exp(-\gamma_o[L_1 + \beta_{L1}]) \ . \tag{3.14}$$

Also for R_2

$$R_2 = \exp(-\gamma_o[L_2 + \beta_{L2}]) \ . \tag{3.15}$$

The routine requires that the length corrections be within a prescribed range which represents physical measurement uncertainty. The length of the sample L is completely determined by

$$L = L_{air} - (L_1 + L_2 + \beta_{L1} + \beta_{L2}) \tag{3.16}$$

and is also implicitly parameterized by the values of β_{L1} and β_{L2}.

Due to inaccuracies in machining of the sample holder there is an uncertainty in the cutoff wavelength of the guide. We account for this by the introduction of an additional optimization parameter $\lambda_c \rightarrow \lambda_c + \beta_\lambda$. We constrain this variation to be within measurement accuracy.

The model can use various combinations of the available data to estimate both the relative permeability and permittivity from scattering data. For example, S_{21} or S_{11} alone

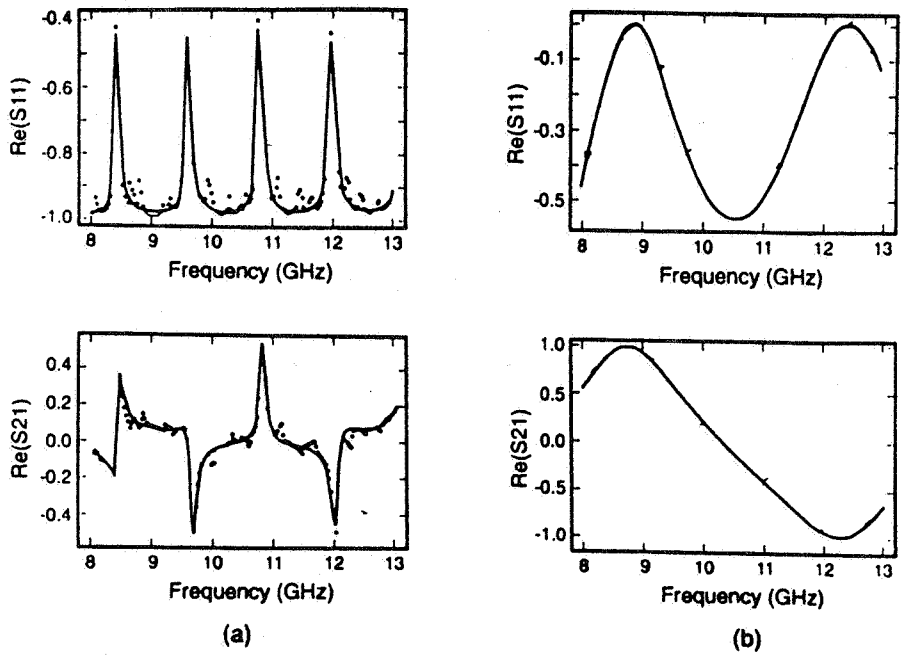

Figure 3.2: Predicted (solid line) and observed (dots) parameters for a barium titanate compound (a) and cross-linked polystyrene in (b).

can be used to obtain both permeability and permittivity. This can be contrasted with point-by-point techniques where both S_{21} and S_{11} are required. Also, magnitude alone can similarly be used. Magnitude data have the advantage of requiring no reference plane rotation.

The technique works well for short-circuit line measurements. For short-circuit lines it is possible with this technique to obtain both the complex permittivity and permeability from a single broadband measurement on one sample at a single position in the line.

3.3.2 Numerical Results

The model predictions are formed by inserting eqs(3.11) and (3.12) into (2.31) and (2.33) or (4.7) and then finding the unknown coefficients in the equations for ϵ_R^* and μ_R^* that produces the least square error. In figure 3.2 the experimental results are given for a barium titanate compound and cross-linked polystyrene. These samples required 21 and 40 iterations respectively.

The difference between the predicted S-parameter and the observed values reveals the presence of systematic uncertainty, as shown in figure 3.3, in the automatic network analyzer (ANA). Additional tests revealed the source of the systematic error did not appear to be related to the material tested in the waveguide. In fact, uncertainties produced for the cross-linked polystyrene sample closely resemble the S-parameter data for an empty waveguide;

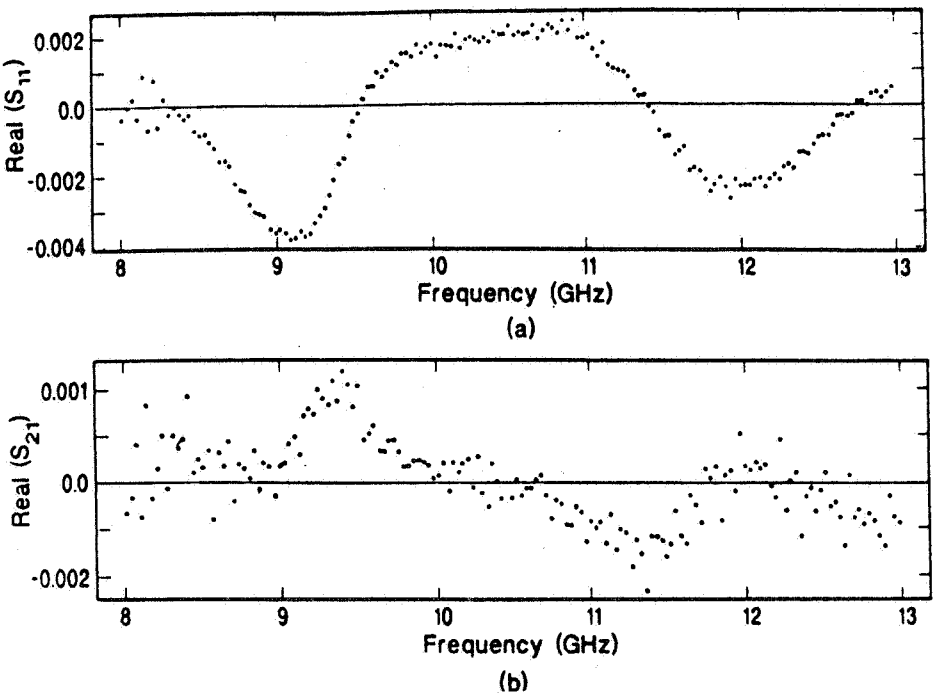

Figure 3.3: Systematic uncertainty as indicated by the residual plot (the difference between the observed and predicted values) for the case on an empty waveguide. The solid line is at 0 residual.

we conclude therefore that much of the systematic error is due to calibration uncertainty and joint losses at connector interfaces. For the barium titanate compound sample there is both the fundamental mode response and smaller resonances related to higher-order modes. As shown in figure C.1, the model interpolates a fundamental mode. This raises the possibility of extending the model to incorporate higher-order modes by extending the theoretical formulation of the problem.

It is easy to move the sample in the holder inadvertently when connecting the sample holder to the port cables. Positioning errors of the sample in the air line can result in large error in computed material parameters. The numerical algorithm can adjust for positioning errors by adjusting L_1 or L_2 slightly. The effects of positioning error can be seen in figure 3.4.

In this example the routine predicted that the position of the sample was off by 0.8 mm.

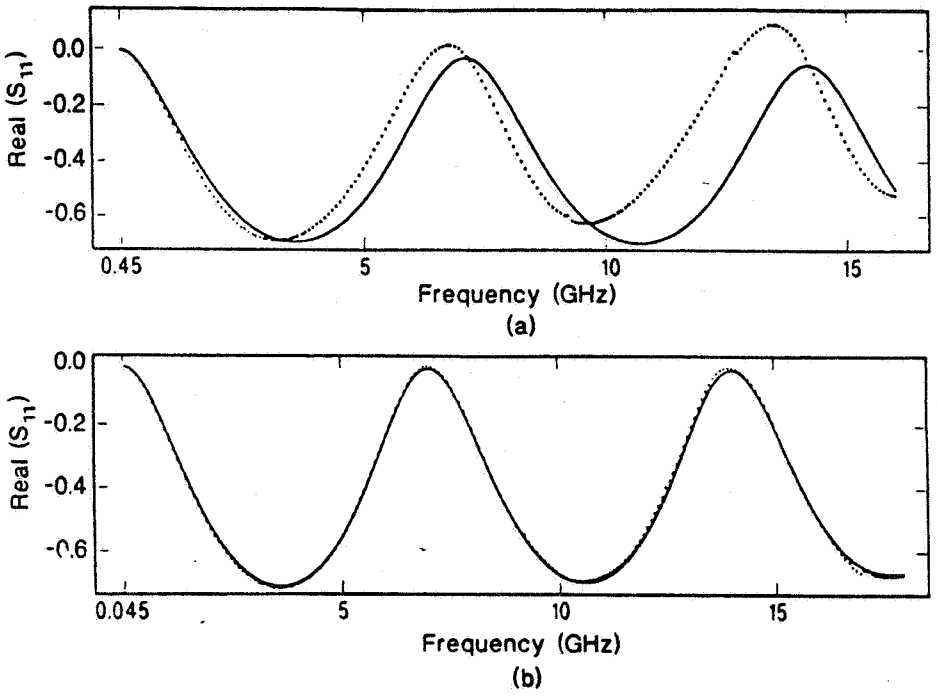

Figure 3.4: Measured real part of S_{11}, measured (. . . .) and predicted (———), for a glass sample (a) with positioning error for L_1 and (b) the solution when the algorithm adjusts for the positioning error.

3.4 Permittivity and Permeability

3.4.1 Measurements

In this section we present the measured and calculated permittivity and permeability. Cross-linked polystyrene and the barium titanate compound are nonmagnetic and therefore $\mu_R^* = 1$. Comparison of the optimized solution to a point-by-point solution is shown in figure 3.5. In figures 3.6 through 3.9 results for four samples are given.

As a check we made an independent measurement of the barium titanate compound in an X-band cavity where the results were $\epsilon_R' = 269$ at 10 Ghz. This result can be compared to the results in figure 3.6. Finally a result of another barium titanate compound is given below.

3.4.2 Robustness of the Procedure

Since the transmission coefficient contains a periodic component, there is more than one solution to the system of equations. Each root of the equation has a neighborhood around which convergence will occur for initial guesses in that region. The robustness of a mathematical procedure is related to how well the algorithm treats the neighborhood around the

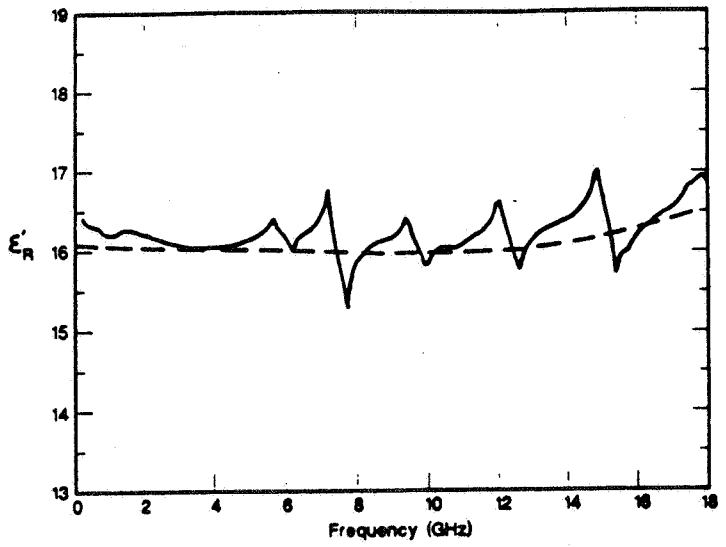

Figure 3.5: Permittivity in the frequency range of $0.045 - 18$ Ghz for the optimized solution (- - - -) and point-by-point technique (——).

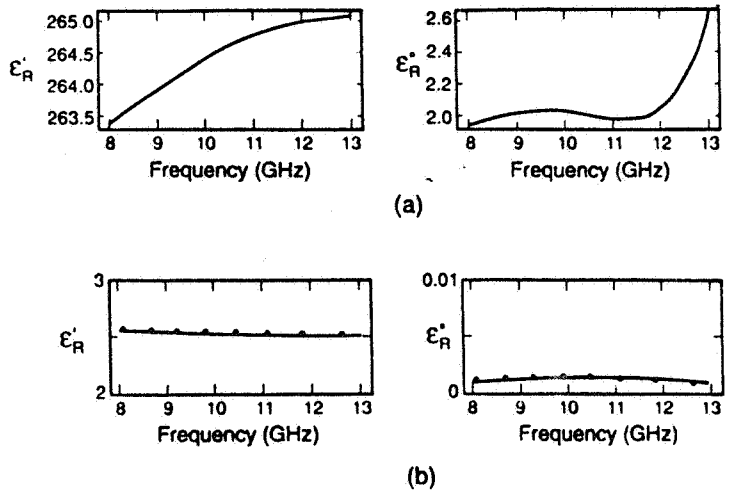

Figure 3.6: Permittivity for barium titanate compound (a) and cross- linked polystyrene (b), point-by-point method (. . . .), optimized solution (——).

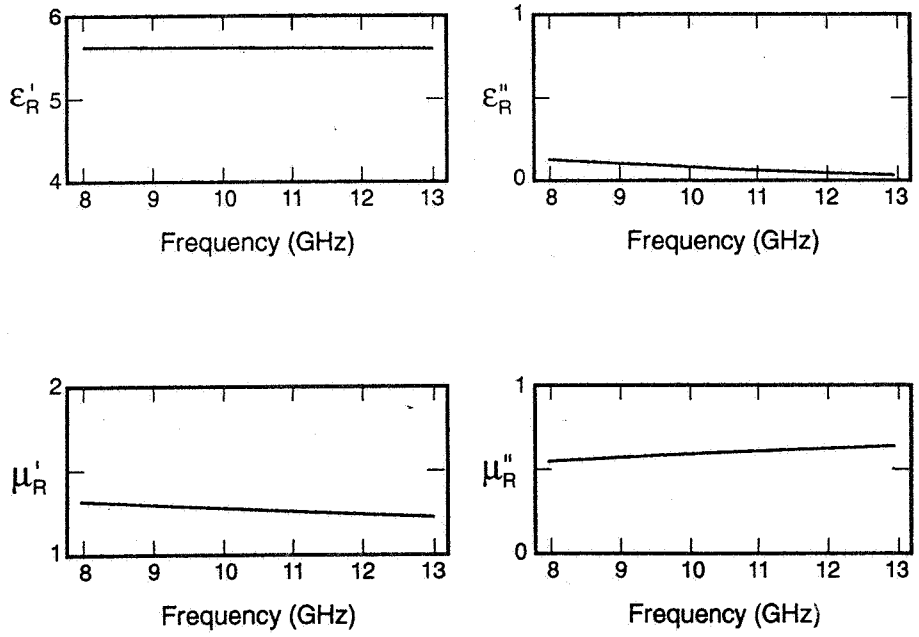

Figure 3.7: Permittivity and permeability for a loaded-polymer, point-by-point method (. . . .) , optimized solution (——).

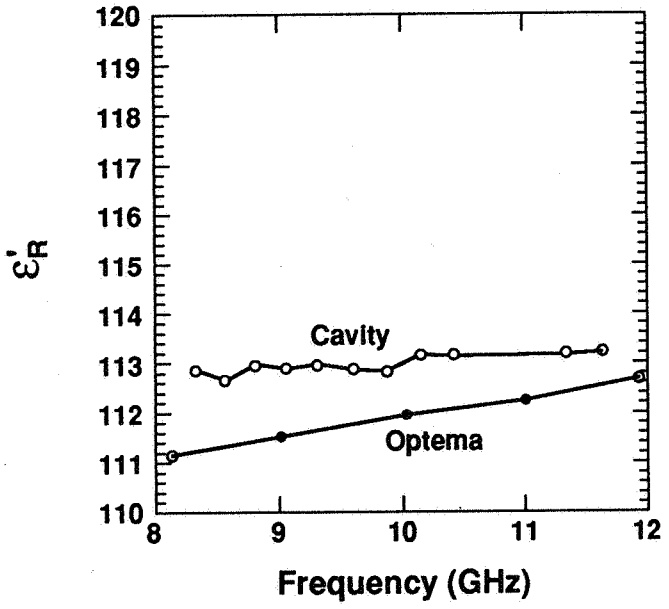

Figure 3.8: Real part of permittivity for a barium titanate compound (o o o) cavity (. . .) optimized solution.

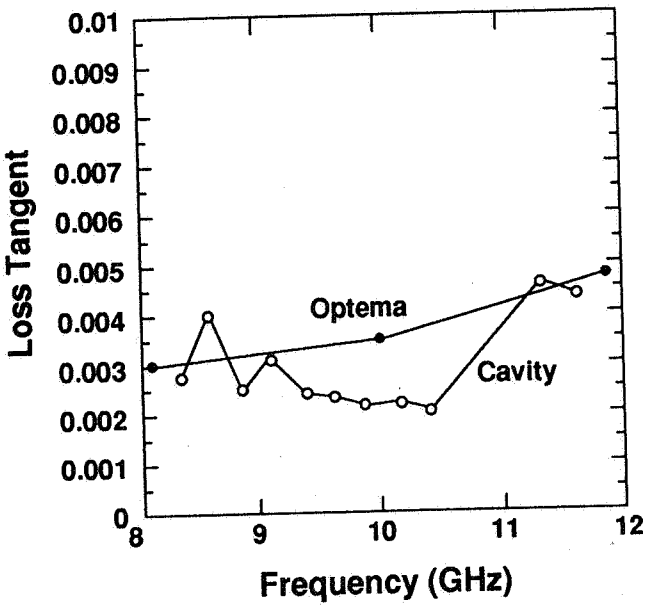

Figure 3.9: Imaginary part of permittivity for a barium titanate compound o o o -cavity and . . . - optimized solution.

correct root. The existence of alternative optima in the mathematical model requires an accurate initial guess in order to converge to the correct solution. Typically convergence occurs after about seven iterations. The use of constraints and the large number of equations enhances the uniqueness of the solution by reducing the dimensions of the solution space.

In point-by-point methods the correct solution is selected from the infinity of possible roots by calculating the slope of the phase curve and comparing the measured and calculated group delays. A group delay constraint is also used as a way of determining the physical solution.

The numerical effectiveness of the entire permeability and permittivity calculation depends on the robustness of the ODRPACK procedure and, more significantly, the robustness of the mathematical model. For the samples used in this study, the robustness of the procedure depended on the sample. For the materials with low dielectric constant the procedure readily determined a solution for a variety of input values with a large radius of convergence. For materials with higher dielectric constant, the procedure often converged quickly, although the existence of alternative local optima in the mathematical model required some testing to make sure that the converged root was the correct root.

3.5 Discussion

An optimization approach to the solution of the scattering equations appears to be a viable alternative to point-by-point techniques. The technique allows a stable solution for a broad range of frequencies. The method works particularly well for short-circuit line measurements. Unlike the point-by-point short-circuit method which requires measurements on two samples or in two positions, the optimized solution can obtain complex permittivity and permeability on a single sample at a single position.

The reflection (S_{11}) data are usually of lesser quality than the transmission data (S_{21}) for low-loss, low- permittivity materials. Therefore S_{11} need not be included in the solution for low-loss materials. However, reflection data S_{11} and S_{22} are very useful in determining the position of the sample in the air line as indicated in figure 3.7. The technique was successful for many isotropic magnetic and relatively high dielectric constant materials. The addition of constraints to the solution is powerful in that it further limits the possible solution range of the system of equations and enhances the uniqueness of the solution. The use of analytic functions for the expansion functions allows a correlation between the real and imaginary parts of the permittivity and permeability. The results shown in figures 3.5 through 3.6 indicate that the method can be used to reduce scattering data of fairly high dielectric constant materials. In fact, in some cases the optimized procedure yields solutions when the point-by-point technique fails completely.

Why does an optimization approach, in many cases, reliably reduce data on higher dielectric constant materials ($\epsilon'_R > 20$), whereas point-by-point techniques generally fail? Scattering data for higher dielectric constant materials contain responses to both primary mode and higher order modes. As indicated in figure 3.2 for the barium titanate compound, the optimization routine selects the primary mode data and places less weight on the higher mode resonance data.

The optimized technique can be used to treat problems where sample lengths, sample holder lengths, and sample positions are not known to high accuracy. Permittivity and permeability can be found from the equations without specifying either sample position or sample length. This result could find application to high-temperature measurements.

Higher-order modes propagate in samples when two conditions are met. The frequencies must be above cutoff in the sample, and there must be inhomogeneities or asymmetries in the sample to excite the higher order modes. Higher-order modes can be incorporated into this type of model by letting the optimization routine select the power in each mode. Higher-order mode models are a subject of our current research.

Chapter 4

Short-Circuit Line Methods

4.1 Theory

In this section we review the mathematical formalism for short-circuit measurements. We consider a measurement of the reflection coefficient (S_{11} for a shorted two-port) as a function of frequency. We begin with a mathematical analysis of the electromagnetic fields in the sample. The details of the field model have been presented previously [26] and only the most essential details will be presented here.

Assumptions on the electric fields in regions I, II, and III shown in figure 4.1 may be made as follows: (1) only the dominant mode is present in the waveguide; (2) the materials are homogeneous and isotropic; (3) only transverse electric fields are present. Under these conditions the electric fields in these regions may be expressed as:

$$E_I = \exp(-\gamma_0 z) + S_{11}\exp(\gamma_0 z) \ , \tag{4.1}$$

$$E_{II} = C_2\exp(-\gamma z) + C_3\exp(\gamma z) \ , \tag{4.2}$$

$$E_{III} = C_4\exp(-\gamma_0(z-L)) + C_5\exp(\gamma_0(z-L)) \ . \tag{4.3}$$

We wish to determine the coefficients in eqs (4.1) through (4.3) by imposing boundary conditions on the system of equations. The boundary conditions are:

- Tangential component of the electric field is continuous at sample interfaces.
- Tangential component of the magnetic field is continuous at sample interfaces.
- The electric field is null at the short-circuit position (perfect reflect).

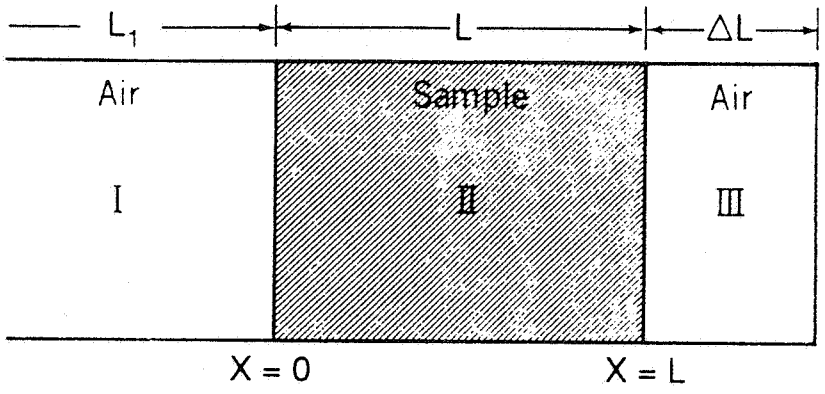

Figure 4.1: A transmission line with a short-circuit termination.

Expressions for the coefficients in eqs (4.1) through (4.3) are presented in reference [26].

Matching boundary conditions of the field equations at the interface and the reflect yields an equation for the permittivity and permeability in terms of the reflection coefficient, $\rho = S_{11} = C_1$. With the sample end face located a distance ΔL from the short,

$$S_{11} = \rho = \frac{-2\beta\delta + [(\delta+1) + (\delta-1)\beta^2]\tanh\gamma L}{2\beta + [(\delta+1) - (\delta-1)\beta^2]\tanh\gamma L} , \tag{4.4}$$

where

$$\beta = \frac{\gamma\mu_o}{\gamma_o\mu} , \tag{4.5}$$

and

$$\delta = \exp(-2\gamma_o\Delta L) . \tag{4.6}$$

In terms of hyperbolic functions

$$S_{11} = \frac{\tanh\gamma L + \beta\tanh\gamma_0\Delta L - \beta(1+\beta\tanh\gamma L\tanh\gamma_0\Delta L)}{\tanh\gamma L + \beta\tanh\gamma_0\Delta L + \beta(1+\beta\tanh\gamma L\tanh\gamma_0\Delta L)} . \tag{4.7}$$

S_{11} for a matched two-port can be obtained as a special case from eq (4.4) by letting $\delta \rightarrow 0$.

Although in the derivation of eq (4.7) it is assumed that the sample plane coincides with the measurement calibration plane, this is not the case in general; however, we can transform the reference plane position by a simple procedure. To accomplish this, we write the most general expression for the reflection coefficient as

$$S_{11(trans)} = R_1^2 S_{11} \ , \tag{4.8}$$

where $S_{11trans}$ is the reflection coefficient at the calibration reference plane position,

$$R_1 = \exp(-\gamma_o L_1) \ , \tag{4.9}$$

and L_1 is the distance from the calibration plane to the sample front face. Equation (4.8) transforms the reflection coefficient from the calibration plane to the plane of sample front face. It is of interest in many applications to eliminate the distance L_1 from eq (4.8). This can be accomplished by measuring S_{11} of the empty sample holder,

$$S_{11(empty)} = -\exp(-2\gamma_o[L_1 + \Delta L + L]) = -\exp(-2\gamma_0 L_{air}) \ , \tag{4.10}$$

and therefore the ratio of the filled to empty holder reflection coefficient is

$$\frac{S_{11(trans)}}{S_{11(empty)}} = -\exp(2\gamma_0[\Delta L + L])S_{11} \ . \tag{4.11}$$

If both the permeability and the permittivity are required, measurement data for two different short-circuit positions are needed. Note that standing waves can be formed in the region between the sample and short-circuit and between the calibration plane and sample front-face. Therefore certain frequencies, depending on sample length and the other lengths, will give better results for permittivity and other frequencies better results for permeability.

The position of the short-circuit is a low electric field and high magnetic field region and a position $\lambda/4$ from the short- circuit is a high electric field and low magnetic field region. Therefore as frequency permits, for permittivity measurements the sample should be moved away from the short-circuit termination. Permeability in isolation can be obtained with the sample at the short-circuit position. Of course when an ANA is used measurements will be taken at many combinations of field strengths and therefore the uncertainty will vary with frequency.

4.1.1 Two Samples of Different Lengths

It is possible to solve for the permeability and permittivity when the scattering parameters with samples of two differing lengths are measured. To see this, let us consider two samples, one of length L and one of length αL as indicated in figure 4.2.

Then for independent measurements on the two samples we have

$$S_{11(1)} = \frac{\Gamma - Z^2}{1 - \Gamma Z^2} \ , \tag{4.12}$$

and

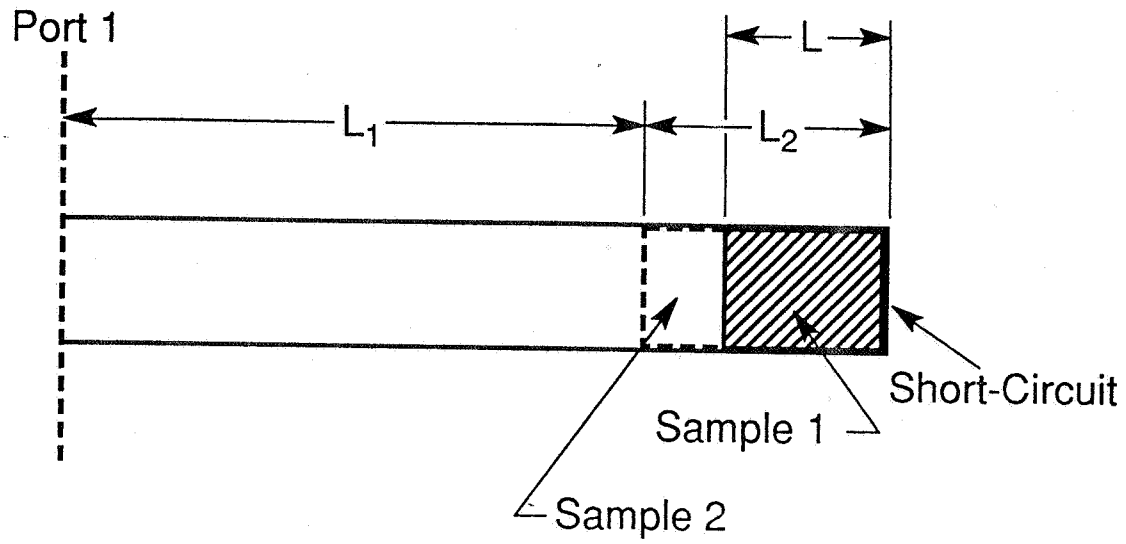

Figure 4.2: A transmission line with a short-circuit termination in two sample magnetic measurements.

$$Z = \exp(-\gamma L) \; . \tag{4.13}$$

The reflection coefficient Γ is given by eq (2.37). The scattering 1-port parameter is given by

$$S_{11(2)} = \frac{\Gamma - Z^{2\alpha}}{1 - \Gamma Z^{2\alpha}} \; . \tag{4.14}$$

Therefore we can solve for Z in eq (4.12),

$$Z^2 = \frac{S_{11(1)} - \Gamma}{S_{11(1)}\Gamma - 1} \; , \tag{4.15}$$

and substitute it into eq (4.14) to obtain

$$S_{11(2)} = \frac{\Gamma - \left[\frac{S_{11(1)}-\Gamma}{S_{11(1)}\Gamma-1}\right]^{\alpha}}{1 - \Gamma\left[\frac{S_{11(1)}-\Gamma}{S_{11(1)}\Gamma-1}\right]^{\alpha}} \; . \tag{4.16}$$

Equation (4.16) is solved iteratively for Γ and then Z is found from eq (4.15). The permittivity and permeability can then be obtained, if we define

$$\frac{1}{\Lambda^2} = -[\frac{1}{2\pi L}\ln(\frac{1}{Z})]^2 \; , \tag{4.17}$$

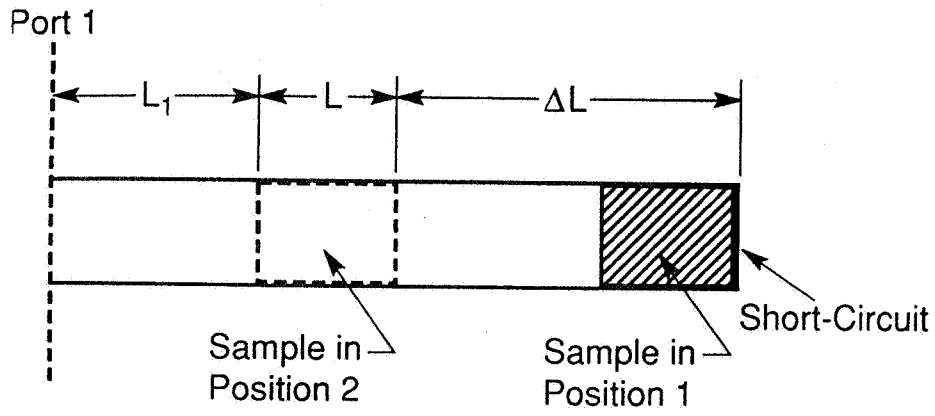

Figure 4.3: A transmission line with a short-circuit termination for two-position measurements.

$$\epsilon_R^* = \frac{\lambda_0^2}{\mu_R^*}[\frac{1}{\lambda_c^2} - \frac{1}{\Lambda^2}] \,, \tag{4.18}$$

$$\mu_R^* = \frac{1+\Gamma}{(1-\Gamma)\Lambda\sqrt{\frac{1}{\lambda_0^2} - \frac{1}{\lambda_c^2}}} \,, \tag{4.19}$$

where λ_0 is the free-space wavelength and λ_c is the cutoff wavelength. Equation (4.17) has an infinite number of roots for magnetic materials because the logarithm of a complex number is multi-valued. In order to pick out the correct root it is necessary to compare the measured to the calculated group delay.

4.1.2 Single Sample at Two Short-Circuit Positions

It is possible to obtain an explicit solution to eq (4.4) when measurements at two different short-circuit positions are taken. The explicit solution is obtained by solving eq (4.4) at a given short-circuit position (position 1) for $\tanh \gamma L$ and then substituting this expression into eq (4.4) at another short-circuit position (position 2) as indicated in figure 4.3.

For two different short-circuit positions at the same frequency we obtain ρ_1 and ρ_2 for positions 1 and 2:

$$\rho_1 = \frac{2\beta\delta_1 - [(\delta_1+1)+(\delta_1-1)\beta^2]\tanh\gamma L}{-2\beta + [(\delta_1-1)\beta^2-(\delta_1+1)]\tanh\gamma L}\,, \tag{4.20}$$

$$\rho_2 = \frac{2\beta\delta_2 - [(\delta_2+1)+(\delta_2-1)\beta^2]\tanh\gamma L}{-2\beta + [(\delta_2-1)\beta^2-(\delta_2+1)]\tanh\gamma L}\,, \tag{4.21}$$

where δ_1, δ_2 denote the phases calculated from eq (4.6) for $\Delta L_1, \Delta L_2$ respectively. These equations yield

$$\tanh\gamma L = \frac{2\beta(\delta_1+\rho_1)}{\beta^2(\rho_1+1)(\delta_1-1)+(1-\rho_1)(\delta_1+1)}\,, \tag{4.22}$$

$$\gamma = \frac{1}{L}\left(\tanh^{-1}\left[\frac{2\beta(\delta_1+\rho_1)}{\beta^2(\rho_1+1)(\delta_1-1)+(1-\rho_1)(\delta_1+1)}\right] + 2n\pi j\right)\,, \tag{4.23}$$

where n is an integer. Since the arctangent is multi-valued, the correct value of n is determined from the group delay arguments given in section 3.2.1. Also

$$\beta^2 = \frac{\delta_1(\delta_2(\rho_1-\rho_2)+\rho_1\rho_2+1-2\rho_2)-(\delta_2(\rho_1(\rho_2-2)+1)+\rho_2-\rho_1)}{\delta_1(\delta_2(\rho_1-\rho_2)+\rho_1\rho_2+1+2\rho_2)-(\delta_2(\rho_1(\rho_2+2)+1)+\rho_2-\rho_1)}\,. \tag{4.24}$$

Once β is known, eqs(4.22) and (4.24) can be used to find permittivity and permeability.

4.2 Measurements

In the SCL technique the scattering parameter S_{11} is measured broadband, with the sample at a given position in the sample holder. The distance from the sample to the short-circuit termination must be known to a high degree of accuracy. If both permeability and the permittivity are required then the sample must be moved in the line and the S-parameters again taken.

Depending on the position of the short-circuit, the sample may be immersed in either a region of high electric field or high magnetic field. A strong electric field is advantageous for permittivity determination, whereas a strong magnetic field is advantageous for permeability determination. Generally, the sample end will be in a region of high magnetic field when the sample is in closest physical contact with the short. It is possible to take advantage of the fluctuating electric and magnetic field distributions when performing permittivity and permeability measurements. When taking broadband measurements on an ANA it is possible to predict when the sample is immersed in the various field strengths. Then one can select the measurements to be used for permittivity and permeability calculations [35].

Measurements were made on an ANA for various samples. Using eq (4.4) we obtain the permittivity and permeability which are shown in figures 4.4 and 4.5.

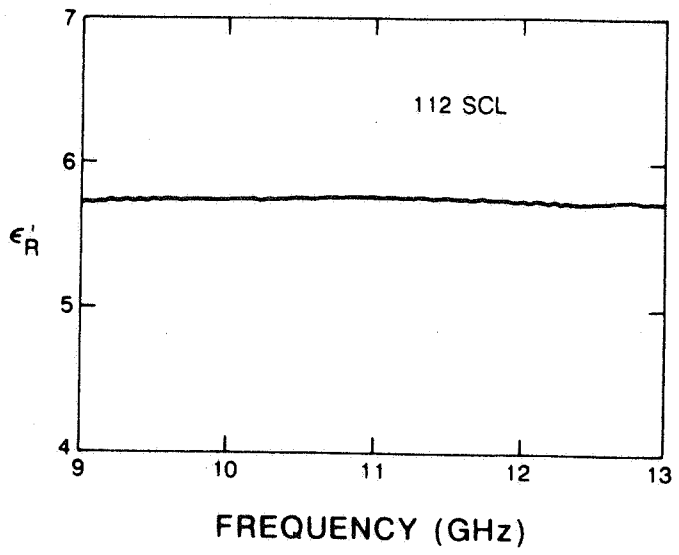

Figure 4.4: ϵ'_R without gap correction using SCL for a loaded polymer mixture.

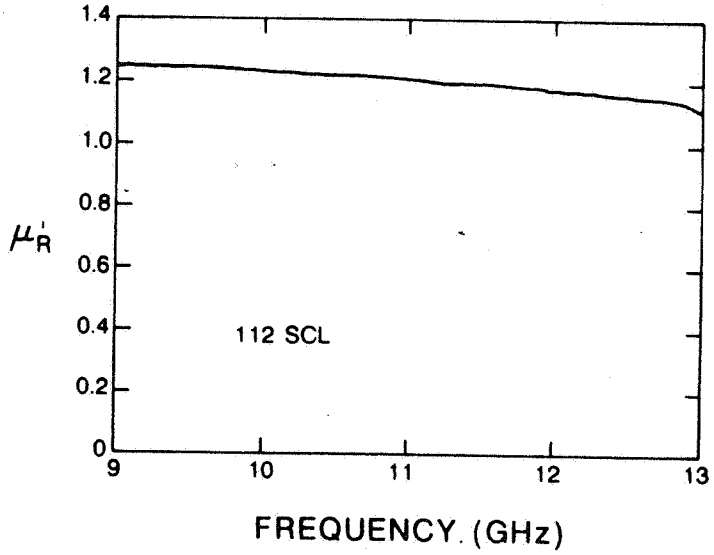

Figure 4.5: μ'_R without gap correction using SCL for a loaded polymer mixture.

4.3 Uncertainty of Short-Circuit Line Measurements

For magnetic materials it is necessary to make two independent measurements at a given frequency. Independent measurements can be obtained either by measuring samples of two different lengths or by taking measurements of a given sample at two locations in the line. The special case of measurement of two samples of varying lengths (L_1, L_2) can be obtained from the solution presented below by substituting $L \rightarrow L_1$, $\gamma_0 \rightarrow \gamma$ and $\Delta L \rightarrow L_2 - L_1$.

The uncertainty involved in two position measurements is explored in this section. The uncertainty incurred with the equations expounded in this report is estimated. The sources of uncertainty in the SCL measurement include

- Uncertainties in measurements of the magnitude and phase of the scattering parameters.
- Gaps between the sample and sample holder.
- Dimensional variations in the sample holder.
- Uncertainty in sample length.
- Short-circuit and line losses and connector mismatch.
- Uncertainty in positions of the reference plane and sample in holder.

Adjustment for errors due to gaps around the sample is obtained from equations available in the literature [33,34,35]. The formulas given in the literature generally under-correct for the real part of the permittivity and over-correct for the imaginary part of the permittivity. All measurements of permittivity are assumed to have been corrected for air gaps around the sample before the following uncertainty analysis is applied.

In order to evaluate the uncertainty introduced by the measured scattering parameters, we assume that a differential uncertainty analysis is applicable. This assumption implies that uncertainties are of small enough magnitude so that a local Taylor series can be applied. We assume that a Taylor series approximates deviations of the function from a given point. We assume that the worst case uncertainty due to the S-parameters and sample lengths can be written

$$\frac{\Delta\epsilon'_R}{\epsilon'_R} = \frac{1}{\epsilon'_R}\sqrt{\left(\frac{\partial\epsilon'_R}{\partial|S_{11}|}\Delta|S_{11}|\right)^2 + \left(\frac{\partial\epsilon'_R}{\partial\theta_{11}}\Delta\theta_{11}\right)^2 + \left(\frac{\partial\epsilon'_R}{\partial L}\Delta L\right)^2 + \left(\frac{\partial\epsilon'_R}{\partial d}\Delta d\right)^2}, \qquad (4.25)$$

$$\frac{\Delta\epsilon''_R}{\epsilon''_R} = \frac{1}{\epsilon''_R}\sqrt{\left(\frac{\partial\epsilon''_R}{\partial|S_{11}|}\Delta|S_{11}|\right)^2 + \left(\frac{\partial\epsilon''_R}{\partial\theta_{11}}\Delta\theta_{11}\right)^2 + \left(\frac{\partial\epsilon''_R}{\partial L}\Delta L\right)^2 + \left(\frac{\partial\epsilon''_R}{\partial d}\Delta d\right)^2}, \qquad (4.26)$$

where $\Delta\theta$ is the uncertainty in the phase of the scattering parameter, $\Delta|S_{11}|$ is the uncertainty in the magnitude of the scattering parameter, Δd is the uncertainty in the air gap around the sample, and ΔL is the uncertainty in the sample length. The gap correction uncertainty is given in [26]. The uncertainties used for the S-parameters depend on the specific ANA used for the measurements. In general uncertainties due to flange bolt torquing and connector repeatability must be added to these uncertainties.

Let us define the variables

$$a = \tanh \gamma L \ , \tag{4.27}$$

$$b = \tanh \gamma_0 \Delta L \ . \tag{4.28}$$

We wish to obtain explicit relations for the derivatives of ϵ_R^* and μ_R^* with respect to independent variables $|S_{11(i)}|$ and θ_i, $i = 1, 2$. We define $S_{11(1)}$ as the reflection at short position 1 and $S_{11(2)}$ as the reflection at short position 2. Next define

$$f = \frac{\tanh \gamma L + \beta \tanh \gamma_0 \Delta L - \beta(1 + \beta \tanh \gamma L \tanh \gamma_0 \Delta L)}{\tanh \gamma L + \beta \tanh \gamma_0 \Delta L + \beta(1 + \beta \tanh \gamma L \tanh \gamma_0 \Delta L)} - S_{11} = 0 \ . \tag{4.29}$$

We assume the following as independent variables $S_{11}(i)$, $i = 1, 2$, L, ΔL, and d. Derivatives of eq (4.29) with respect to the independent variables can be found analytically. By the chain rule we have

$$\underbrace{\left[\frac{\partial f}{\partial a}\frac{\partial a}{\partial \gamma}\frac{\partial \gamma}{\partial \mu_R^*} + \frac{\partial f}{\partial \beta}\frac{\partial \beta}{\partial \mu_R^*}\right]}_{a_1}\frac{\partial \mu_R^*}{\partial |S_{11}(m)|} + \underbrace{\left[\frac{\partial f}{\partial a}\frac{\partial a}{\partial \gamma}\frac{\partial \gamma}{\partial \epsilon_R^*} + \frac{\partial f}{\partial \beta}\frac{\partial \beta}{\partial \epsilon_R^*}\right]}_{a_2}\frac{\partial \epsilon_R^*}{\partial |S_{11}(m)|} = \exp(j\theta_m) \ , \tag{4.30}$$

This equation is evaluated at position one.

$$\underbrace{\left[\frac{\partial f}{\partial a}\frac{\partial a}{\partial \gamma}\frac{\partial \gamma}{\partial \mu_R^*} + \frac{\partial f}{\partial \beta}\frac{\partial \beta}{\partial \mu_R^*}\right]}_{b_{1m}}\frac{\partial \mu_R^*}{\partial |S_{11}(m)|} + \underbrace{\left[\frac{\partial f}{\partial a}\frac{\partial a}{\partial \gamma}\frac{\partial \gamma}{\partial \epsilon_R^*} + \frac{\partial f}{\partial \beta}\frac{\partial \beta}{\partial \epsilon_R^*}\right]}_{b_{2m}}\frac{\partial \epsilon_R^*}{\partial |S_{11}(m)|} = \exp(j\theta_m) \ . \tag{4.31}$$

This equation is evaluated at position two. The four derivatives can be written

$$a_1\frac{\partial \mu_R^*}{\partial |S_{11(m)}|} + a_2\frac{\partial \epsilon_R^*}{\partial |S_{11(m)}|} = \exp(j\theta_m)\delta_{1,m} \ , \tag{4.32}$$

$$b_1\frac{\partial \mu_R^*}{\partial |S_{11(m)}|} + b_2\frac{\partial \epsilon_R^*}{\partial |S_{11(m)}|} = \exp(j\theta_m)\delta_{2,m} \ , \tag{4.33}$$

where $\delta_{i,m}$ is the Kronecker delta function.

At the first position the derivatives with respect to length are

$$[\frac{\partial f}{\partial a}\frac{\partial a}{\partial \gamma}\frac{\partial \gamma}{\partial \mu_R^*} + \frac{\partial f}{\partial \beta}\frac{\partial \beta}{\partial \mu_R^*}]_m \frac{\partial \mu_R^*}{\partial L} + [\frac{\partial f}{\partial a}\frac{\partial a}{\partial \gamma}\frac{\partial \gamma}{\partial \epsilon_R^*} + \frac{\partial f}{\partial \beta}\frac{\partial \beta}{\partial \epsilon_R^*}]_m \frac{\partial \epsilon_R^*}{\partial L} + \frac{\partial f}{\partial a}\frac{\partial a}{\partial L} = 0 \ , \qquad (4.34)$$

or

$$a_1 \frac{\partial \mu_R^*}{\partial L} + a_2 \frac{\partial \epsilon_R^*}{\partial L} + \frac{\partial f}{\partial a}\frac{\partial a}{\partial L} = 0 \ , \qquad (4.35)$$

and for the second short-circuit termination position

$$b_1 \frac{\partial \mu_R^*}{\partial L} + b_2 \frac{\partial \epsilon_R^*}{\partial L} + \frac{\partial f}{\partial a}\frac{\partial a}{\partial L} = 0 \ . \qquad (4.36)$$

The derivatives with respect to the distance from the sample back face to the short-circuit termination can similarly be calculated

$$[\frac{\partial f}{\partial a}\frac{\partial a}{\partial \gamma}\frac{\partial \gamma}{\partial \mu_R^*} + \frac{\partial f}{\partial \beta}\frac{\partial \beta}{\partial \mu_R^*}]_m \frac{\partial \mu_R^*}{\partial \Delta L} + [\frac{\partial f}{\partial a}\frac{\partial a}{\partial \gamma}\frac{\partial \gamma}{\partial \epsilon_R^*} + \frac{\partial f}{\partial \beta}\frac{\partial \beta}{\partial \epsilon_R^*}]_m \frac{\partial \mu_R^*}{\partial \Delta L} + \frac{\partial f}{\partial b}\frac{\partial b}{\partial \Delta L} = 0 \ , \qquad (4.37)$$

$$a_1 \frac{\partial \mu_R^*}{\partial \Delta L} + a_2 \frac{\partial \epsilon_R^*}{\partial \Delta L} + \frac{\partial f}{\partial b}\frac{\partial b}{\partial \Delta L} = 0 \ , \qquad (4.38)$$

and for the second short-circuit position

$$b_1 \frac{\partial \mu_R^*}{\partial \Delta L} + b_2 \frac{\partial \epsilon_R^*}{\partial \Delta L} + \frac{\partial f}{\partial b}\frac{\partial b}{\partial \Delta L} = 0 \ . \qquad (4.39)$$

The derivatives can be calculated explicitly to yield

$$\frac{\partial f}{\partial a} = \frac{1 - \beta^2 \tanh \gamma_0 \Delta L}{\tanh \gamma L + \beta \tanh \gamma_0 \Delta L + \beta(1 + \beta \tanh \gamma L \tanh \gamma_0 \Delta L}) - \frac{\tanh \gamma L + \beta \tanh \gamma_0 \Delta L + \beta(1 + \beta \tanh \gamma L \tanh \gamma_0 L)}{(\tanh \gamma L + \beta \tanh \gamma_0 \Delta L + \beta(1 + \beta \tanh \gamma L \tanh \gamma_0 \Delta L)^2} \times (1 + \beta^2 \tanh \gamma_0 \Delta L) \ , \qquad (4.40)$$

$$\frac{\partial f}{\partial b} = \frac{\beta - \beta^2 \tanh \gamma L}{\tanh \gamma L + \beta \tanh \gamma_0 \Delta L + \beta(1 + \beta \tanh \gamma L \tanh \gamma_0 \Delta L}) - \frac{\tanh \gamma L + \beta \tanh \gamma_0 \Delta L + \beta(1 + \beta \tanh \gamma L \tanh \gamma_0 L)}{(\tanh \gamma L + \beta \tanh \gamma_0 \Delta L - \beta(1 + \beta \tanh \gamma L \tanh \gamma_0 \Delta L)^2} \times (\beta + \beta^2 \tanh \gamma L) \ , \qquad (4.41)$$

$$\frac{\partial f}{\partial \beta} =$$

$$\frac{\tanh\gamma_0\Delta L - 1 - 2\beta\tanh\gamma L\tanh\gamma_0 L}{\tanh\gamma L + \beta\tanh\gamma_0\Delta L + \beta(1+\beta\tanh\gamma L\tanh\gamma_0\Delta L}) \\ -\frac{\tanh\gamma L + \beta\tanh\gamma_0\Delta L + \beta(1+\beta\tanh\gamma L\tanh\gamma_0 L)}{(\tanh\gamma L + \beta\tanh\gamma_0\Delta L - \beta(1+\beta\tanh\gamma L\tanh\gamma_0\Delta L)^2} \times$$

$$(\tanh\gamma_0\Delta L + 1 + 2\beta\tanh\gamma L\tanh\gamma_0\Delta L) \; . \tag{4.42}$$

The following derivatives will be needed in the forthcoming analysis

$$\frac{\partial a}{\partial \gamma} = L\mathrm{sech}^2\gamma L \; , \tag{4.43}$$

$$\frac{\partial \gamma}{\partial L} = \gamma\mathrm{sech}^2\gamma L \; , \tag{4.44}$$

$$\frac{\partial b}{\partial \Delta L} = \gamma_0\mathrm{sech}^2\gamma_0\Delta L \; , \tag{4.45}$$

$$\frac{\partial \beta}{\partial \gamma} = \frac{1}{\mu_R^*\gamma_0} \; , \tag{4.46}$$

$$\frac{\partial \beta}{\partial \mu_R^*} = \frac{\partial \gamma}{\partial \mu_R^*}\frac{1}{\mu_R^*\gamma_0} - \frac{\gamma}{\gamma_0}\frac{1}{\mu_R^{*2}} \; , \tag{4.47}$$

$$\frac{\partial \beta}{\partial \epsilon_R^*} = \frac{\partial \gamma}{\partial \epsilon_R^*}\frac{1}{\epsilon_R^*\gamma_0} - \frac{\gamma}{\gamma_0}\frac{1}{\epsilon_R^{*2}} \; , \tag{4.48}$$

$$\frac{\partial \beta}{\partial \epsilon_R^*} = \frac{\partial \gamma}{\partial \epsilon_R^*}\frac{\partial \beta}{\partial \gamma} \; , \tag{4.49}$$

$$\frac{\partial \beta}{\partial \epsilon_R^*} = \frac{\partial \gamma}{\partial \epsilon_R^*}\frac{1}{\mu_R^*\gamma_0} \; , \tag{4.50}$$

$$\frac{\partial \gamma}{\partial \mu_R^*} = -\frac{\omega^2/c_{vac}^2\epsilon_R^*}{2\gamma} \; , \tag{4.51}$$

$$\frac{\partial \gamma}{\partial \epsilon_R^*} = -\frac{\omega^2/c_{vac}^2\mu_R^*}{2\gamma} \; , \tag{4.52}$$

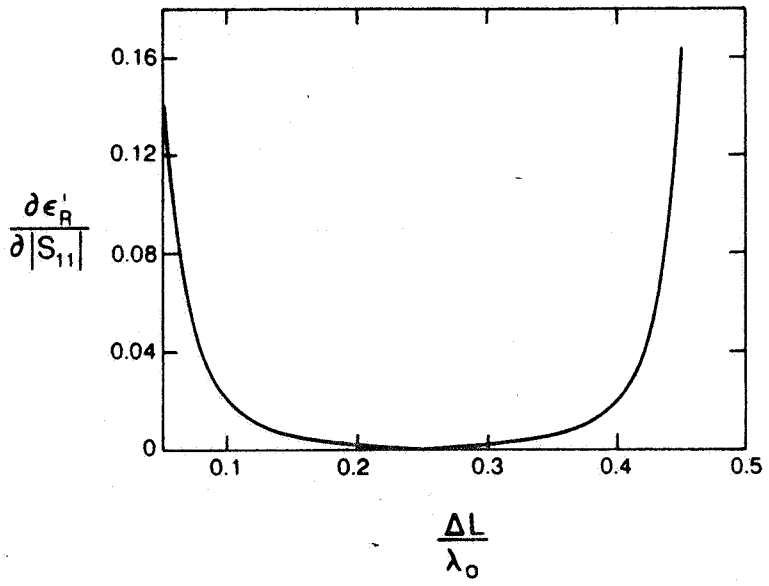

Figure 4.6: A plot of the derivative of ϵ_R' with respect to $|S_{11}|$ as a function of the distance from the short-circuit termination for the case of thin samples $L \ll \lambda_m$.

$$\frac{\partial \mu_R^*}{\partial \theta_i} = -j|S_{11(i)}|\frac{\partial \mu_R^*}{\partial |S_{11(i)}|}\ , \tag{4.53}$$

$$\frac{\partial \mu_R^*}{\partial |S_{11}|} = -\frac{b_2}{b_1}\frac{\partial \epsilon_R^*}{\partial |S_{11(1)}|}\ , \tag{4.54}$$

$$\frac{\partial \epsilon_R^*}{\partial |S_{11(1)}|} = \frac{\exp(j\theta_1)b_1}{a_2b_1 - a_1b_2}\ , \tag{4.55}$$

$$\frac{\partial \mu_R^*}{\partial |S_{11(2)}|} = -\frac{a_2}{a_1}\frac{\partial \epsilon_R^*}{\partial |S_{11(2)}|}\ , \tag{4.56}$$

$$\frac{\partial \epsilon_R^*}{\partial |S_{11(2)}|} = -\frac{\exp(j\theta_2)a_1}{a_2b_1 - a_1b_2}\ . \tag{4.57}$$

In figures 4.6 and 4.7 $\partial \epsilon_R^*/\partial |S_{11}|$ is plotted as a function of the distance from the short circuit termination. We see that in the case of electrically thin samples the minimum uncertainty occurs when the second sample measurement is at $\lambda_0/4$ from the short-circuit termination. As shown in figure 4.7, this is not the case for samples that are not electrically thin.

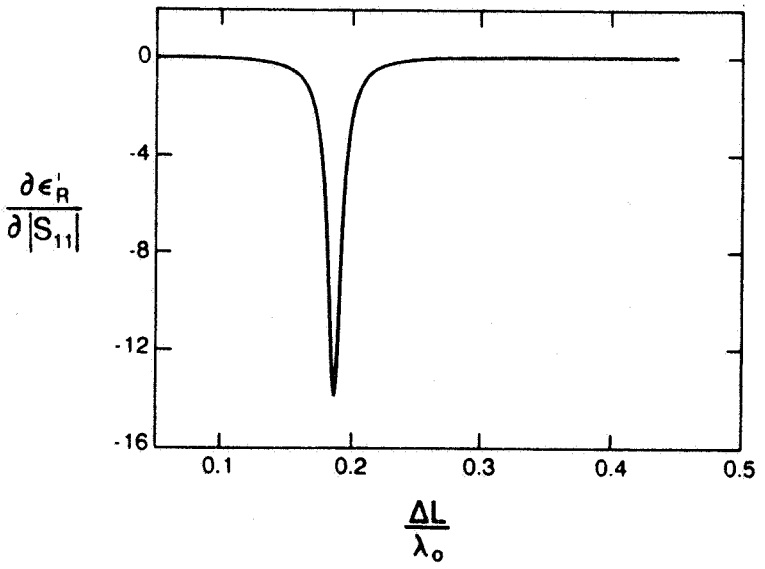

Figure 4.7: A plot of the derivative of ϵ'_R with respect to $|S_{11}|$ as a function of the distance from the short-circuit termination for the case of long samples $L \approx \lambda_m$.

Chapter 5

Discussion

We have presented an overview of the theory and the measurements for both the TR method and the SCL method for dielectric and magnetic materials. In addition, relevant uncertainty analyses have been developed. Equations were presented for TR and SCL measurements that are reference plane invariant. These equations can be solved either by iteration or explicitly.

There are two common problems in the data reduction techniques for transmission line measurements. These problems are the existence of higher mode resonances and the problem that for low- loss materials the solution of the equations become ill-conditioned at integral multiples of one-half wavelength in the sample. The one-half wavelength instability occurs because the phase of S_{11} contains a large uncertainty when $|S_{11}| \rightarrow 0$ and also because the equations in this limit yield only the phase velocity. For dielectric and magnetic measurements, the uncertainty is a function of the sample length. In general for low-loss materials, samples long in relation to wavelength give more accurate results, however overmodes may be produced. Thus for broadband measurements of low-loss low-dielectric materials, it is preferable to use longer samples. However, with lossy materials, very long samples result in only front face reflection information and the results have a relatively large uncertainty. For relatively lossy materials, sample lengths on the order of one attenuation length are optimum. Longer samples allow the propagation of higher order modes, and therefore higher mode responses will be contained in measured scattering data. However, the uncertainty in the spectrum between over-moded resonance regions will be lower for longer samples than for electrically short samples.

For thicker samples the problem is more complicated and a knowledge of the uncertainty analysis is important for interpreting the results. For permeability measurements in a short-circuit line the numerical reduction procedure becomes divergent when there is an integral multiple of one-half wavelength in the sample. For TR and SCL measurements we can summarize our conclusions as follows

- For SCL measurements, length of samples should be such that $|S_{11}| \geq -20$ dB.
- The one-sample techniques appear to allow a better reduction of the scattering data.
- The optimized solution and the reference plane invariant solution appear to be the most accurate and stable methods. However, local minima have to be avoided.
- The short-circuit line is a simple way to obtain permittivity and permeability simultaneously. For low-loss materials it does suffer from numerical instabilities.
- In SCL permittivity measurements, minimum uncertainty is obtained when the sample is $\lambda/4$ from the short. This is only true for electrically thin samples.
- Minimum uncertainty magnetic measurements can be made for single frequency measurements by taking one measurement at a maximum electric field position and another measurement at a maximum magnetic field position.

The various TR and SCL techniques are compared in table 5.1 and 5.2.

Table 5.1: Dielectric and magnetic TR measurement techniques compared.

Technique	Applicability	Strong Points	Weak Points
Full 2-port, one sample	Dielectric	Requires one sample	———
Full 2-port, one sample	Magnetic	Requires one sample	Unstable at $n\lambda_m/2$
NRW Technique	Magnetic	Simple Solution	Unstable at $n\lambda_m/2$
Two-Position Technique	Magnetic	———	Doesn't exist for TR techniques
Two sample technique	Magnetic	Stable over all frequencies	Requires two samples
Multi-point techniques	Magnetic	Very stable	non-global minima

Table 5.2: Dielectric and magnetic SCL measurement techniques compared.

Technique	Applicability	Strong Points	Weak Points
One-position Technique	Dielectric	Stable	—
Two-Position Technique	Magnetic	Requires only one sample	Unstable at $n\lambda_m/2$
Two sample technique	Magnetic	Stable over all frequencies	Requires two samples
Multi-point techniques	Magnetic	Very stable	Alternative minima

We would like to thank Eleanor Livingston for her excellent comments and suggestions, Paul Domich for collaboration on the optimized solution, Chris Jones for help with measurements and plotting, William Kissick, Claude Weil, and Howard Bussey for various discussions and as sources of encouragement. Finally we would like to thank Ramon Jesch, Bill Daywitt, and Lydell Frasch for reviewing the manuscript.

References

[1] Belhadj-Tahar, N.; Fourrier-Lamer, A.; and de Chanterac, H., "Broadband simultaneous measurement of complex permittivity and permeability using a coaxial discontinuity," *IEEE Trans. Microwave Theory Tech.*, vol. 2, pp. 1–7, January 1990.

[2] Deschamps, G. A., "Determination of reflection coefficients and insertion loss of a wave-guide junction," *J. Appl. Phys.*, vol. 2, pp. 1046-1050, August 1953.

[3] "Measuring dielectric constant with the HP 8510 network analyzer," Product note no. 8510-3, Hewlett Packard, 1985.

[4] Freeman, M. S.; Nottenburg, R. N.; and DuBow, J. B., "An automated frequency domain technique for dielectric spectroscopy of materials," *J. Phys. E: Sci. Instrum.*, vol. 12, pp. 899–903, 1979.

[5] Nicolson, A. M.; and Ross, G. F., "Measurement of the intrinsic properties of materials by time domain techniques," *IEEE Trans. Instrum. Meas.*, vol. IM-19, pp. 377–382, November 1970.

[6] Weir, W. B., "Automatic measurement of complex dielectric constant and permeability at microwave frequencies," *Proc. IEEE*, vol. 62, pp. 33-36, January 1974.

[7] Stuchly, S.; and Matuszewski, M., "A combined total reflection transmission method in application to dielectric spectroscopy," *IEEE Trans. Instrum. Meas.*, vol. IM-27, pp. 285–288, September 1978.

[8] Delecki, Z. A.; and Stuchly, S. S., "Uncertainties in the determination of dielectric properties in the infinite sample method," *IEEE Trans. Instrum. Meas.*, vol. 38, pp. 902–906, June 1989.

[9] Franceschetti, G., "A complete analysis of the reflection and transmission methods for measuring the complex permeability and permittivity of materials at microwave," *Alta Frequenzia*, vol. 36, pp. 757–764, August 1967.

[10] Ligthardt, L. P., "A fast computational technique for accurate permittivity determination using transmission line methods," *IEEE Trans. Microwave Theory Tech.*, vol. MTT-31, pp. 249-254, March 1983.

[11] Roberts, S.; and von Hippel, A., "A new method for measuring dielectric constant and loss in the range of centimeter waves," *J. Appl. Phys.*, vol. 7, pp. 610–616, July 1946.

[12] Brydon, G. M.; and Hepplestone, D. J., "Microwave measurements of permittivity and $\tan\delta$ over the temperature range $20 - 700°C$," *Proc. Inst. Elec. Eng.*, vol. 112, pp. 421–425, 1965.

[13] Szendrenyi, B. B.; Kazi, K.; and Mojzes, I., "An alternative broadband method for automatic measurement of the complex permeability and permittivity of materials at microwave frequencies," *Microwave Theory and Tech. Digest*, vol. 1, no. 1, pp. 743–745, 1988.

[14] Mattar, K. E.; and Brodwin, M. E., "A variable frequency method for wide-band microwave material characterization," *IEEE Trans. Instrum. Meas.*, vol. 39, pp. 609–614, August 1990.

[15] Maze, G.; Bonnefoy, J. L.; and Kamarei, M., "Microwave measurement of the dielectric constant using a sliding short-circuited waveguide method," *Microwave J.*, pp. 77- -88, October 1990.

[16] Dakin, T. W.; and Works, C. N., "Microwave dielectric measurements," *J. Appl. Phys.*, vol. 18, pp. 789–796, September 1947.

[17] Bowie, D. M. and Kelleher, K. S., "Rapid measurement of dielectric constant and loss tangent," *IEE Trans. Microwave Theory Tech.*, vol. MTT-4, pp. 137–140, 1956.

[18] Sequeira, H. B., "Extracting μ_r and ϵ_r from one- port phasor network analyzer measurements," *IEEE Trans. Instrum. Meas.*, vol. 39, pp. 621–627, August 1990.

[19] Chao, S., "An uncertainty analysis for the measurement of microwave conductivity and dielectric constant by the short- circuited line method," *IEEE Trans. Instrum. Meas.*, vol. IM-35, pp. 36–41, March 1986.

[20] Miles, P. A., Westphal, W. P. and von Hippel, A., "Dielectric spectroscopy of ferromagnetic semiconductors," *Rev. Mod. Phys.*, vol. 29, no. 3, pp. 279–307, 1957.

[21] Solymar, L. and Walsh, D., *Lectures on Electrical Properties of Materials.* New York: Oxford University Press, 1988.

[22] Ramo, S., Whinnery, J. R. and Duzer, T. V., *Fields and Waves in Communication Electronics.* New York: John Wiley and Sons, 1984.

[23] Gilbert, T. A., "Constitutive relations," Tech. Rep., Armour Research Foundation, 1955.

[24] Hord, W. E., *Ferrite Control Components*, pp. 238–272. John Wiley and Sons, 1989.

[25] Soohoo, R. F, *Theory and Application of Ferrites.* Englewood Cliffs, NJ: Prentice-Hall, Inc., 1960.

[26] Baker-Jarvis, J., "Transmission/reflection and short-circuit line permittivity measurements," Nat. Inst. Stand. Tech. (U.S.), Tech. Note 1341, 1990.

[27] Baker-Jarvis, J., Vanzura, E. and Kissick, W. "Improved technique for determining complex permittivity with the transmission/reflection method," *IEEE Trans. Microwave Theory Tech.*, vol. 38, pp. 1096–1103, August 1990.

[28] Kerns, D. M. and Beatty, R. W., *Basic Theory of Waveguide Junctions and Introductory Microwave Network Analysis.* New York: Pergamon Press, 1967.

[29] Rasmussen, A. L., Enfield, A. W. and Hess, A. "Advances in the design and application of the radiofrequency permeameter," *Nat. Bur. Stand. (U.S.) J. Res.*, vol. 56, no. 5, pp. 261–267, 1960.

[30] Hoer, C. A. and Rasmussen, A. L., "Equations for the radiofrequency magnetic permeameter," *Nat. Bur. Stand. (U.S.) J. Res.*, vol. 67C, no. 1, pp. 69–76, 1963.

[31] Powell, R. C. and Rasmussen, A. L., "A radio-frequency permittimeter," *IRE Trans. Instrum.*, vol. I-9, no. 2, pp. 179–184, 1960.

[32] Goldfarb, R. B. and Bussey, H. E., "Method for measuring complex permeability at radio frequencies," *Rev. Sci. Instrum.*, vol. 58, no. 4, pp. 624–627, 1987.

[33] Bussey, H. E., "Measurement of rf properties of materials a survey," *Proc. IEEE*, vol. 55, pp. 1046–1053, June 1967.

[34] Westphal, W. P., "Techniques of measuring the permittivity and permeability of liquids and solids in the frequency range 3 c/s to 50 kmc/s," Laboratory for Insulation Res. Tech. Report, MIT. 1950.

[35] Bussey, H. E.; and Gray, J. E., "Measurement and standardization of dielectric samples," *IRE Trans. Instrum.*, vol. I-11, no. 3, pp. 162–165, 1962.

[36] Domich, P. A.; Baker-Jarvis J.; and Geyer, R. G., "Optimization techniques for permittivity and permeability determination," J. Res.,vol. 96, no. 5, pp. 565–575, 1991.

[37] Wallin, S. R., *Dielectric Properties of Heterogeneous Media.* PhD thesis, University of Wyoming, 1985.

[38] Papoulis, A., *Signal Analysis.* New York: McGraw-Hill, 1977.

[39] Boggs, P. T.; Donaldson, J. R; Byrd, R. H.; and Schnabel, R. B., "ALGORITHM 676 ORDPACK: software for weighted orthogonal distance regression," *ACM Trans. Math. Software*, vol. 15, no. 4, pp. 348–364, 1989.

[40] Marcuvitz, N., *Waveguide Handbook.* New York: Dover Publications, 1951.

[41] Champlin, K. S.; and Glover, G. H, "Influence of waveguide contact on measured complex permittivity of semiconductors," *J. Appl. Phys.*, vol. 37, pp. 2355–2360, May 1966.

[42] Schwinger, J. and Saxon, D. S., *Discontinuities in Waveguides.* New York: Gordon and Breach Science Publishers, 1968.

[43] Jesch, R. L., "Dielectric measurements of five different soil textural types as functions of frequency and moisture content," Nat. Bur. Stand. (U.S.) Tech. Rep., 1978.

[44] Jesch, R. L., "Dielectric measurements of oil shale as functions of temperature and frequency," *IEEE Trans. Geosci. Remote Sensing*, vol. GE-22, pp. 99–105, March 1984.

[45] Ben-Menahem, A. and Singh, S. J., *Seismic Waves and Sources.* New York: Springer-Verlag, 1981.

Chapter 7

Appendices

Appendix A

Magnetism in Matter

A.1 Description of Magnetic Phenomena

The origin of magnetism is related to the electrostatic coulomb repulsion between electrons and is intimately related to the spin and orbital angular momentum of electrons, nuclei, and other charged particles. Stern and Gerlach proved the existence of discrete magnetic moments by observing the deflection of silver atoms passing through a spatially varying magnetic field. The quantum mechanical relation between magnetic moment and angular momentum of an electron is $\vec{m}_J = -g\frac{e\hbar}{2m}\vec{J}$, where g is the Lande *g-factor* ≈ 2.002319114, $\frac{e\hbar}{2m} = 9.2742 \times 10^{-24}\ (J - m^2/W)$ is the *Bohr magneton*, $\vec{J}$ is the total quantum mechanical angular momentum, e is the electronic charge, $\hbar$ is Planck's constant, and m is the mass. The gyromagnetic ratio is defined as

$$\gamma_g = \frac{\text{magnetic dipole moment}}{\text{angular momentum}} = g\frac{e}{2m}\ . \tag{A.1}$$

There is a diversity of magnetic phenomena due to the existence of various coupling schemes of angular momenta quanta. Types of magnetism include *paramagnetism*, which is due to spin and angular momentum of individual electrons, *diamagnetism* which has its origin in the orbital angular momentum of the electron, and *ferromagnetism* originates from the formation of domains with each domain containing a large number of aligned spins.

A.1.1 Field Description of Electromagnetic Phenomena

It has been found that dielectric and magnetic phenomena are adequately described by a set of field vectors. These vectors represent the electric field, $\vec{E}$ and magnetic field, $\vec{H}$, the displacement field, $\vec{D}$, the induction field, $\vec{B}$, the polarization field, $\vec{P}$, and magnetization

field $\vec{M}$. Maxwell's equations define the spatial and temporal evolution of these field vectors. Constitutive relations between field quantities and material properties are necessary to describe electromagnetic phenomena. The displacement field is related to the electric field by $\vec{D} = \overline{\overline{\epsilon}} \cdot \vec{E}$, where $\overline{\overline{\epsilon}}$ is the permittivity tensor. For linear materials the permittivity does not depend on the field strength. The permittivity is a measure of electronic, ionic, and dipolar polarization. The permittivity is frequency dependent with dipolar polarization occurring below 10^{10} Hz, ionic polarization below 10^{13} Hz, and electronic polarization above 10^{13} Hz. The permittivity of free space is $\epsilon_0 = 8.85419\ F/m$. The magnetic field is related to the induction field by $\vec{B} = \overline{\overline{\mu}} \cdot \vec{H}$, where $\overline{\overline{\mu}}$ is the permeability tensor. The permeability of a material is a measure of the degree to which it allows the penetration by an external magnetic field. The permeability of free space is $\mu_0 = 4\pi \times 10^{-7} H/m$. The permittivity and permeability of free space are related to the speed of light in vacuum $c = 1/\sqrt{\epsilon_0 \mu_0} = 2.99792458 \times 10^8$m/sec. The electric field may contain sources, so that $\nabla \cdot \vec{E} = \rho$, where ρ is the free charge density. Induction fields are sourceless, expressed mathematically by $\nabla \cdot \vec{B} = 0$. For a charge e moving with velocity $\vec{v}$ through and electric field $\vec{E}$ and magnetic field $\vec{B}$, the Lorentz force on the charge is $F = e[\vec{E} + (\vec{v} \times \vec{B})]$.

The electronic properties of isotropic substances can be described macroscopically by scalar material properties in terms of the relative complex permittivity and permeability, ϵ_R^* and μ_R^*:

$$\epsilon = \epsilon' - j\epsilon'' = (\epsilon_R' - j\epsilon_R'')\epsilon_0 = \epsilon_R^* \epsilon_0 \ , \tag{A.2}$$

$$\mu = \mu' - j\mu'' = (\mu_R' - j\mu_R'')\mu_0 = \mu_R^* \mu_0 \ . \tag{A.3}$$

The electric and magnetic fields are modified by the presence of matter in the space-time region in and around the body. The presence of magnetism in matter is described by the magnetization vector $\vec{M}$ which quantifies the number of magnetic dipoles per unit volume. The magnetic field $\vec{H}$ is related to the induction and magnetic moment vectors by

$$\vec{H} = \frac{1}{\mu_0}\vec{B} - \vec{M} \ , \tag{A.4}$$

where μ_0 is the permeability of free space. The magnetic field is also related to the magnetization field, $\vec{M}$ by a constitutive relationship in terms of the susceptibility χ_m. For a linear medium the relation is

$$\vec{M} = \chi_m \vec{H} \ . \tag{A.5}$$

The permeability and susceptibility are related through eqs (A.4) and (A.5)

$$\mu = \mu_0(1 + \chi_m) \ . \tag{A.6}$$

Similarly, the electric field is related to the displacement field ($\vec{D}$) and the polarization field ($\vec{P}$) by

$$\vec{D} = \epsilon_0 \vec{E} + \vec{P} = \epsilon \vec{E} \ . \tag{A.7}$$

It is useful to define a constitutive relation between polarization and electric fields using the electric susceptibility (χ_{el})

$$\vec{P} = \epsilon_0 \chi_{el} \vec{E} \ , \tag{A.8}$$

and therefore

$$\epsilon = \epsilon_0 (1 + \chi_{el}) \ . \tag{A.9}$$

A.1.2 Types of Magnetism

Magnetic materials are classified by the values of permeability.

- diamagnetic $\mu' < \mu_0$,
- paramagnetic $\mu' > \mu_0$,
- ferromagnetic $\mu' >> \mu_0$.

The susceptibilities of the various classes of magnetic phenomena are

- diamagnetic $\chi_m < 0$,
- paramagnetic $\chi_m > 0$,
- ferromagnetic $\chi_m >> 0$.

Due to the complicated quantum-mechanical origin of magnetism with various competing effects, it is not always possible to classify a material into one of the categories. For example, a ferrite may be diamagnetic in X-band and paramagnetic at lower frequencies.

A.2 Paramagnetism

Paramagnetism arises from the alignment of individual spins and angular momentum of particles in external magnetic fields. Paramagnetism is an interaction between the tendency for the electron spins to be aligned with the field on the one hand and thermal agitation which tends to randomize the spins on the other hand. Paramagnetic phenomena in insulators is temperature dependent and follows Curie's law. In metals paramagnetism is strongly influenced by the conduction electrons and has minimal temperature dependence. Paramagnetic materials are primarily the rare earth and transition ions with incomplete atomic shells. There are two types of paramagnetism

- Spin paramagnetism,
- Orbital paramagnetism.

Spin paramagnetism is due to alignment of electron spins and is only slightly temperature dependent. Spin paramagnetism or Pauli paramagnetism occurs in metals. Orbital paramagnetism, caused by alignment of orbital magnetic moments, is strongly temperature dependent. This type of paramagnetism occurs in insulators.

A.2.1 Diamagnetism

Diamagnetism is the magnetic effect that is due to orbital angular momentum effects. *Larmor diamagnetism* occurs in filled-shell insulators. The origin of diamagnetism in materials is the orbital angular momentum of the electrons in applied fields. Diamagnetic materials have a negative susceptibility and generally it is not sensitive to temperature variations at least for nonsuperconducting materials. Diamagnetic materials do not have a strong magnetic response.

A.2.2 Ferromagnetism

In ferromagnetic materials, spin coupling allows regions of aligned spins to be formed, called *domains*. In each domain the spins are more or less aligned. However, adjacent domains as a whole may be arranged in a random fashion. As a magnetic field is applied the domains more or less align with the field.

The difference between paramagnetism and ferromagnetism is that in the case of the former, spins interact minimally, whereas in ferromagnetism the spins strongly interact to cause alignment. Ferromagnetic materials can exist in a nonmagnetized state since magnetic energy is at a minimum when the domains are randomly situated or in a state of maximum entropy. This random arrangement of domains is possible because it is found in a detailed analysis that it is energetically more favorable for many ferromagnetic materials to be magnetically neutral. The boundaries between the oriented spin regions, called *domain walls* require energy for formation. There is a detailed balance between the magnetic field energy caused by alignment of spins in a domain on the one hand and the energy required for domain wall formation on the other hand. Dipolar energy is decreased by wall formation, but exchange energy is increased by the Pauli exclusion principle. Domain walls are normally of 0.01 - 10 μ m thick and can deform under applied fields or mechanical stresses.

As the temperature increases in a ferromagnetic material the kinetic energy can overwhelm the magnetic energy and the preferential alignment of spins can be broken. The

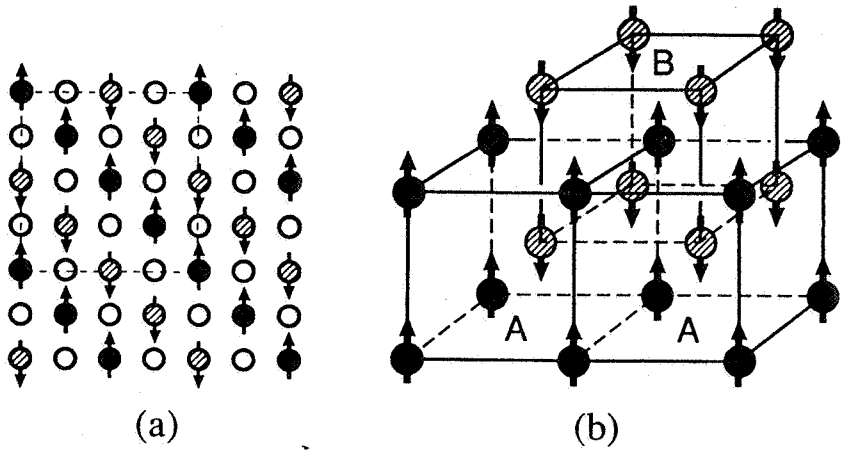

Figure A.1: Lattice structure of antiferromagnetic and ferrite materials. In one lattice the spins are up and in the other lattice the spins are down.

temperature where the kinetic thermal energy becomes predominant over the magnetic energy is called the *Curie temperature*.

If a ferromagnetic material is immersed in an increasing external field its magnetization increases. However as the external field is removed the magnetization curve does not necessarily follow the reverse curve back to the initial state; rather a slightly different curve is followed.

This phenomenon is called *hysteresis* and is caused by the irreversible movement of the domain walls. The irreversibility is caused by defects in the domain wall lattice. Thus, ferromagnetic behavior depends on the past history of the sample and is not totally reversible. Materials with large hysteresis effects are called *hard* and materials with small hysteresis effects are called *soft*.

A.2.3 Ferrites and Antiferromagnetism

Antiferromagnetism is a property possessed by many transition elements and some metals. In these materials the atoms form an ordered array with alternating spin moments so as to give zero for the net magnetic moment of the material. Antiferromagnetic materials are composed of two interpenetrating lattices. Each lattice has all spins more or less aligned, but the lattices as a whole are inverse structures as indicated in figure A.1.

Antiferromagnetic materials do not generally support permanent magnetization and do

not have a strong magnetic response to an applied field. Ferrite materials also consist of two overlapping lattices whose spins are oppositely directed, but with a larger magnetic moment in one lattice than the other. Since spin angular momentum is not canceled totally between the lattices these materials have a magnetic response to an applied field. The magnetic response increases with temperature. Antiferromagnetic materials are paramagnetic above the *Neel* temperature.

Most ferrites are mixtures of oxides such as magnetite of the generic form $XO.Fe_2O_3$ where X is a divalent metallic ion such as Fe (magnetite), Ni (nickel ferrite), Cu (copper ferrite), Mg (manganese ferrite), Co (cobalt ferrite), or Li (lithium ferrite). There are also many other spinel class ferrites that contain additional components, for example, zinc and aluminum. The spinels have either a normal or an inverse lattice structure formed by controlled quenching. Many ferrites have few free electrons and therefore are useful in microwave frequency components since the absence of free electrons prevents eddy-current losses that occur in conducting materials at high frequencies.

A.3 Equations of Motion for the Magnetization Vector

A.3.1 The Torque Equation

In this section we will develop macroscopic equations of motion that underlie the coupling of angular momentum and magnetic fields. As a model [22], we consider a spinning particle exhibiting angular momentum $\vec{J}$, immersed in a magnetic field. The presence of spin induces a magnetic moment $\vec{m} = \gamma_g \vec{J}$, where the γ_g is the gyromagnetic ratio. The magnetic field will interact with the angular momentum by inducing a torque $\vec{\tau}$

$$\vec{\tau} = \frac{d\vec{J}}{dt} . \tag{A.10}$$

We define a magnetic moment, $\vec{m} = \gamma_g \vec{J}$. The equation of motion of the spin system in an applied field $\vec{B}$ is

$$\vec{\tau} = \vec{m} \times \vec{B} , \tag{A.11}$$

or

$$\frac{d\vec{m}}{dt} = \gamma_g (\vec{m} \times \vec{B}) . \tag{A.12}$$

If we average over a significant number of these particles we obtain a macroscopic magnetic moment

$$\vec{M} = N\vec{m} \ , \tag{A.13}$$

where N = number of magnetic moments. We obtain the following equation of motion for the magnetization

$$\frac{d\vec{M}}{dt} = \gamma_g \mu(\vec{M} \times \vec{H}) + \frac{A}{\tau} \ , \tag{A.14}$$

where A is a constant and τ is a characteristic relaxation time of the system. As we will see in the next section it is possible to obtain a tensorial constitutive relation between $\vec{H}$ and $\vec{B}$ by use of eq (A.14) for a magnetic moment in an external magnetic field. This constitutive relationship will define the susceptibility and permeability tensors.

In real materials there always exists some dissipation due to damping. Dissipation is caused by such effects as magnetic dipole radiation and magneto-elastic coupling with lattice phonons. The effect of a dissipation torque can be modelled as a source term added to eq (A.14). One approximation for the dissipation torque yields the Landau equation of motion

$$\frac{d\vec{M}}{dt} = \mu\gamma_g(\vec{M} \times \vec{H}) + \underbrace{\frac{\mu\gamma_g\alpha}{|\vec{M}|}[\vec{M} \times (\vec{M} \times \vec{H})]}_{\text{damping}} \ , \tag{A.15}$$

where α is a parameter that determines the damping. This can be reduced for small damping to

$$\frac{d\vec{M}}{dt} = \mu\gamma_g(\vec{M} \times \vec{H}) + \frac{\alpha}{|\vec{M}|}[\vec{M} \times \frac{d\vec{M}}{dt}] \ . \tag{A.16}$$

This equation is due to Gilbert [23] and neglects terms nonlinear in α. The damping introduces a nonlinearity into the problem.

A.3.2 Magnetized Magnetic Material: The Polder Matrix

The constitutive relation between the induction field and the magnetic field in ferrite materials is represented by the Polder matrix. In order to derive an expression for the Polder permeability tensor we use as a model a magnetic dipole of moment $\vec{m}$, [22,24], in the presence of an external magnetic field, $H(t)$. The net torque experienced by the dipole of magnetic moment m_d is

$$\tau = -\mu m_d H(t) \sin\theta \ , \tag{A.17}$$

where θ is the angle between the dipole axis and field. In the presence of a z-axis magnetic field the dipole will precess with a characteristic Larmor frequency of $\omega_0 = |\gamma_g| H_z$ where γ_g is the gyromagnetic ratio. There are also non-conservative frictional forces present to damp the rotation.

We will assume that in the presence of a time independent d.c. magnetic field in the z direction (H_z), the magnetization is essentially at the saturated value M_s. We further assume a combined d.c. field and an alternating field $\vec{h}$, we obtain $\vec{H}(t) = H_z\vec{e}_3 + \vec{h}\exp(j\omega t)$, where $\vec{e}_3$ is the unit vector in the z direction. The magnetic moment can be approximated by $\vec{M} = M_z\vec{e}_3 + \vec{m}\exp(j\omega t)$, where M_z is time independent. When we substitute these into eq (A.16) we obtain a system of equations

$$j\omega\vec{m} = \mu\gamma_g M_s(\vec{e}_3 \times \vec{h}) + (\omega_0 + j\omega\alpha)(\vec{e}_3 \times \vec{m}) + \vec{m} \times \vec{h}\exp(j\omega t) \ , \tag{A.18}$$

where $\omega_0 = -\gamma_g H_z$ [25] and we assume $|\vec{M}| = M_s \approx M_z$. In the analysis we will neglect the last term in eq (A.18). If

$$\vec{m} = \sum_{i=1}^{3} m_i\vec{e}_i \ , \tag{A.19}$$

$$\vec{h} = \sum_{i=1}^{3} h_i\vec{e}_i \ , \tag{A.20}$$

then by substitution into eq (A.18)

$$j\omega m_x = -(\omega_0 + j\omega\alpha)m_y - \mu\gamma_g M_s h_y \ , \tag{A.21}$$

$$j\omega m_y = \gamma_g\mu M_s h_x + (\omega_0 + j\omega\alpha)m_x \ , \tag{A.22}$$

$$j\omega m_z = 0 \ . \tag{A.23}$$

Therefore

$$m_x = -\frac{(\omega_0 + j\omega\alpha)\mu\gamma_g M_s}{(\omega_0 + j\omega\alpha)^2 - \omega^2}h_x - \frac{j\omega\mu\gamma_g M_s}{(\omega_0 + j\omega\alpha)^2 - \omega^2}h_y \ , \tag{A.24}$$

$$m_y = \frac{j\omega\mu\gamma_g M_s}{(\omega_0 + j\omega\alpha)^2 - \omega^2}h_x - \frac{(\omega_0 + j\omega\alpha)\mu\gamma_g M_s}{(\omega_0 + j\omega\alpha)^2 - \omega^2}h_y \ . \tag{A.25}$$

The system of eqs (A.24) through (A.25) for the linear susceptibility relation between $\vec{M}$ and $\vec{H}$ can be expressed as

$$\mu\begin{pmatrix} \chi & -j\kappa & 0 \\ j\kappa & \chi & 0 \\ 0 & 0 & 0 \end{pmatrix}\begin{pmatrix} h_x \\ h_y \\ h_z \end{pmatrix} = \begin{pmatrix} m_x \\ m_y \\ m_z \end{pmatrix} \ , \tag{A.26}$$

where

$$\chi = \frac{(\omega_0 + j\omega\alpha)\omega_M}{(\omega_0 + j\omega\alpha)^2 - \omega^2} \ , \tag{A.27}$$

and

$$\kappa = \frac{-\omega\omega_M}{(\omega_0 + j\omega\alpha)^2 - \omega^2} , \tag{A.28}$$

and

$$\omega_M = -\gamma_g M_s . \tag{A.29}$$

We can separate out the real and imaginary components to yield

$$\chi' = \frac{\omega_M\omega_0[(\omega_0^2 - \omega^2) + \alpha^2\omega^2]}{[\omega_0^2 - \omega^2(1+\alpha^2)]^2 + 4\omega^2\omega_0^2\alpha^2} , \tag{A.30}$$

$$\chi'' = -\frac{\omega_M\omega\alpha[\omega_0^2 + \omega^2(1+\alpha^2)]}{[\omega_0^2 - \omega^2(1+\alpha^2)]^2 + 4\omega^2\omega_0^2\alpha^2} , \tag{A.31}$$

$$\kappa' = \frac{-\omega_M\omega[\omega_0^2 - \omega^2(1+\alpha^2)]}{[\omega_0^2 - \omega^2(1+\alpha^2)]^2 + 4\omega^2\omega_0^2\alpha^2} , \tag{A.32}$$

$$\kappa'' = \frac{2\omega_0\omega^2\alpha\omega_M}{[\omega_0^2 - \omega^2(1+\alpha^2)]^2 + 4\omega^2\omega_0^2\alpha^2} . \tag{A.33}$$

Note that we have assumed that the magnetization is at the saturated value M_s. That is all of the magnetic moments are assumed to be aligned with the external field. This is not always a good assumption. For this special case the Polder matrix is

$$\bar{\bar{\mu}} = \mu(\bar{\bar{I}} + \bar{\bar{\chi}}) = \mu \begin{pmatrix} \chi + 1 & -j\kappa & 0 \\ j\kappa & \chi + 1 & 0 \\ 0 & 0 & 1 \end{pmatrix} . \tag{A.34}$$

We see that in the limit as $H_z \rightarrow 0$ and $M_z \rightarrow 0$ the off-diagonal components of the permeability tensor vanish and the diagonal components reduce to the isotropic permeability, $\bar{\bar{\mu}} = \mu\ \bar{\bar{I}}$, where $\bar{\bar{I}}$ is the identity matrix.

Appendix B

Fields in Waveguides

B.1 Summary of Maxwell's Equations

Maxwell's equations are

$$\nabla \times \vec{E} = -j\omega\vec{B} \ , \tag{B.1}$$

$$\nabla \times \vec{H} = \vec{J} + j\omega\vec{D} \ , \tag{B.2}$$

$$\nabla \cdot \vec{D} = \rho \ , \tag{B.3}$$

$$\nabla \cdot \vec{B} = 0 \ . \tag{B.4}$$

The boundary conditions at material interfaces are

$$\vec{n} \times (\vec{E}_2 - \vec{E}_1) = 0 \ , \tag{B.5}$$

$$\vec{n} \times (\vec{H}_2 - \vec{H}_1) = \vec{J}_s \ , \tag{B.6}$$

$$\vec{n} \cdot (\vec{D}_2 - \vec{D}_1) = \Omega \ , \tag{B.7}$$

$$\vec{n} \cdot (\vec{B}_2 - \vec{B}_1) = 0 \ , \tag{B.8}$$

where J_s is the surface current density and Ω is the surface charge density.

B.2 Modes

B.2.1 TE Modes

The longitudinal coordinate is assumed to be z. If the H_z mode exists, it is the generator of the TE mode [22]. The TE modes satisfy the boundary value problem,

$$\{\nabla_T^2 + k_c^2\} H_{z(TE)} = 0 \ , \tag{B.9}$$

where $k_c^2 = k^2 + \gamma^2$ are real, positive eigenvalues. The boundary conditions are

$$\vec{n} \cdot (\nabla H_{(z(TE))})|_{on\ conductor} = 0 \ , \tag{B.10}$$

where $\vec{n}$ is the normal vector. Also

$$E_{z(TE)} = 0 \ . \tag{B.11}$$

The other field components are then

$$\vec{H}_{T(TE)} = -\frac{\gamma}{k_c^2} \nabla_T H_z \ , \tag{B.12}$$

$$\vec{E}_{T(TE)} = -Z_{TE}(\vec{z} \times \vec{H}_{T(TE)}) \ . \tag{B.13}$$

B.2.2 TM Modes

For the case of TM waves

$$\{\nabla_T^2 + k_c^2\} E_{z(TM)} = 0 \ , \tag{B.14}$$

where $k_c^2 = k^2 + \gamma^2$ are real, positive eigenvalues determined by boundary information on the waveguide.

The boundary conditions are

$$E_{(z(TM))}|_{on\ conductor} = 0 \ , \tag{B.15}$$

$$H_{z(TM)} = 0 \ . \tag{B.16}$$

The other field components are

$$\vec{E}_{T(TM)} = -\frac{\gamma}{k_c^2} \nabla_T E_z \ , \tag{B.17}$$

$$\vec{H}_{T(TM)} = \frac{1}{Z_{TM}} (\vec{z} \times \vec{E}_{T(TM)}) \ , \tag{B.18}$$

$$\gamma = j\sqrt{k^2 - k_c^2} \ . \tag{B.19}$$

B.2.3 TEM Modes

The propagation of *TEM* modes are possible in addition to the *TE* and *TM* modes in coaxial cable . The cutoff wave numbers for higher order *TM* waves in coaxial line are given by the roots of:

$$\frac{N_n(k_c R_1)}{J_n(k_c R_1)} - \frac{N_n(k_c R_4)}{J_n(k_c R_4)} = 0 \ , \tag{B.20}$$

[22], and for *TE* waves in coaxial line by

$$\frac{N'_n(k_c R_1)}{J'_n(k_c R_1)} \frac{N'_n(k_c R_4)}{J'_n(k_c R_4)} = 0 \ , \tag{B.21}$$

where J and N denote the Bessel functions of the first and second kind and R_1 and R_4 are the inner and outer radii respectively. The cutoff wavelengths are given approximately by:

$$\lambda_c \approx \frac{2}{q}(R_4 - R_1) \quad q = 1, 2, 3, \ldots \ . \tag{B.22}$$

For example the *TM* mode cutoff frequency in 7 mm coaxial line for eq (B.22) is approximately 34 GHz.

Appendix C

Gap Correction

C.1 Frequency-Dependent Gap Correction

C.1.1 Waveguide

We consider a sample in a rectangular waveguide of dimensions a x b with a small gap (b-d). The dielectric constant in the gap is ϵ_{Rg} and of sample ϵ_{Rs}. The measured or observed value is ϵ_{Ro}.

A transverse resonance condition yields [40]:

$$\tan(k_{1c}d) + X\tan(k_{2c}(b-d)) = 0\ , \tag{C.1}$$

where

$$k_{1c} = \frac{\omega}{c_{lab}}\sqrt{\epsilon_{Rs} - \epsilon_{Ro}}\ , \tag{C.2}$$

$$k_{2c} = \frac{\omega}{c_{lab}}\sqrt{\epsilon_{Rg} - \epsilon_{Ro}}\ , \tag{C.3}$$

and

$$X = \frac{\epsilon_{Rs}}{\epsilon_{Rg}}\frac{\sqrt{\epsilon_{Rg} - \epsilon_{Ro}}}{\sqrt{\epsilon_{Rs} - \epsilon_{Ro}}}\ . \tag{C.4}$$

For our case of waveguide $(b-d) \approx 2.54 \times 10^{-5}$ m and $b = 0.01016$ m. Equation (C.1) must be solved by iteration, but for low frequencies and low dielectric constants we can obtain a approximate solution. This equation reduces to Westphal's equation, [34] in the appropriate low frequency limit.

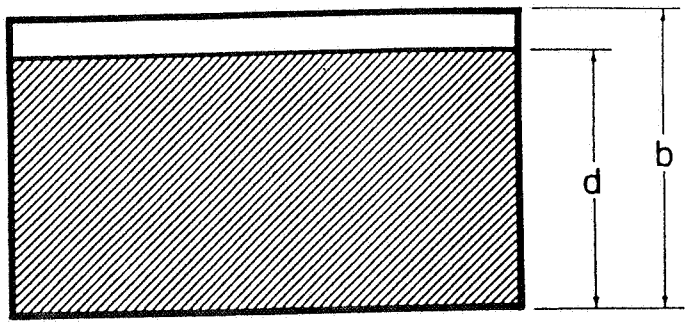

Figure C.1: Sample in waveguide with air gap.

C.1.2 Coaxial Line

For coaxial line the matching of transverse impedance yields the resonance condition [40]:

$$\mathrm{ct}(x_2, x_1) = X\,\mathrm{ct}(x_2', x_3') \;, \tag{C.5}$$

where

$$x_1 = k_{1c} R_1 \;, \tag{C.6}$$

$$x_2 = k_{1c} R_2 \;, \tag{C.7}$$

$$x_2' = k_{2c} R_1 \;, \tag{C.8}$$

$$x_3' = k_{2c} R_2 \;, \tag{C.9}$$

and X, k_{1c}, and K_{2c} are given in the previous section. The functions ct are defined as

$$\mathrm{ct}(x, y) = \frac{J_1(x)N_0(y) - N_1(y)J_0(x)}{J_0(x)N_0(y) - N_0(x)J_0(y)} \;, \tag{C.10}$$

where J_0, J_1, N_0, and N_1 are the Bessel functions of zero and first order of the first and second kind respectively.

C.2 Frequency-Independent Approaches

Various researchers have approached the gap problem by representing the sample with air gap as a layered capacitor [33,34,41]. This approach assumes that the gaps between transmission line and sample are effectively modeled by a set of capacitors in series. Champlin [41] approached the problem using as a starting point the perturbation formula developed by Schwinger [42]. By substituting into the perturbation formula approximations to the field distribution in the various regions, they obtain an estimate for the effective permittivity. Their answer turns out to be fully equivalent to the capacitor model of Westphal [34]. Champlin showed that Bussey's theory [33] is the first two terms in an expansion of Westphal [34] and Champlin's models.

The capacitor model is frequency independent and thus is strictly valid only at lower frequencies and dc. We expect the capacitor model to break down at higher frequencies because the wavelength decreases with increasing frequency to a point where multiple scattering dominates. In order to account for multiple scattering, it is necessary to develop a theory that is frequency dependent.

C.2.1 Coaxial Capacitor Model for Dielectric Materials

Consider a capacitor consisting of layers of dielectric and layers of air in a coaxial line [43,44]. The dimensions are shown in figure C.2.

We treat the system as capacitors in series, so

$$\frac{1}{C_m} = \frac{1}{C_1} + \frac{1}{C_2} + \frac{1}{C_3} \,. \tag{C.12}$$

We know that for a coaxial line the electric field distribution is given by

$$E_r = \frac{V}{\ln(\frac{b}{a})r} \,, \tag{C.13}$$

and the voltage between the conductors is given by

$$V = -\int_a^b E(r)dr \,. \tag{C.14}$$

The capacitance of a coaxial line of length L is given by

$$C = \frac{2\pi\epsilon L}{\ln\frac{R_2}{R_1}}; \tag{C.15}$$

thus, for a system of three capacitors in series we have

$$\frac{\ln\frac{R_4}{R_1}}{\epsilon'_m} = \frac{\ln\frac{R_2}{R_1}}{\epsilon'_1} + \frac{\ln\frac{R_3}{R_2}}{\epsilon'_c} + \frac{\ln\frac{R_4}{R_3}}{\epsilon'_1} \,, \tag{C.16}$$

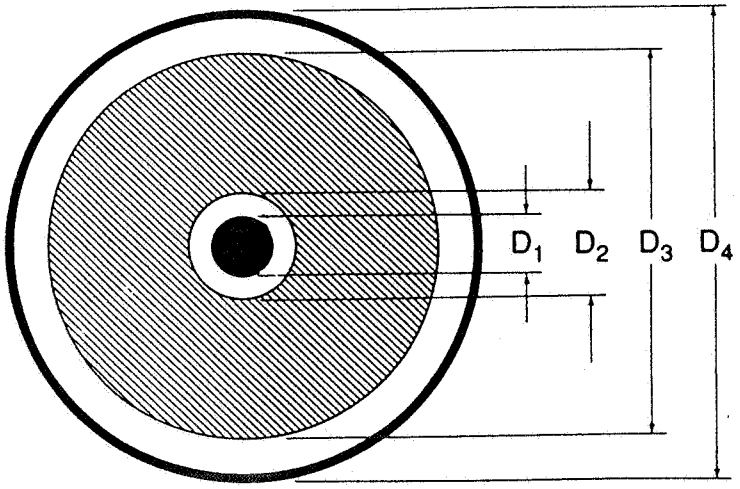

Figure C.2: A coaxial sample in holder with air gaps near conductors with diameters denoted by D_i.

where ϵ'_c, ϵ'_m are the corrected and measured values of the real part of the permittivity and ϵ'_1 is the real part of the permittivity of the air gap

$$\epsilon'_{cR} = \frac{L_2(\epsilon'_{mR}L_3 - \epsilon''^2_{mR}L_1 - \epsilon'^2_{mR}L_1)}{\epsilon'^2_{mR}L_1^2 - 2\epsilon'_{mR}L_1L_3 + \epsilon''^2_{mR}L_1^2 + L_3^2}\ , \tag{C.16}$$

$$\epsilon''_{cR} = \frac{L_2L_3\epsilon''_{mR}}{\epsilon'^2_{mR}L_1^2 - 2\epsilon'_{mR}L_1L_3 + \epsilon''^2_{mR}L_1^2 + L_3^2}\ . \tag{C.17}$$

An approximate expression is given by

$$\epsilon'_{cR} = \epsilon'_{mR}\frac{L_2}{L_3 - \epsilon'_{mR}L_1}\ , \tag{C.18}$$

$$\tan\delta_c = \tan\delta_m[1 + \epsilon'_{mR}\frac{L_1}{L_2}]\ , \tag{C.19}$$

where

$$L_1 = \ln\frac{R_2}{R_1} + \ln\frac{R_4}{R_3}\ , \tag{C.20}$$

$$L_2 = \ln\frac{R_3}{R_2}\ , \tag{C.21}$$

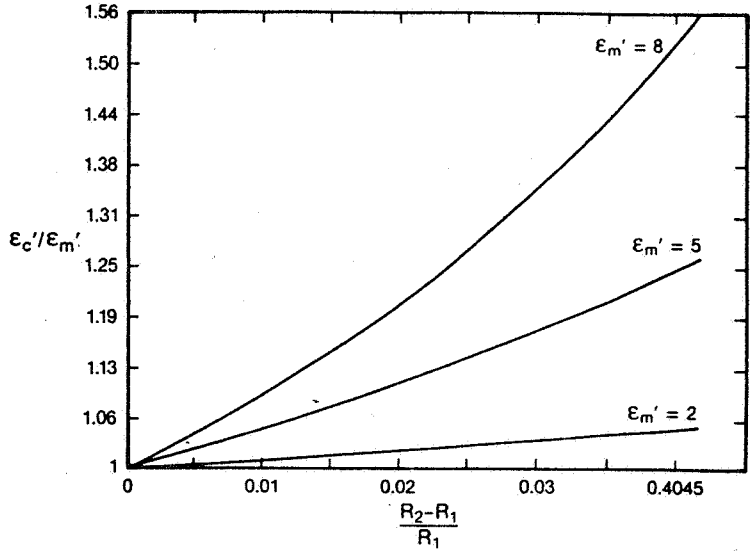

Figure C.3: The gap correction calculated for various values of ϵ'_R, where R_2, R_1 are the radii of the inner conductor and sample respectively.

$$L_3 = \ln \frac{R_4}{R_1} \,. \tag{C.22}$$

Equation (C.18) breaks down when $\epsilon'_{mR} \geq L_3/L_1$. An example is plotted in figure C.3 for a 7 mm coaxial line.

C.2.2 Rectangular Waveguide Model

For the case of a rectangular guide of short dimension b with sample thickness d and long dimension b_1 and sample thickness d_1 the E-plane gap correction is

$$\epsilon'_{cR} = \frac{d(b(\epsilon'_{mR} - \epsilon'^2_{mR} - \epsilon''_{mR}) + d(\epsilon'^2_{mR} + \epsilon''^2_{mR}))}{b^2(\epsilon'^2_{mR} - 2\epsilon'_{mR} + \epsilon''^2_{mR} + 1) - 2bd(\epsilon'^2_{mR} - \epsilon'_{mR} + \epsilon''^2_{mR}) + d^2(\epsilon'^2_{mR} + \epsilon''^2_{mR})} \,, \tag{C.23}$$

$$\epsilon''_{cR} = \frac{db\epsilon''_{mR}}{b^2(\epsilon'^2_{mR} - 2\epsilon'_{mR} + \epsilon''^2_{mR} + 1) - 2bd(\epsilon'^2_{mR} - \epsilon'_{mR} + \epsilon''^2_{mR}) + d^2(\epsilon'^2_{mR} + \epsilon''^2_{mR})} \,. \tag{C.24}$$

C.3 Gap Correction for Magnetic Materials

C.3.1 Coaxial Line

For the calculation of the gap correction for the permeability a pure inductance model is useful. We model the transmission line as

a series of inductors for the E-field gap

$$L_m = L_c + L_{air} \ , \tag{C.25}$$

where c, m, and air denote corrected value, measured value, and air space. Therefore the corrected value is

$$L_c = L_m - L_{air} \ . \tag{C.26}$$

The inductance is the flux penetrating the circuit divided by the current flowing in the circuit

$$L = \frac{\phi}{I} \ , \tag{C.27}$$

where

$$\phi = \int \vec{B} \cdot d\vec{S} \ . \tag{C.28}$$

Ampere's law is

$$\int \vec{H} \cdot d\vec{l} = I \ , \tag{C.29}$$

which yields

$$B_\phi = \frac{\mu' I}{2\pi r} \ . \tag{C.30}$$

Therefore

$$\phi = \frac{1}{2\pi} \mu' I \ln b/a \ , \tag{C.31}$$

so

$$L = \frac{1}{2\pi} \mu' \ln b/a \ . \tag{C.32}$$

Therefore we can write for the corrected permeability

$$\mu'_{cR} = \frac{\mu'_{mR} \ln R_4/R_1 - [\ln R_2/R_1 + \ln R_4/R_3]}{\ln R_3/R_2} \ , \tag{C.33}$$

$$\mu''_{cR} = \mu''_{mR} \frac{\ln(R_4/R_1)}{\ln(R_3/R_2)} \ . \tag{C.34}$$

Gap corrections are given in figures C.4- C.7. The corrections for permeability in coaxial line are much less than for permittivity. This is due to the fact the azimuthal magnetic

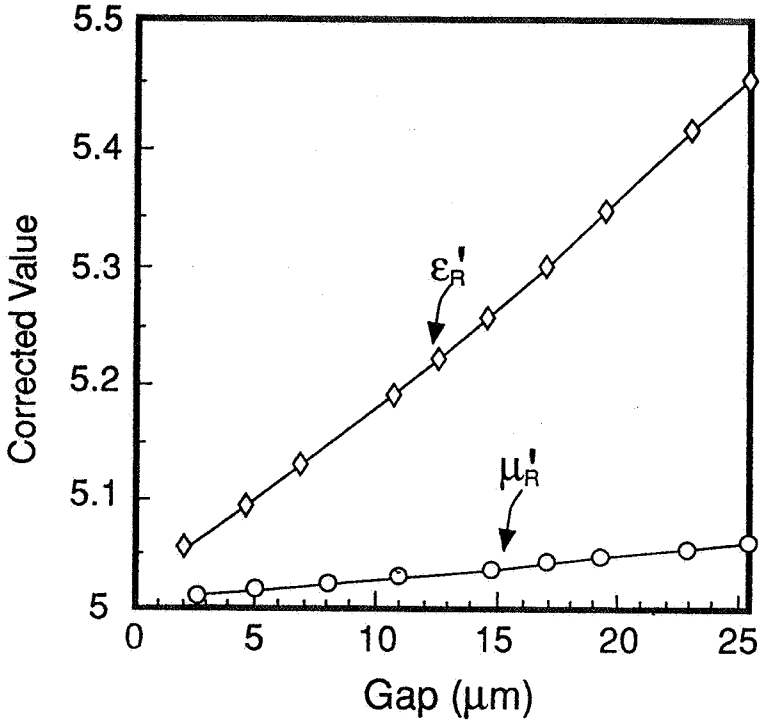

Figure C.4: Corrected permeability and permittivity as a function of inner conductor gap for a 7 mm sample. The gap around the outer conductor is assume to be zero. In this case the uncorrected (measured) was $\mu_R' = 5$, $\epsilon_R' = 5$.

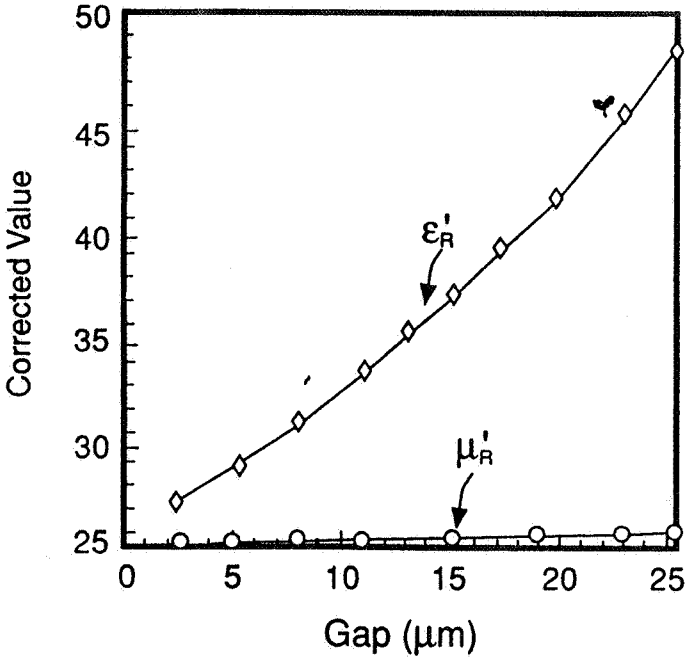

Figure C.5: Corrected permeability and permittivity as a function of inner conductor gap for a 7 mm sample. The gap around the outer conductor is assume to be zero. In this case the uncorrected (measured) was $\mu_R' = 25$, $\epsilon_R' = 25$.

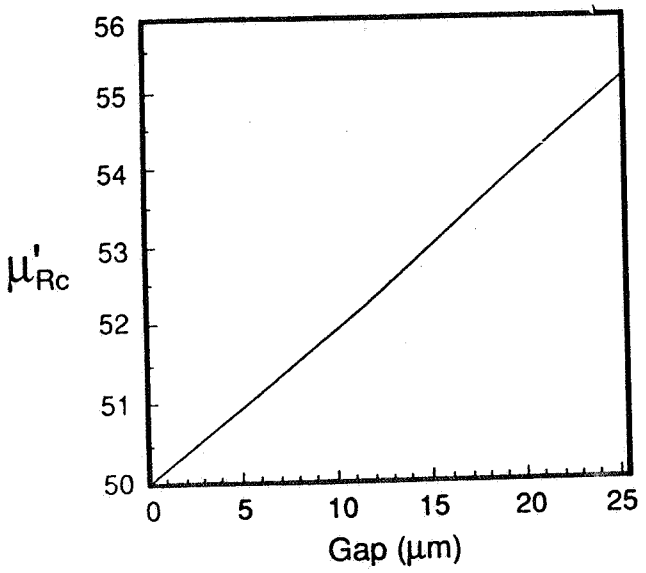

Figure C.6: Corrected permeability as a function of inner conductor gap for a 7 mm sample. The gap around the outer conductor is assume to be zero. In this case the uncorrected (measured) was $\mu'_R = 50$.

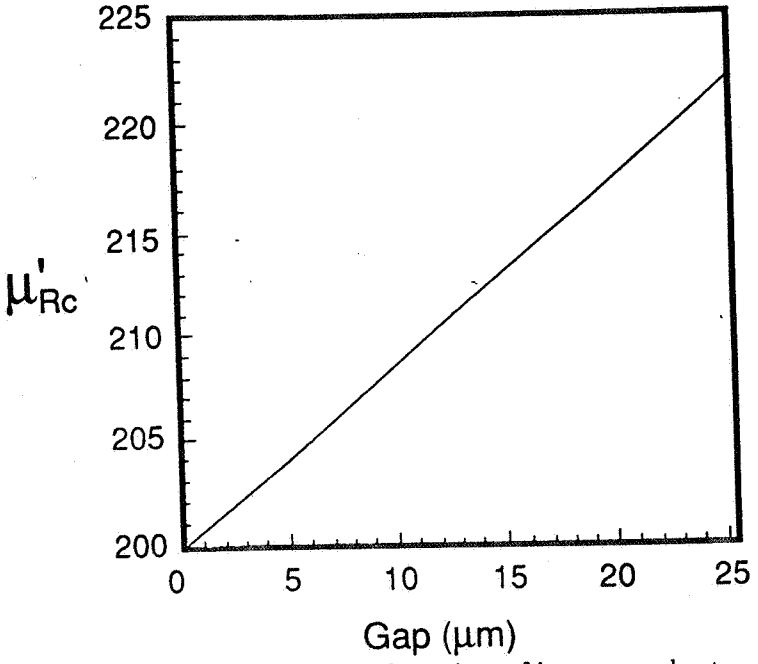

Figure C.7: Corrected permeability as a function of inner conductor gap for a 7 mm sample. The gap around the outer conductor is assume to be zero. In this case the uncorrected (measured) was $\mu'_R = 200$.

field is continuous across the discontinuity, whereas the radial electric field is discontinuous across the discontinuity.

(C.35)

C.3.2 Waveguide

E-plane Gaps

For magnetic materials in waveguide for the TE_{10} mode the E- plane gap is less severe than the H-field gap. The corrections can be obtained using inductances in series. These are

$$\mu'_{cR} = \mu'_{mR}\left(\frac{b}{d}\right) - \left(\frac{b-d}{d}\right) , \tag{C.36}$$

$$\mu''_{cR} = \mu''_{mR}\left(\frac{b}{d}\right) . \tag{C.37}$$

H-plane gaps

For the long width of the waveguide there is a discontinuity in the magnetic field for the TE_{10} mode. The corrections can be obtained using inductances in parallel. We assume a long waveguide width of b_1 and sample width d_1

$$\mu'_{cR} = \frac{d_1(b_1(\mu'_{mR} - \mu'^2_{mR} - \mu''_{mR}) + d_1(\mu'^2_{mR} + \mu''^2_{mR}))}{b_1^2(\mu'^2_{mR} - 2\mu'_{mR} + \mu''^2_{mR} + 1) - 2b_1d_1(\mu'^2_{mR} - \mu'_{mR} + \mu''^2_{mR}) + d_1^2(\mu'^2_{mR} + \mu''^2_{mR})} , \tag{C.38}$$

$$\mu''_{cR} = \frac{d_1b_1\mu''_{mR}}{b_1^2(\mu'^2_{mR} - 2\mu'_{mR} + \mu''^2_{mR} + 1) - 2b_1d_1(\mu'^2_{mR} - \mu'_{mR} + \mu''^2_{mR}) + d_1^2(\mu'^2_{mR} + \mu''^2_{mR})} . \tag{C.39}$$

C.4 Gap Correction Formulas Derived Directly From Maxwell's Equations

Consider Maxwell's equations in a coaxial line

$$\nabla \times \vec{E} = -j\omega\vec{B} . \tag{C.40}$$

The radial electric field is discontinuous at the air gap interface, but the displacement vector $\vec{D}$ is continuous across the interface. Also H_ϕ is continuous across the interface, whereas $\vec{B}$ is discontinuous. Let us assume that there are no sources so that $\vec{J} = 0$. Then, we can write eq (C.40) as

$$\nabla \times \frac{\vec{D}}{\epsilon} = -j\omega\mu\vec{H} \ . \tag{C.41}$$

If we now average eq (C.41) over the cross-sectional area of a coaxial line, we obtain

$$2\pi \int_a^b \nabla \times \frac{\vec{D}}{\epsilon} dr = -j\omega 2\pi \int_a^b \mu\vec{H} dr \ . \tag{C.42}$$

Continuity of the displacement field and tangential magnetic field and the fact that $D_r \propto 1/r$ and $H_\phi \propto 1/r$ is imposed and integrations are performed. Comparing these results to an effective medium equation, we obtain the same form as the previously developed capacitor and inductance models for the corrected permittivity and permeability:

$$\frac{\ln \frac{R_4}{R_1}}{\epsilon'_m} = \frac{\ln \frac{R_2}{R_1}}{\epsilon'_1} + \frac{\ln \frac{R_3}{R_2}}{\epsilon'_c} + \frac{\ln \frac{R_4}{R_3}}{\epsilon'_1} \ , \tag{C.43}$$

$$\mu'_{mR}[\ln R_4/R_1] = \mu'_{cR} \ln R_3/R_2 + [\ln R_2/R_1 + \ln R_4/R_3] \ . \tag{C.44}$$

The analogous calculation can be performed for waveguide. These effective media formulas are the Voigt approximation for the permeability (layers in series) and the Reuss approximation (layers in parallel) for the permittivity. The previously developed capacitor model can be derived directly from Maxwell's equations.

From the perspective of Maxwell's equation the limitations of the capacitor and inductance models can be assessed. In order for these models to apply, we assume that

- The fundamental mode is the only propagating mode.
- The air gap and sample are azimuthally symmetric.

The air gap modifies the modal structure in the waveguide. The model assumption that only a TEM mode is propagating in a coaxial line with an air gap around the sample becomes less and less valid as the air gap increases in size. In fact, since the phase velocity in the air gap region is much larger than the phase velocity in the sample, a distortion of the wave can be expected. Longitudinal components of the electric field and therefore TM modes will form as a result of an air gap if above cutoff. If the air gap or sample are not azimuthally symmetric, H_ϕ is no longer the only nonzero magnetic field component. This asymmetry will allow higher order TE modes to propagate, when they are above cutoff. When the assumption that the only propagating mode is the fundamental mode breaks down, equations of the same form as eqs (C.43) and (C.44) hold with the logarithmic constants replaced by more complicated expressions.

C.5 Mitigation of Air Gap Effects

It is possible to minimize the effects of air gaps by placing a conducting material in the air gap. This material may be a conducting paint, indium-gallium solder alloy, or a conducting grease. The conducting material will change the line impedance and line loss to a degree. However, for relatively small gaps, the improvements in dielectric and magnetic property measurements far outweigh any changes in line impedance. The loss measurement will be influenced by this procedure. Application of the conducting material is an art.

Appendix D

Causal Functions and Linear Response

D.1 Introduction

We call a temporal function *causal* if it is 0 for all times less than 0. The goal of this section is to review the basic mathematics used to describe causal systems.

In the analysis to follow we assume that an impulse is applied to a system at $t = 0$. We can model a linear system by an input function $f(t)$, an output function $g(t)$, and an impulse response function $a(t)$. It is possible for either or both of $f(t)$ and $a(t)$ to be causal. A more general approach would be to study nonlinear response with linear response as a very special case. Linear response theory is usually valid when the underlying probability density function can be approximated as an equilibrium distribution.

If both $f(t)$ and $a(t)$ are causal, the linear response is given by [45]

$$g(t) = \int_0^t f(\tau)a(t-\tau)d\tau \ . \tag{D.1}$$

In this case, the output is a convolution over all past times. If only $f(t)$ is causal then

$$g(t) = \int_0^\infty f(\tau)a(t-\tau)d\tau \ . \tag{D.2}$$

We assume that $a(t) = 0$ for $t < 0$. The interpretation of the function $f(t)$ can be obtained from the relationship

$$f(t) = \int_{-\infty}^\infty f(\tau)\delta(t-\tau)d\tau \ . \tag{D.3}$$

If we identify the left side of eq (D.3) as the response function, then the impulse response $a(t)$ is delta function in the special case of no distortion. Of course, in real systems the impulse response will be broader than a delta function.

We can define the step response function $h(t)$ as

$$\frac{dh(t-\tau)}{dt} = a(t-\tau) \ , \tag{D.4}$$

and it is assumed that $h(0) = 0$. If we use the step response for $g(t)$ in eq (D.1) we obtain

$$g(t) = f(0)h(t) + \int_0^t \frac{df(\tau)}{d\tau} h(t-\tau) \ . \tag{D.5}$$

D.2 Transfer Functions

If we send a signal $\exp(j\omega t)$ into a system, the response of the system is called the *transfer function* and is denoted by S. The transfer function is defined as the Fourier transform of the impulse response function

$$S(\omega) = \int_{-\infty}^{\infty} a(t) e^{j\omega t} dt \ . \tag{D.6}$$

As a consequence of the reality of $a(t)$, $S(-\omega) = S^*(\omega)$. If $F(\omega)$ is the Fourier transform of $f(t)$ we have, using the inverse Fourier transform

$$g(t) = \frac{1}{2\pi} P \int_{-\infty}^{\infty} F(\omega) S(\omega) e^{j\omega t} d\omega \ . \tag{D.7}$$

D.3 Kramers-Kronig Relations

The real and imaginary components of any causal function are related by a dispersion relation. The complex permittivity is a causal function whose real and imaginary components are related by the Hilbert transform [45]

$$\epsilon_r'(\omega) - \epsilon_{r\infty} = -\frac{2}{\pi} \int_0^{\infty} \frac{[\theta \epsilon_r''(\theta) - \omega \epsilon_r''(\omega)]}{\theta^2 - \omega^2} d\theta \ , \tag{D.8}$$

$$\epsilon_r''(\omega) = -\frac{2\omega}{\pi} \int_0^{\infty} \frac{[\epsilon_r'(\theta) - \epsilon_r'(\omega)]}{\theta^2 - \omega^2} d\theta \ . \tag{D.9}$$

The following summarizes some of the features of the Kramers-Kronig relations:

- The Hilbert transform relates real and imaginary components of a causal function.

- Direct solution requires complete data over full spectrum for one component.
- Equation (D.8) can be thought of as an integral equation for the unknown component when there are some data for the other component.

Another form of the dispersion relations is

$$\epsilon'_r(\omega) - \epsilon'(\omega_o) = -\frac{\omega - \omega_o}{\pi} P \int_{-\infty}^{\infty} \frac{\epsilon''_r(\theta) d\theta}{(\theta - \omega)(\theta - \omega_o)} , \tag{D.10}$$

$$\epsilon''_r(\omega) - \epsilon''(\omega_o) = \frac{\omega - \omega_o}{\pi} P \int_{-\infty}^{\infty} \frac{\epsilon'_r(\theta) d\theta}{(\theta - \omega)(\theta - \omega_o)} , \tag{D.11}$$

where P denotes principal value.

*U.S. GOVERNMENT PRINTING OFFICE:1994-573-013/89064